Delineating the impact of binding-domain affinity and kinetic properties on Chimeric Antigen Receptor T cell function

Anne Marijn Kramer

A dissertation submitted in partial fulfilment

of the requirements for the degree of

Doctor of Philosophy

of

University College London.

Great Ormond Street Institute of Child Health

University College London

April 30, 2017

I, Anne Marijn Kramer, confirm that the work presented in this thesis is my own. Where information has been derived from other sources, I confirm that this has been indicated in the work.

This project was supported by a NIHR GOSH/UCL ICH BRC PhD Scholarship.

This work is dedicated to Alexander and opa & oma Muntendam.

"A good head and a good heart are always a formidable combination."

Nelson Mandela, 1918-2013

Abstract

CD19 Chimeric Antigen Receptor (CAR) therapy represents a breakthrough in the treatment of relapsed/refractory acute lymphoblastic leukaemia and early-phase clinical trials with CAR-modified-T cells have shown unprecedented responses. A CAR is a recombinant receptor that combines a single chain variable fragment (scFv) against a tumour-associated antigen and an intracellular activation domain of the T cell receptor (TCR), recognizing membrane-bound antigen, typically with a higher affinity compared to TCR-pMHC affinity. We compared the influences of differences in on- and off-rates underlying the binding kinetics of CD19 CARs on downstream CAR T cell responses and constructed a novel CAR derived from the CAT hybridoma demonstrating a lower affinity as a result of a greater off-rate, whilst maintaining an on-rate nearly identical to FMC63, the scFv most-used in clinical trials. Using *in vitro* pre-clinical models we demonstrated that CAT-CAR$^+$ T cells showed increased proliferation, higher cytotoxic responses, and increased cytokine production, as well as a greater number of interactions between CAT-CAR$^+$ T cells and target cells and a greater motility in comparison to FMC63. *In vivo* CAT-CAR$^+$ T cells showed an enhanced ability to clear disease, proliferate and produce cytokines, displaying markers characteristic for improved T cell fitness. We believe that, analogous to the natural TCR, a lower overall binding affinity might be mitigated by a relatively faster off-rate in the setting of a constant on-rate and propose that this may enhance CAR T cell function through serial triggering, where increased target:effector interaction time, may lead to exhaustion and activation induced cell death. These data have important implications for the development of future CARs.

Acknowledgements

There are many people I am eternally grateful to for their encouragement throughout the duration of this PhD project at the Great Ormond Street Institute of Child Health, I could have not done this alone.

First and foremost, this PhD project would not have happened if professor Persis Amrolia would not have allowed me to work under his supervision and support after an unfortunate start, for which I extend a huge thank you. Together with Dr. Martin Pule, who conceived the project and offered guidance and expertise throughout, and Dr. Sara Ghorashian who has been far more than a mentor, providing support on many different levels, which I know will stand me in great stead for what comes next, I could have not wished for a better supervisory team around me.

Next, I would like to thank everyone in the Amrolia and Pule labs. It has been an absolute joy working with you throughout the years. I feel very privileged having been surrounded by such enthusiastic and experienced scientists. Your support as a colleague and as a friend have meant a lot to me.

Thank you to all my lovely colleagues among the lab members at MCI and Developmental Biology and Cancer, past and current included, for making the past 3 years so enjoyable. All the help, great laughs, pep talks, coffees, chats and countless cakes have been unforgettable.

I feel very privileged to be surrounded by an amazing group of friends, both in the Netherlands as well as in the United Kingdom. There is a whole world outside of work, of which you very much helped to remind me, providing me with the right amount of distraction I needed to keep me sane(ish) during the course of this PhD.

My family has been the cornerstone of my professional and personal development, extending much further than this PhD. Thank you for your unconditional love and support and the laughs, the tears, and all our memories together that I cherish. Even in difficult times you proved to be strong and resilient, which has been an enormous inspiration. The perk of having returned to Amsterdam is definitely being so much closer to you all.

Last but definitely not least, my never-ending thankfulness goes to my fiancé, Alexander. I could have not wished for a more loving, caring and supportive person to share my life with. We started our journey together before London, but in December 2015 in Hyde Park this changed into what will hopefully turn out to be a life-long adventure. I cannot wait for the future together with you, I love you dearly.

Contents

List of Figures

List of Tables

Abbreviations

ACT	Adoptive T cell therapy
AICD	Activation induced cell death
ALAT	Alanine transaminase
ALL	Acute lymphoblastic leukaemia
APC	Antigen presenting cell
ASAT	Aspartate aminotransferase
B-ALL	B-lymphoblastic leukaemia
BLI	Bioluminescent imaging
BUN	Blood urea nitrogen
CAR	Chimeric antigen receptor
CCR	C-C Chemokine Receptor
CDR	Complementarity determining region
CEA	Carcinoembryonic antigen
Cr	Chromium
CRP	C-reactive protein
CRS	Cytokine release syndrome
CSF	Cerebrospinal fluid
CTL	Cytotoxic lymphocyte
CTLA-4	Cytotoxic T-lymphocyte antigen 4
D10	Dulbeccos Modified Eagle Medium + 10% FCS
DNA	Deoxyribonucleic acid
E:T	Effector to target ratio
EBV	Epstein Barr virus

ELISA	Enzyme linked immunoassay
Erk	Extracellular-signal-regulated kinase
FACS	Fluorescence activated cell sorting
FCS	Fetal calf serum
ffLuc	Firefly luciferase
GFP	Green fluorescent protein
GEMs	Glycolipid-enriched membrane microdomains
HER2	Human epidermal growth factor receptor 2
HLA	Human leukocyte antigen
HSCT	Haematopoietic stem cell transplantation
i.v.	Intravenous
ICOS	Inducible costimulator
IFN-γ	Interferon γ
Ig	Immunoglobulin
IL	Interleukin
ITAMs	Immunoreceptor tyrosine-based activation motifs
k_a	Association rate/On rate
K_D	Dissociation equilibrium constant
k_d	Dissociation rate/Off rate
LAG-3	Lymphocyte activated gene-3
LAT	Linker of activated T cells
LDH	Lactate dehydrogenase
MART-1	Melanoma antigen recognized by T cells 1
MFI	Median fluorescence intensity
MHC	Major Histocompatability Complex
MIP-1β	Macrophage inflammatory protein 1 β
NCAM	Neural small adhesion molecule
ORR	Overall response rate
PAMPs	Pathogen-associated molecular patterns
PBMCs	Peripheral blood mononuclear cells

PCR	Polymerase chain reaction
PD1	Programmed Death 1
pMHC	Peptide-MHC Complex
r/r	Relapsed/refractory
R10	Roswell Park Memorial Insitute + 10% FCS
RFS	Relapse free survival
RNA	Ribonucleic acid
scFv	Single chain variable fragment
Sgp130	Soluble IL-6-Receptor
SOC	Super Optimal broth with catabolite repression
SPR	Surface plasmon resonance
STAT3	Signal transducer and activator of transcription 3
$t_{1/2}$	Half-life
TAA	Tumour associated antigen
TCR	T cell receptor
TGF-β	Transforming growth factor beta
Th1	T helper 1 subset
Th2	T helper 2 subset
TIL	Tumour infiltrating lymphocyte
TIM-3	T cell Ig and mucin domain containing protein-3
TNF	Tumour Necrosis Factor
TNFRSF	TNF receptor super family
Tregs	Regulatory T cells
WBC	White blood cell
xeno-GvHD	Xenogeneic Graft versus Host Disease

Chapter 1

Introduction

"Natural forces within us are the true healers of disease"

–Hippocrates–

1.1 Acute lymphoblastic leukaemia

Acute lymphoblastic leukaemia (ALL) is generally classified into B-lymphoblastic and T-lymphoblastic leukaemias, and further subclassified according to specific genetic abnormalities. Within the context of this thesis, I will focus on B-lymphoblastic leukaemias (B-ALL).

B-ALL is seen in both children and adults, but is the commonest childhood cancer, comprising approximately 30% of all childhood malignancies [1]. with a peak incidence between ages 2 and 5 years. The pathogenesis of ALL is believed to be multi-factorial, including exogenous or endogenous exposures, genetic susceptibility, and chance [2]. Predictions of prognosis depend on several factors including initial white blood cell (WBC) count, age, cytogenetic abnormalities, immunologic subtype - including early B cell, mature B cell and T cell lineage - and early response to cytoreductive therapy.

1.1.1 Genetic profile risk stratification

Next generation sequencing and microarray analysis have provided considerable understanding and insights into the pathogenesis and clinical course of ALL. Most ALL genomes contain sequence and structural DNA alterations involving coding genes, as well as alterations of noncoding elements such as noncoding RNAs and

enhancer elements[3]. Chromosomal alterations are characteristic for ALL. Frequencies of distinct genetic profiles and their association with outcome are summarized in table 1.1

1.1.2 Treatment

Current treatment regimens utilise risk based therapy to avoid over- or under-treatment of individual patients and include chemotherapy, radiation therapy and bone marrow transplantation [4], resulting in 5-year event-free survival rates that exceed 85% in children, as illustrated in figure 1.1. However, therapeutic failure leading to relapse has been associated with a poor outcome, and ALL remains the leading cause of cancer-related death in children and young adults [5–7]. The largely non-specific nature of these treatments leads to acute toxic side effects, resulting in severe short- and long term co-morbidities, such as infertility and secondary malignancies, with a 10-year cumulative risk ranging from 3.2% to 9.9% [8]. This underscores the need to further improve survival whilst reducing side-effects.

Table 1.1: **Frequencies and related risk stratification of genetic alterations in paediatric pre-B ALL**

Adapted from Hunger and Mullighan [3]

Subtype	Prevalence %	Comments
Hyperdiploidy with $>$ 50 chromosomes	20-30	Excellent prognosis
Hyperdiploidy with $<$ 44 chromosomes	2-3	Poor prognosis; high frequency of Ras pathway and Ikaros gene family mutations
t(12;21)(p13;q22) translocation encoding ETV6-RUNX1	15-25	Excellent prognosis
t(1;19)(q23;p13) translocation encoding TCF3-PBX1	2-6	Increased incidence in African-Americans; generally excellent prognosis; association with CNS relapse
t(9;22)(q34;q11.2) translocation encoding BCR-ABL1	2-4	Historically poor outcome; improved with addition of tyrosine kinase inhibitors (TKI)
Ph-like ALL	10-15	Multiple kinase-activating lesions; associated with older age, elevated white blood cell count, and IKZF1 alteration; potentially amenable to TKI therapy
t(4;11)(q21;q23) translocation encoding MLL-AF4 fusion	1-2	Common in infant ALL (especially age $<$6 mo); poor prognosis
t(8;14)(q24;q32), t(2;8)(q12;q24), t(2;8)(q12;q24) encoding; MYC rearrangement	2	Favourable prognosis with short-term high-dose chemotherapy
CRLF2 rearrangement (IGH-CRLF2; P2RY8-CRLF2)	5-7	Common in Down syndrome and Ph-like ALL ($\approx$ 50% each); associated with IKZF1 deletion and/or mutation and JAK1/2 mutation and poor prognosis in nonDown syndromeassociated ALL
ERG-dysregulated ALL	$\approx$ 7	Distinct gene expression profile; the majority have focal ERG deletions and favourable outcome despite IKZF1 alterations
PAX5 rearrangement	$\approx$ 2	Multiple partners, commonly from dic(7;9), dic(9;12), and dic(9;20)
iAMP21	$\approx$ 2	Complex structural alterations of chromosome 21; rarely associated with a constitutional Robertsonian translocation rob(15;21)(q10;q10)c; poor prognosis

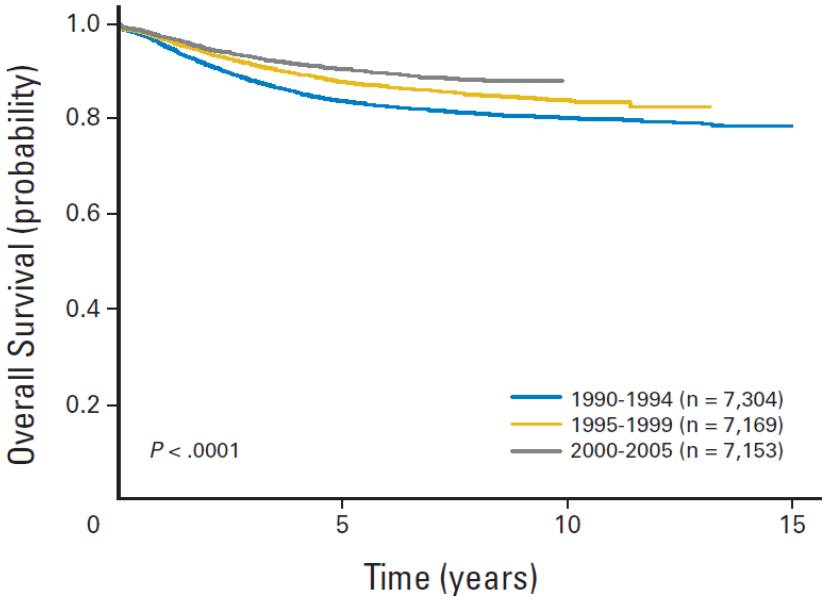

Figure 1.1: **Overall survival probability by treatment era**

Patients enrolled onto Childrens Oncology Group trials in 1990-1994, 1995-1999, and 2000-2005
Source: [9]

1.2 Adaptive immunity: focus on T cells

The human immune system has evolved into a powerful highly sophisticated defence mechanism, equipped with innate and adaptive arms to eliminate a wide variety of pathogens. A fundamental feature of the immune system is its ability to distinguish between structural aspects of a pathogen (non-self) and its host tissue (self), which is carefully confined to limit toxicity to the host. The innate effector cells of the immune system specialise in the recognition of pathogen-associated molecular patterns (PAMPs), that are common on microbes or other host-invading organisms and act rapidly upon encounter of its ligands [10]. The adaptive arm, formed by B and T lymphocytes, is capable of undergoing somatic rearrangements of antigen receptor genes, to generate an extensive repertoire of antigen-binding molecules, which mediate humoral and cellular immune responses.

Random recombinations of gene elements encoding for the T cell receptor (TCR) result in a diverse and polymorphic T-cell repertoire in the thymus. These somatic rearrangements result in an estimated 10^{18} TCRs of two types: $\alpha\beta$ and $\gamma\delta$[11]. Intrathymic selection events then result in a repertoire of peripheral T-cell cells, that are self-MHC restricted and not reactive to self-antigens.

1.2.1 T cell subsets

The majority of peripheral T cells in the circulation express the $\alpha\beta$ TCR on their surface, which is the main population of interest within the context of this thesis. The TCR on the surface of each T cell recognizes its antigenic peptide bound to major histocompatibility complex (MHC) molecules. The co-receptors CD8 and CD4 bind a conserved membrane-proximal region on MHC-I and II respectively [12]. They do not specifically facilitate adhesion and/or binding to MHC as its major function, but rather play an important role in TCR signalling.

$CD8^+$ cytotoxic T lymphocytes are, as their name reflects, capable of killing infected or neoplastic cells. They harness an arsenal of cytotoxins, stored in specialized lytic granules and cytokines, such as Granzyme B, perforin, Tumour Necrosis Factor (TNF), Interferon-γ (IFN-γ), and macrophage inflammatory protein 1β (MIP-1β), resulting in different anti-pathogenic effects.

Helper T lymphocytes, or $CD4^+$ T cells, can be divided into different subsets, Th1, Th2, Th17 and Tfh, all conferring varying levels of protection against different pathogens and employing different helper responses. Specifically Th1 cells, of importance when intracellular pathogens are targeted, activate macrophages and release cytokines that attract macrophages to the site of infection [13].

1.2.2 TCR signalling

In addition to the variable α and β chains, composed of antigen-binding clonotypic heterodimers with a single antigen-binding site, the TCR complex contains different accessory chains. The CD3 complex is made up from CD3 γ, δ, ε and the ζ chain, a largely intracytoplasmic homodimer [13]. These subunits are devoid of kinase activity, but become phosphorylated and induce the assembly of a larger multiprotein complex that is required to diversify the signal for the expression of multiple genes [14]. Following TCR agonist stimulation, Src kinase family member Lck phosphorylates the tyrosine residues of immunoreceptor tyrosine-based activation motifs (ITAMs) exposed on CD3, therein allowing Zap-70 recruitment, inducing the phosphorylation of the adaptor proteins LAT (linker for activation of T cells) and SLP76 (SRC homology 2 (SH2)-domain-containing leukocyte protein of 76 kDa) [14, 15]. This initiates a signalling cascade that leads to $Ca2^+$ mobilization as well as to the activation of the mitogen-activated protein kinase (MAPK) signalling pathway.

The magnitude of ITAM phosphorylation depends on the half-life of the TCR/peptide MHC-complex (pMHC) interaction [16] and the presence of activated Lck [14]. By delivering and sequestering Lck into the TCR-pMHC interaction, CD4 and CD8 co-receptors optimize TCR signalling [15]. Lck must be anchored to glycolipid-enriched membrane microdomains (GEMs) and its activity is regulated by different elements including CD45, a transmembrane protein tyrosine phosphatase (PTP), regulating Lck independently of TCR engagement [14].

Cytoskeleton organization is tightly integrated with T cell activation and signalling. When T cells recognize APCs, the immunological synapse (IS) is formed. The IS is the spatial frame of the TCR engaging with MHC and multiple accessory molecules, promotes sustained T cell-APC interactions and serves as a platform

for exchange of information between the two cells [17]. The adhesion and signal transduction depend on physical forces exerted by actin cytoskeletal dynamics. IS-associated signalling molecules are physically linked to actin filaments. Conformational changes exerted by these forces are needed for full T cell activation [18].

1.2.3 T cell receptor affinity

The binding and interaction of the TCR to a specific pMHC complex is pivotal in regulating the activity and specificity of the T cell, setting off a cascade of intracellular signals leading to cytokine production, proliferation and release of cytotoxic granules. The extent of TCR mediated signal transduction in individual T cells (lasting for circa a few hours) and the duration of TCR/pMHC binding half-lives (lasting a few seconds) are critical parameters in T cell activation [19]. The binding kinetics of TCRs to pMHC complexes are determined by the association rate, on-rate, the dissociation rate, off-rate, and their derivative, the dissociation constant (K_D) that is reciprocally related to the affinity of binding [20].

Affinity is a measure of the strength of the monomeric reversible binding between an epitope and an antibody's antigen binding site or the TCR/pMHC complex. High affinity antibodies will bind a greater amount of antigen in a shorter period of time. The avidity is a measure of the overall strength, which is dependent on the affinity, the structural arrangement and the valency of both the antibody and the antigen. Viewed from the perspective of the TCR/pMHC, expression levels of the antigen and TCR, and interactions of MHC with co-receptors CD4 or CD8 also play a role. Interaction between the CD8 or CD4 co-receptor and MHC class I or II stabilises T cell receptor-antigen complexes at the cell surface. Functional T cell avidity is considered as the ability of T cells to respond to a given concentration of cognate peptide antigen [21].

Both K_D, the off-rate specifically, and the density of the target peptide presented on MHC influence T cell activation. TCR agonists for mature T cells are of relatively low affinity (1-10 μM) and have fast off-rates [14]. The half-lives of the interactions between a TCR and foreign-pMHC agonists are characteristically

2-10 seconds [20]. T cells display an extraordinary sensitivity to low density antigen. The sensitivity and polyfunctionality of T cells are controlled by TCR affinity, where there is a threshold above which a higher affinity does not lead to a better T cell function and very high affinity TCRs show cross-reactivity with self-derived peptides [22]. These finding showed to be consistent among studies of various groups. Irving *et al* observed that there were maximal T cell responses at lower affinities, with a plateau of functional output between 1 μM and 5 μM [23]. Reducing the TCR affinity further however, has been demonstrated to affect different parameters of T cell activation such as the phosphorylation of CD3ζ, the activation of the MAP kinase pathways and the ability to recruit cytotoxic granules [16, 24, 25]. A positive association has been described between TCR affinity and the degree of polyfunctionality for $CD8^+$ T cells within the earlier described window of TCR affinity, which allows improved recognition of a tumour associated epitope in the absence of apparent cross reactivity with other self-derived pMHC molecules [22]. Thus, within natural TCR responses, lower affinity in the setting of similar receptor and antigen expression would be expected to result in lower functional avidity and therefore reduced antigen-specific responses.

1.2.4 T cell activation

1.2.4.1 The 2-signal model of activation

The 2-signal model of T cell activation, distinguishes between the interaction between the TCR and the co-receptors with the pMHC complex, known as signal 1, and secondary co-stimulation by antigen presenting cells (APCs), known as signal 2. As mentioned earlier, signal 1 leads to CD3 and ζ-chain ITAMs phosphorylation by active Lck, resulting in the recruitment of Zap-70 that subsequently phosphorylates the key adapter protein linker for activation of T cells (LAT), leading to the recruitment of downstream signalling proteins[27].

Signal 1 alone is not sufficient to activate a T cell and, when delivered solely, could result in anergy [26]. For activation and proliferation to occur signal costimulation is required, as provided by the 2 main receptor families; 1) the CD28 family, including CD28, ICOS, interacting with CD80/CD86 and B7-H2, and 2) the TNF

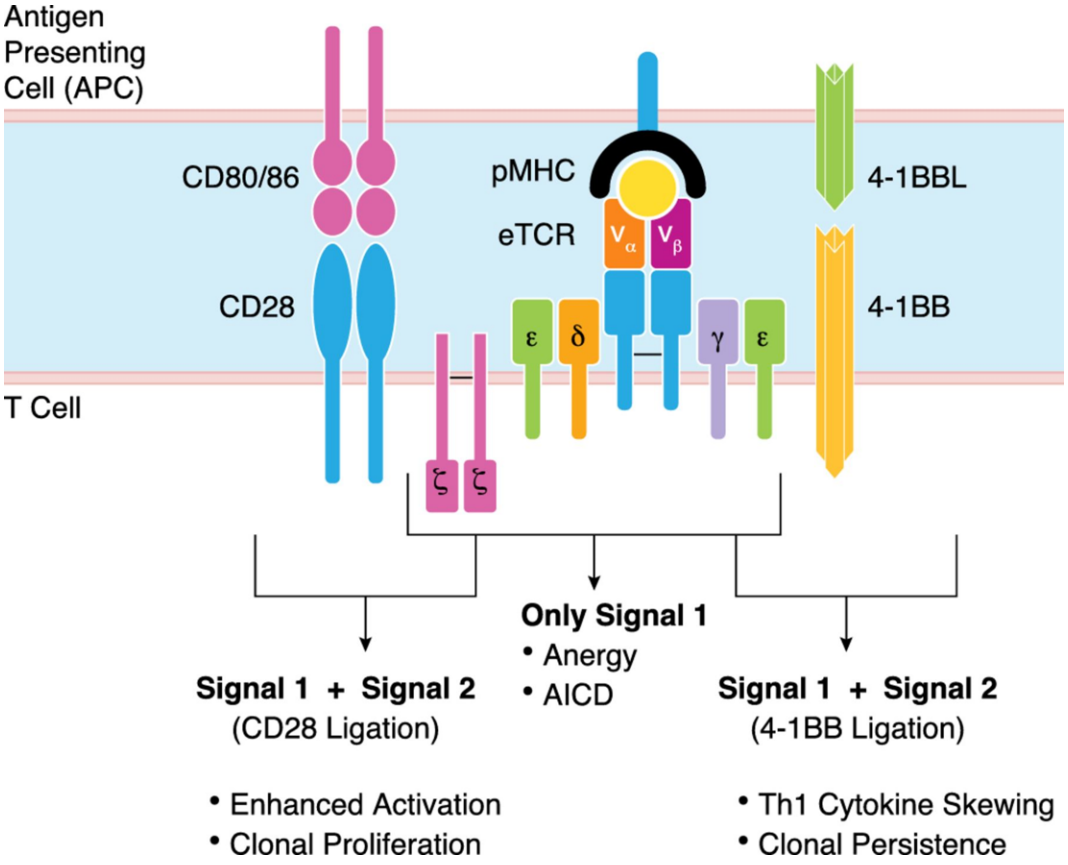

Figure 1.2: **The 2-signal model of T cell activation**

Source: [26]

Receptor Super Family (TNFRSF), including 4-1BB, CD27, CD40 and OX40, interacting with 4-1BBL, CD70 (CD27L), CD40L and OX40L on antigen presenting cells. These costimulatory signals have varying effects on T cell behaviour, such as survival, effector function and formation of memory [26], as shown in figure 1.2. CD28 is thought to be of particular importance in early activation of naive T cells, whereas the TNFRSF associated co-stimulatory domains are fundamental for memory formation and persistence.

1.2.4.2 Kinetic models of T cell activation

The mechanisms underlying TCR sensitivity and specificity are not yet fully understood. There are several models proposed to interpret how T cell signal amplification takes place, following binding between TCR and pMHC. With a relatively low affinity and generally a quick off-rate, T cells remain highly sensitive and specific to an antigen [28].

Kinetic Proofreading Model

The kinetic proofreading model proposes a signal is not immediately generated when a ligand binds to its receptor that utilizes a tyrosine kinase in signalling. Binding of pMHC to TCR induces a series of biochemical reactions in the T cell. If pMHC dissociates when these reactions are complete, the T cell receives a positive activation signal. However, dissociation of pMHC following completion of the first reaction but prior to generation of the final products results in partial T cell activation, which acts to suppress a positive response [29]. Short-lived nonspecific complexes should usually fail to signal before dissociating [30]. However, experimental evidence from Thomas *et al* contradicts this model, by exploring in detail how TCR affinities spanning the natural range and extending 700-fold into the supraphysiological range affected the kinetics and the sensitivity of primary human $CD8^+$ T cell responses. The functional analysis revealed that affinity maturation beyond the physiological range accelerates $CD8^+$ responses, but disrupts the serial triggering that is needed to maximize recognition of low-density peptide ligands. They showed that optimal peptide sensitivity was achieved with $t_{1/2}$ of 9.3 seconds, and that increasing the dissociation half time to 348, 1320, and 3120 seconds resulted in a progressive loss of peptide sensitivity [31, 32]. Kalergis *et al.* show that T cell activation can be impaired by mutations that either decrease or increase the binding half-life of the TCR-pMHC interaction. Their data indicate that efficient T cell activation occurs within an optimal dwell-time range of TCR-pMHC interaction[33]. These studies both suggest that simply increasing immunoreceptor interaction time does not result in a linear increase in T cell activation and suggesting a more complex relationship between these parameters.

Serial triggering model

The serial triggering model was proposed as an alternative, suggesting there is sequential binding of TCRs by a single pMHC, consistent with the short-lived nature of the majority of TCR/pMHC interactions, thereby rendering T cells sensitive for very low level of antigen [34]. However, it should be noted that this model was based not on visualisation of TCR/pMHC interactions, but on the conjectural con-

sequence, namely TCR down-regulation, as a read out of TCR occupancy. A more recent study suggests, by using a single-molecule imaging technique, that even a single-agonist pMHC can trigger cytokine production from some naive T cells [35].

Different studies elucidate the high sensitivity of T cells to antigenic stimulation, as well as the importance of sustained signalling for T cell activation [28]. Figure 1.3 shows there is a defined window of half-life of TCR-ligand interactions and number of TCRs engaged. While very short half-lives prevent productive TCR triggering, half-lives exceeding the optimum interaction time decrease the efficiency of TCR serial engagement. An interesting systematic analysis of T cell responses by Lever *et al.* concluded that a peak amplitude of bell-shaped dose-response is independent of affinity, but that a low to intermediate affinity ligand produces largest response at low doses pMHC [36].

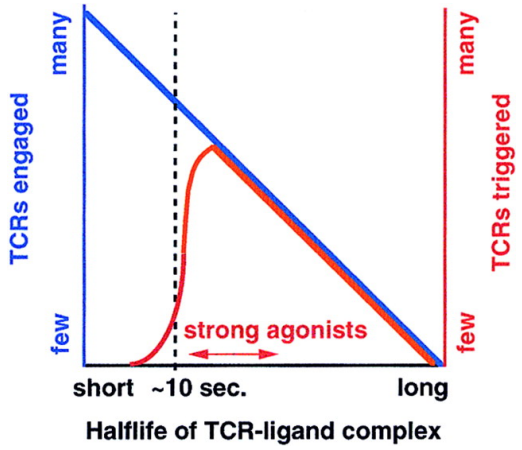

Figure 1.3: **A kinetic window defines strong TCR agonists**

Source: [37]

1.2.5 Cancer immunoediting

"It is by no means inconceivable that small accumulations of tumour cells may develop and because of their possession of new antigenic potentialities provoke an effective immunological reaction, with regression of the tumour and no clinical hint of its existence." In 1957 Sir Macfarlane Burnet instigated the concept that is now known as cancer immunoediting [38].

Several decades following have taught us there are different aspects in which the immune system plays a role in cancer biology. The importance of T cells in immune surveillance has been demonstrated by an abundance of studies demonstrating an improved survival of patients with a higher number tumour infiltrating lymphocytes in solid tumours such as Non-Small Cell Lung Cancer, Breast Cancer, Squamous Cell Carcinomas, Melanoma, and Brain Tumours [39–44], as well as the increased incidence of tumours (particularly EBV associated lymphomas), in patients with primary immunodeficiency and those who are immunosuppressed after organ transplant [45].

A study by Matsushita *et al.* showed that, by using a genomic approach, there is a T cell dependent immunoselection process, leading to preferential outgrowth of clones lacking immunodominant rejection antigens [46]. The clinical relevance of these findings has been underlined by a study, showing that immunoediting occurs as a consequence of immunotherapy in melanoma patients, revealing that in the majority of patients that had relapsed, there was a loss of antigen that was initially targeted [47, 48].

The cancer immunoediting hypothesis is hotly debated and has set out the principles for understanding both the tumour directed response of the immune system as well as its tumour sculpting actions [49]. Many labs have unambiguously shown that immunity can induce cellular transformation, but also prevent or control tumour growth and influence the immunogeneicity of the tumours [49]. These paradoxical roles are determined by their temporal occurrence relative to tumour formation, the different effectors of immunity involved, the transformational process and the tumour associated antigens expressed on the transformed cell. The tumour immu-

noediting hypothesis is composed of three phases; Elimination, Equilibrium and Escape.

Elimination

In the elimination phase, the balance is towards anti-tumour immunity. Both the innate and adaptive arms of the immune system together partake in the detection and destruction of early tumour development, as shown in figure 1.4 [50].

Equilibrium

In the Equilibrium phase, the tumour is held in a state of dormancy. Genetic and epigenetic changes result in tumour cell variants that exhibit antigen loss or persistent tolerogenic antigen, and are therefore more resistant to immune recognition, or the induction of immunosuppression by the expression of PD-L1 for example [50].

Escape

In the Escape phase, clinical disease becomes apparent after the immune system has failed to restrict tumour growth, through many different mechanisms. Immune recognition is evaded by the tumour cells (by mechanisms such as the absence of strong tumour antigens, or loss of MHC class I, class I-like, or co-stimulatory molecules), tumour cells now express molecules of increased resistance (STAT-3), survival (Bcl-2) and immunosuppression (PD-L1 for example) and the tumour microenvironment facilitates tumour growth by the expression of immunoregulatory molecules and the secretion of immunosuppressive cytokines (IL-10, TGF-β). T cells including regulatory T cells (Tregs) may also upregulate inhibitory receptors such as PD-1, CTLA-4, TIM-3 and LAG-3 that suppresses anti-tumour immune responses and favour tumour outgrowth [50].

The aim of cancer immunotherapy is to tip this balance towards the favourable elimination phase, by employing the patient's own immune system and re-eliciting the anti-tumour response.

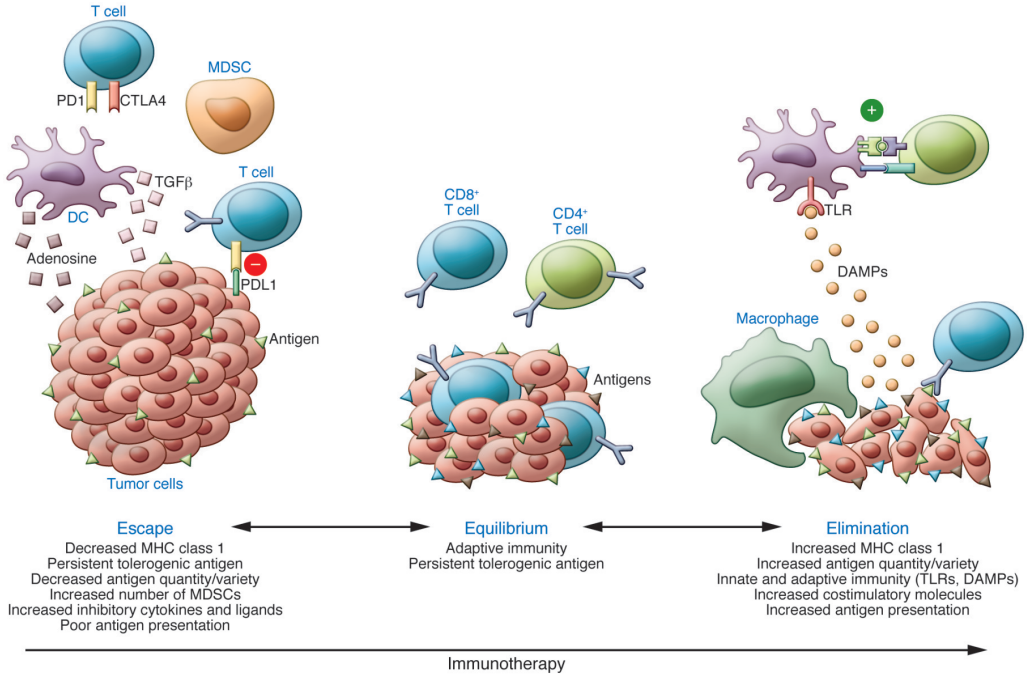

Figure 1.4: **Cancer immunoediting**

In the immunoediting hypothesis, the tumour immune system balance shifts among tumour escape (to mutation-specific antigens), equilibrium, and elimination.
Source: [50]

1.3 Adoptive T cell therapy

As far back as the late 19th century, William B. Coley discovered that when tumours were infected with a bacteria they shrank. Apparently, activation of the immune system, caused by the infection, had a favourable outcome on the tumour. Coley's idea, far ahead of his time, lies at the basis of modern immunotherapy; targeted tumour cell killing by use of the immune system's cytotoxic mechanisms. Both humoral and cellular components of the immune system are employed to enhance the anti-tumour response, however only the latter will be discussed further. By isolating and expanding tumour reactive T cells *ex vivo* before infusing them back into a patient - known as adoptive T cell therapy (ACT) - one seeks to enhance antitumour immunity by passive transfer.

ACT has several advantageous properties that make it effective for cancer therapy: 1) The specificity of the T cell response allows potential differentiation between healthy and cancerous cells; 2) Following specific activation there is a robust clonal expansion; 3) T cells are able to traffic to different sites where the antigen of interest is expressed, and are thereby able to potentially target both the primary tumour as well as metastases; 4) T cells are capable of a so called recall response by antigen-specific memory T cells, resulting in ongoing tumour surveillance.

The adoptive T cell therapy field first started with using non-gene modified T cells for the treatment of viral and non-viral malignancies. Several reports in the early nineties described that by transfer of antigen-specific T cell clones reactivation of CMV or EBV after haematopoietic stem cell transplantation (HSCT) was prevented [51, 52]. Shortly thereafter, different groups started reporting about adoptive T cell therapy in a non-viral malignant setting, demonstrating that tumour infiltrating lymphocytes could mediate tumour regression in melanoma patients [53] and that donor lymphocytes could successfully be applied as a treatment for chronic myelogenous leukaemia relapsing after stem cell transplant [54].

One of the earliest reports of a T cell receptor (TCR) gene transfer using gamma retroviral vector transduction described the introduction of a tumour associated antigen (TAA) specific TCR targeting MART-1 [55]. TCR gene transfer since

then has been intensively studied and modification in the TCR α and β chain sequences and the introduction of a disulfide bond linking the constant domains have reduced the risk of mispairing, which has proven to result in a lethal autoimmune reaction in mice [56]. Most effective in avoiding mispairing has been the concomitant knockdown of expression of the endogenous TCR by gene editing. TCR gene transfer endows specificity against tumour associated antigens that can be derived from the entire protein composition of tumour cells, including intracellular proteins as well as specific mutant proteins that are restricted to tumour cells [57]. However, there is a requirement for HLA-matching, owing to the restricted nature of TCR function.

Investigating the modularity of the TCR structure, Eshhar *et al.* developed a method where they coupled a single chain variable fragment (scFv) of an antibody to CD3ζ of the TCR [58]. Initially this method was named a T-body, after the combination of an antibody with the T cell activation. Since then the generally used term is Chimeric Antigen Receptor (CAR).

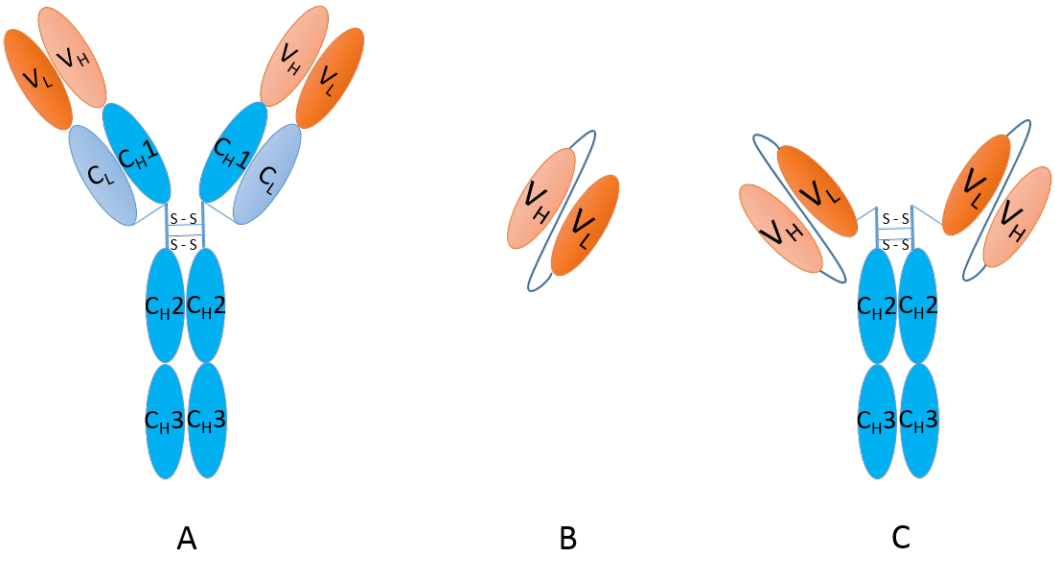

Figure 1.5: **Antibody structure and derived scFv**

A. Full length IgG (˜150 kDa) B. scFv fragment (˜30 kDa) C.scFv-Fc (˜105 kDa)

.

1.3.1 Chimeric Antigen Receptors

An scFv is an engineered antibody consisting of the immunoglobulin light chain variable region (V_L) and the heavy chain variable region (V_H) linked by a peptide linker sequence into a single polypeptide chain, retaining its specificity and affinity, as illustrated in figure 1.5. A CAR is a recombinant receptor construct that combines an scFv against a tumour-associated antigen and an intracellular activation domain of the TCR (Fig.1.6). These receptors are capable of recognizing intact membrane proteins irrespective of HLA restriction or antigen processing so that, in contrast to natural TCRs, CARs do not need to be matched to the patient's tissue type and a single CAR can be used to target all patients. Upon binding of their ligand CAR transduced T cells are then activated in a way very similar to that of the endogenous TCR. As most tumour-associated targets are self-antigens that are also expressed in normal tissues, a major advance in adoptive T cell therapy is the ability to efficiently endow patients T cells with reactivity for tumour antigens through the adoptive transfer of CAR expressing T cells [59, 60]. In table 1.2 a direct comparison of TCR engineered versus CAR T cell therapy is explained. The design of CARs and their structural evolution will be discussed in more detail in section 1.3.3, prompting the research aims of this PhD project.

T cell receptor genes	**Chimeric Antigen Receptors**
Targets processed intra- & extracellular peptide antigens	Restricted to antigens expressed on cell surface
Requires HLA matching	HLA independent antigen recognition
Triggers through the signal transduction machinery used by the native TCR	Signal amplification derived by synthetic biology
Subject to the same counter-regulatory circuits that physiologically downregulate TCR signaling	Possible tonic signaling, leading to unrestrained cellular activation that results in apoptosis
Low affinity interaction	Antibody mediated high affinity interaction
Risk of TCR mispairing	No mispairing

Table 1.2: **Gene-engineered T cells for cancer therapy**

Chimeric antigen receptor (CAR) compared to the T-cell receptor (TCR)

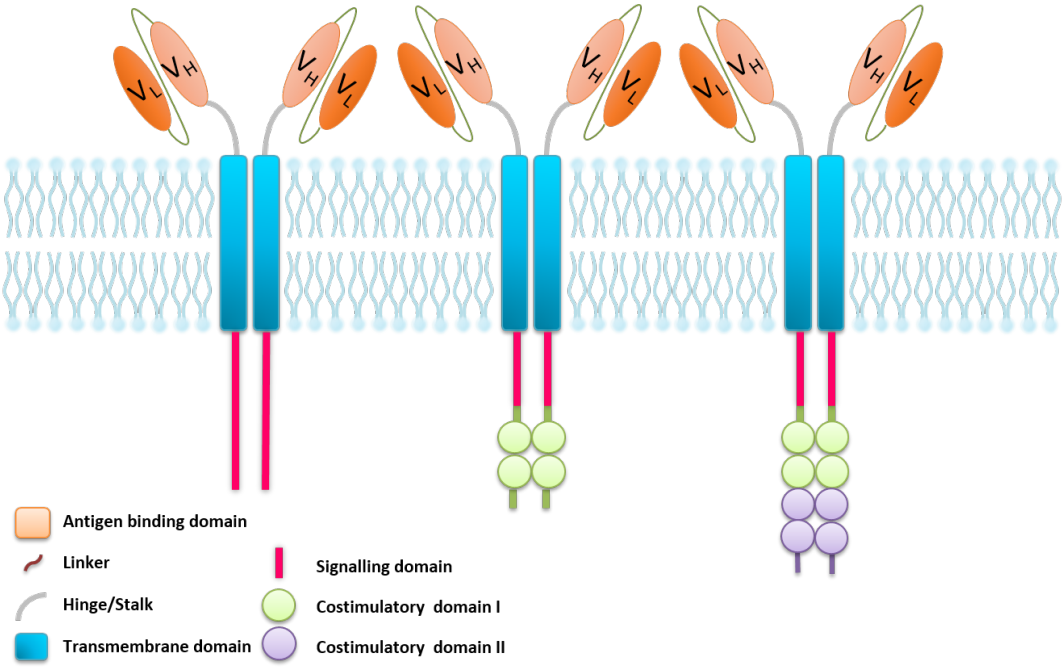

Figure 1.6: **Evolution of Chimeric Antigen Receptors.**

Schematic representation of 1st, 2nd and 3rd generation CARs

1.3.1.1 Genetic modification of primary T cells

Effective genetic modification of T cells requires methods that facilitate adequate gene delivery and adequate expression of functional transgenes [61]. The level and duration of expression depend on the function required, but in general when sustained expression is required in highly proliferative T cells, efficient integration of the vector system and sufficient expression levels are needful.

Viruses are obligate intracellular parasites. Members of the Retroviridae family, including γ-retroviruses and lentiviruses, are able to retrotranscribe their RNA genome into a cDNA copy, which is then stably integrated into the host cell genome. Following reports of the occurrence of severe adverse events related to the mutagenic side effects of retroviral insertion in stem cells [62–64], the potential genotoxicity of clinical vectors was significantly reduced following the development of U3-deleted SIN vectors, the use of cellular promoters rather than viral promoter elements and the switch to lentiviral integration. Lentiviral gene delivery utilizes viral replication to provide integration of a desired gene, allowing a stable integration at sites distant from transcriptional start sites which is inherited and expressed over clonally expanding and persisting T cells. Key for lentiviral vectors is the production of self-inactivating particles, allowing for delivery of the desired sequence whilst reducing the potential recombination with other retroviruses or retrovirus-like elements that could reconstitute an infectious HIV-like retrovirus[65, 66], T cell activation or proliferation is not absolutely required for genomic integration.

Lentivectors have been steadily improved over time to increase both their efficiency and biosafety. In the second generation lentivectors, the packaging plasmid encodes gag-pol, rev and tat, but lacks the rest of viral accessory genes (vif, vpr, vpu, nef) [65]. Production of infectious virus-like particles carrying the genome of interest is accomplished by co-transfecting the plasmid encoding the principally defective virus genome (transfer vector) with the plasmids that encode the structural genes (packaging plasmid) and an envelope glycoprotein (envelope plasmid). Figure 1.7 shows a schematic representation of the three plasmids forming the second generation lentivector system. The packaging and the envelope plasmids contain

a CMV promoter, which controls the expression of HIV-1 proteins. In this figure the transfer vector contains an expression cassette, made of an internal promoter of choice controlling the expression of the gene of interest. The packaging signal is represented as Ψ and the rev response element as RRE.

Both γ-retroviral and lentiviruses have been used in clinical trials of gene-engineered mature T cells, as shown in table 1.3. To date, no case of insertional mutagenesis has been reported in either, with a follow up of more than 500 patient years [67]. CAR gene transfer in this project was achieved using a lentiviral vector, for its stable integration and safety. However one should take in mind the disadvantages of this method, such as the difficulty of generating of a stable producer cell line and the resulting costs of this laborious process to produce the vector on a large scale.

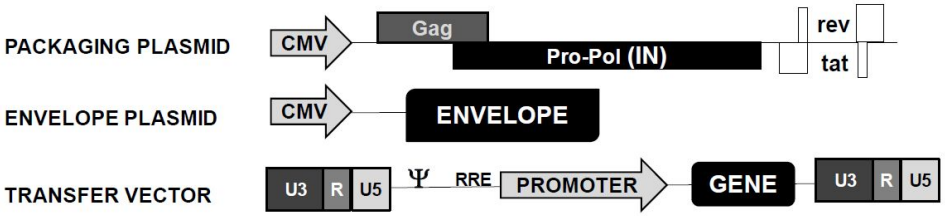

Figure 1.7: **Engineering of lentivector system**

Adapted from Liechtenstein *et al.* [65].

There are other (non-) viral methods exploited such as Clustered Regularly Interspaced Short Palindromic Repeats (CRISPR)-CRISPR associated protein 9 (Cas9) system using electroporation or lipid based transfection for genome editing and efficient sequence-specific interventions. CRISPR-Cas9 technology, originates from bacteria and provide them with adaptive immunity against viruses and plasmids by using CRISPR RNAs (crRNAs) to guide the silencing of invading nucleic acids by introducing double-stranded (ds) breaks in target DNA [68]. The most commonly used type is CRISPR/Cas9 including a conjugation of the tracrRNA (trans-activating crRNA)-crRNA complex to a single guide RNA and Cas9. This same mechanism can be used to introduce site-specific therapeutic genes by the use of synthetic crRNA/tracrRNA structures, but these still entail a risk of in-

sertional mutagenesis and they share many of the same safety concerns as retroviral approaches such as toxicity or immunogenicity of the transgene and delivery modality [32, 69].

In a recent publication from the Sadelain lab it was shown that targeting a CD19-specific CAR coding sequence to the TCR α constant (TRAC) locus, placing it under the control of endogenous regulatory elements by the use of the CRISPR/Cas9 system, not only results in uniform CAR expression in human peripheral blood T cells, but also enhances T cell potency, averting tonic signaling and establishing effective internalization and re-expression of the CAR following repeated exposure to antigen [70]. They designed a guide RNA, to disrupt the TRAC locus and place the CD19-specific 1928z CAR under its transcriptional control. Approximately 95% of CAR^+ cells were TCR-negative, validating the 2-in-1 TCR-knockout and CAR-knock-in strategy [70]. Another application of CRISPR/Cas9 in CD19 CAR therapy has been described in a study where PD-1 deficient CD19 CAR T cells were generated, to reduce CAR T cell exhaustion as a result of high levels of PD-L1 expression on tumour cells [71]. PD-1 disruption augmented CAR T cell mediated killing of tumour cells *in vitro* and enhanced clearance of $PD\text{-}L1^+$ tumour xenografts *in vivo*. Both these studies demonstrate improved therapeutic efficacy of Cas9-edited CAR T cells and highlight the potential of precision genome engineering to enhance next-generation cell therapies.

1.3.2 CAR T cell therapy for cancer

The first publications of clinical trials using CAR technology were published in 2006 [72, 73], followed by series of successive publications that gave great insights [74–79]. Successful B cell tumour eradication was obtained with different CD19 CARs [80–82], and multiple early-phase clinical trials with CAR-modified T-cells, targeting the CD19 molecule, have shown unprecedented responses in the United States, even in patients with chemorefractory and relapsed disease. The largest studies of patients with B-ALL treated with CD19-CAR therapy in the United States and Europe, are summarized in table 1.3 [83–86]. Similar clinical studies are under way in different European countries, with the majority to be conducted in the United Kingdom. Clinical evaluation of CD19 CAT-CAR is being undertaken in the CARPALL trial (clinicaltrials.gov, NCT02443831), in which we aim to specifically study disease response in relation to T cell persistence and T cell fitness.

A number of different groups have attempted to extend the successful findings in the CD19-field to patients with solid tumours, but the clinical efficacy unfortunately has been modest. One of the targets overexpressed in many different types of cancer, and therefore prioritised as a potential immunotherapy target, was human epidermal growth factor receptor 2 (HER2) [91]. Although efficacy was reported in very preliminary studies [92], in a patient, treated for metastasised colon cancer with a HER2-targeted CAR, severe dyspnea was observed followed by hypoxia, pulmonary infiltrates and severe cytokine release syndrome (CRS), and the patient succumbed most likely due to recognition of low levels of HER2 on lung epithelial cells, ultimately leading to multi-organ failure [93].

Other targets such as mesothelin, GD2, CD123, MUC16 and others are being tested both in a pre-clinical as well as a clinical setting, but are outside of the scope of this thesis.

Table 1.3: CAR T cell design and production and clinical aspects of largest clinical trials to date investigating CD19-targeted CAR T cells in the treatment of B-ALL, table adapted from Geyer & Brentjens [7]

Institution (reference)	No. of patients	Gene transfer method	scFv	Co-stimulatory domain	Median age (range), y	Disease-related outcomes
CHOP [86]	30 (25 children, 5 adults)	Lentivirus	FMC63	4-1BB	Paediatric ALL: 11 (5-22) Adult ALL: 57 (36-60)	CR: 90% (MRD-negative in 88% of those who achieved CR) 6-month EFS: 67% 6-month OS: 78%
NCI [86]	20	γ Retrovirus	FMC63	CD28	Paediatric ALL: 15 (5-27)	CR: 70% (MRD-negative in 60% of those who achieved CR) OS: 52% at 7.8 months LFS: 79% at 4.8 months 10 of 12 in MRD-negative CR underwent AlloHSCT
NCI [85]	5	γ Retrovirus	FMC63	CD28	Adult ALL	CR: 80% (4/5, all MRD-negative)
MSKCC [83, 87]	51	γ Retrovirus	SJ25C1	CD28	Adult ALL: (22-74)	CR: 82% (MRD-negative in 85% of those who achieved CR) Sixteen of 41 in CR underwent AlloHSCT Median OS: 9 months (in patients with morphologic disease at CAR T cell infusion), not reached (in patients with minimal disease at CAR T-cell infusion)
Fred Hutchinson Cancer Research Center [88]	30	Lentivirus	FMC63	4-1BB	Adult ALL: 40 (20-73)	CR: 10/12 among patients receiving Cy monotherapy 16/17 among patients receiving Flu/Cy
UPenn [89]	27	Lentivirus	FMC63	4-1BB	Adult ALL: 44 (21-72)	CR: 15/27 (across all cohorts)
Multi centre European Study [90]	11	Lentivirus	FMC63	none	Paediatric ALL: 44 (21-72)	Studied use of donor Epstein Barr virus-specific T-cells, relying on the endogenous TCR for proliferation. At median follow-up of 12 months, 10 of 11 patients had relapsed, 2 are alive with disease and 1 alive in CR 3 years.

1.3.2.1 CD19 as tumour associated antigen

Tumour associated antigens (TAAs) are self-antigens which are expressed on healthy tissue but are aberrantly expressed on tumours. CD19 is a 95-kDa transmembrane glycoprotein of the immunoglobulin superfamily containing two extracellular immunoglobulin-like domains and an extensive cytoplasmic tail [94]. Its expression is restricted to lymphocytes of the B-cell lineage and is part of the B cell receptor co-complex. In the bone marrow, CD19 amplifies pre-B cell receptor signalling, inducing the proliferation and differentiation of late pro-B cells. The CD19 pathway in healthy and neoplastic B-lineage cells results in the activation of growth-promoting kinases, via interactions with the CD19 cytoplasmic tail[95].

The density of CD19 on the cell surface is accurately regulated at all stages of maturation and is gradually lost during terminal differentiation to plasma cells. CD19 is not expressed on cells of any other lineage, nor is it expressed on non-haematopoietic cells. The expression of CD19 at normal to high levels, by the vast majority ($>95\%$) of non-Hodgkins lymphomas and B-lineage acute lymphoblastic leukaemia, renders this molecule an attractive target for adoptive T cell therapy, enabling targeting of malignant cells without toxicity to the non-haematopoietic tissue [96].

Although it has been described that the extracellular domains are needed for mature B-cell function, the role of these ectodomains in the proliferation and differentiation of normal B-lineage precursors is unknown, and its role in B-cell neoplasm is not yet understood [95]. Despite the promising clinical responses of relapsed/refractory (r/r) B-ALL patients to CD19-CAR T cell therapies, a significant number of patients still relapses. An interim report on the efficacy and safety of CTL019 in the first US phase II multicenter trial in paediatric r/r ALL stated an overall response rate (ORR) of 90%, only a relapse free survival after 6 months of 66.4%, indicating that about one third of the patients relapses within a short period of time after infusion of the CAR T cells [97]. In this context there are two types of relapses recognized on the basis of their phenotype: 1) CD19+ relapse: these relapses are typically linked to poor T cell function or persistence; 2) CD19-ve re-

lapses resulting from selection of antigen negative variants that can evade tumour surveillance by CD19-CAR T cells. Recent publications have estimated that CD19 epitope loss takes place in 10% to 20% of paediatric B-ALL treated with CD19-directed immunotherapy [86], leading to discussions regarding its importance in neoplastic growth. CD19-ve relapses are observed in B-ALL patients treated with different CAR products, independently of the construct (different costimulation domains) and expansion/clinical protocol [98].

Sotillo *et al's* publication described, for the first time, the characteristics of both CD19 positive and CD19 negative relapsed patient's samples. They characterized those samples, performing whole-exome sequencing and RNA sequencing. Firstly, any increase or changes in methylation of CD19 promoter or enhancer elements were ruled out, which could have potentially led to gene silencing. PAX5, which is the regulator of CD19 transcription was also not downregulated, as shown by qRT-PCR. Interestingly however, *de novo* genomic alterations found to primarily affect exon 2, leading to a N-terminal truncated CD19 Δex2 isoform were seen. These genomic alterations consisted of clustering of nonsense and missense mutations, that in contrast to distributed frameshift mutations did not lead to complete CD19 loss or changes in signalling, required for leukaemic maintenance. This isoform was predominantly located in the cytosol. A novel combinatorial mechanism was identified, by which the CD19 protein was partly conserved by removing the cognate epitope on the cell surface. It has not been clarified yet, whether these mutations are de novo mutations, resulting from actively redirecting the splicing machinery, or whether there is a selective advantage of pre-existing CD19 Δex2 isoform clones.

It has also been demonstrated by Jacoby *et al.*, that persistent CD19 CAR pressure can also lead to lineage switching of the malignant clone as a mechanism of CAR resistance [99]. This lineage switching, determined by the cells inherent lineage plasticity, is a result of reprogramming induced by elimination of the B-cell transcription factors, resulting in complete loss of B-cell developmental pathways.

1.3.2.2 Toxicities of CAR T cells in patients with ALL

Although the summarized studies differ in their CAR design, production protocols and CAR T cell dose, as well as the patient's baseline characteristics, disease burden and prior lymphodepleting chemotherapy, all observed strikingly similar toxicities, relating to cytokine release, neurologic toxicities and off-tumour on-target related B cell aplasia.

Cytokine Release Syndrome

Cytokine Release Syndrome (CRS) is the most common severe toxicity seen after CAR T cell treatment, with potentially fatal outcome [100]. It is characterised by a systemic inflammatory response, that becomes apparent hours to days following CAR T cell infusion. There is a marked increase in pro-inflammatory cytokines, related to T cell activation and expansion (sIL-2Rα, IFN-γ) and activated monocytes/macrophages (IL6, IL10, MIP1β). Clinical features include fevers, myalgias, malaise and, in more severe cases, a capillary leak syndrome associated with hypotension, hypoxia and occasionally renal dysfunction and coagulopathy [7].

Published research suggests that there is a correlation between the occurrence of CRS and clinical outcome, however no strong correlation was found between the degree of CRS and outcome [83, 85, 86]. Recent work of Teachey *et al.*, identifying predictive biomarkers for CRS, conclude that, although there seems to be a correlation between disease burden and CRS severity [83, 86], this alone is not sufficient to predict CRS severity.

When evaluating standard clinical laboratory tests to predict CRS severity, none of the following markers were informative, as they all peaked after patients became ill: ferritin, CRP, LDH, ASAT, ALAT, BUN and Cr. An increase in soluble IL-6-Receptor (Sgp130) and IFN-γ however, was strongly associated with the development of CRS.

The cornerstone treatment of CRS is IL-6 directed therapy. Tocilizumab, an IL-6R inhibitor, has shown to be effective in quickly reducing and resolving the clinical symptoms of CRS, without seemingly affecting the efficacy of the CAR T cells [83, 85, 86].

Additional variables not studied by Geyer *et al.* that may predict severe CRS include T cell phenotype of the product, T cell function of the product, CD19 polymorphisms that may differentially activate CTL019, tumour expression of CD19 or PD-L1, and immune gene polymorphisms [7].

Neurologic toxicities

A broad spectrum of neurological symptoms has been reported, following CAR T cell infusion, occurring apparently independent of CRS. The majority were reversible and self-limiting, and included delirium, encephalopathy, hallucinations, seizures, confusion, aphasia or word-finding difficulties [83]. In adults with ALL, a number of deaths from cerebral oedema has recently led to the cessation of Juno JCART15 programme. The mechanism for neurotoxicity is at present unclear. Interestingly, in all patients reported to show neurological symptoms, CARs were present in their cerebrospinal fluid (CSF). There is no concordance on the diagnostic value of imaging by either CT or MRI, as conflicting results were seen between the UPenn/CHOP cohort and the NCI trial, but it is considered informative to exclude important differential diagnoses.

B-cell aplasia

B cell aplasia is an expected ”on-target, off-tumour” toxicity and considered tolerable. Chronic B cell aplasia can lead to hypogammaglobulinaemia which can effectively be managed by the infusion of replacement therapy gamma-globulins. As CAR T cells target CD19, a part of the B cell receptor complex, both leukaemic and healthy B lymphocytes are eradicated. It serves as quite a useful marker for CAR T cell persistence and functionality.

1.3.3 Evolution of CARs

The general structure of CARs consists of four elements, the antigen binding domain, the hinge or spacer region, the transmembrane domain and the intracellular domain. CAR design has progressed through different generations, via a largely empiric process, to improve its signalling output. The first-generation CAR did not have costimulatory elements incorporated, that later proved to be needed for full T cell activation. Although these CAR T cells were able to generate a cytotoxic response in murine models [101], the clinical outcome of these first generation CARs were disappointing [74, 90]. The subsequent second and third generation CARs contained either one or two costimulatory domains[102–104], as illustrated in figure 1.6. Details and function of the different elements are discussed below.

1.3.3.1 Activation domain

In physiological T cell activation the TCR co-localizes with CD3 - composed of dimers comprising four subunits ζ, δ, ε, γ - which then initiates the first TCR signal. In CARs CD3ζ alone proved to be sufficient to induce signals with similar potency to the normal TCR/CD3 signalling and was chosen as the preferred moiety for CAR signalling [105]. For effective activation however, naive T cells depend upon more than one stimulus. Although the presentation and engagement of a peptide in the context of HLA is essential for the onset of the activation pathway through the TCR, without costimulatory signals the ligation of the TCR alone is insufficient and results in hyporesponsiveness [106]. An early study in which naive/resting T cells of transgenic were transduced with an scFv and TCR ζ -chain confirmed this two-signal hypothesis by demonstrating insufficient proliferative and cytotoxic responses after triggering of the scFvCD3ζ protein [107]. The CD28 signalling domain was first introduced as a costimulatory moiety. After incorporating both the primary and costimulatory signalling domain in a single gene product, T cells transduced with this construct showed enhanced cytokine production [102]. Several following studies demonstrated that the addition of the CD28 costimulatory domain improved activation, proliferation and cytokine production by CAR T cells in vitro and greater tumour cell killing in preclinical animal models using both

solid tumours and leukaemia that lack the expression of the CD28 receptor ligands CD80 and CD86 [108–112]. This has been confirmed in an elegant double marking study in humans which demonstrated T cells transduced with a second generation CAR incorporating CD28 expanded and persisted better than autologous T cells transduced with a CAR lacking a costimulatory domain [113].

CD28 co-stimulation is thought to be fundamental for early activation of naive T cells, but of less significance in memory and effector T cell responses. Additional co-stimulatory molecules cooperate in different T cell subsets at different stages of activation. Inducible co-stimulator (ICOS)2, OX40 (CD134) and 4-1BB (CD137) are expressed upon signalling through CD28 and are thought to be important in extending the T cell response and the origination of T cell memory [114]. ICOS is a B7 receptor family member, OX-40 and 4-1BB are TNF receptor family members and all are expressed on activated T cells. Subsequent to the incorporation of CD28 as a co-stimulatory domain in a CAR, 4-1BB as a co-stimulatory domain was tested in a CAR format. Signalling via 4-1BB was selected because it has been shown to induce expansion of $CD8^+$ cells, and enhancement of $CD8^+$ T cells responses [115, 116], but more notably it causes up-regulation of anti-apoptotic genes which is thought to protect the transduced cells of activation induced cell death (AICD) [117]. Persistence of transduced T cells has been a considerable impediment to the use of these cells for adoptive immunotherapy, as poor *in vivo* persistence has been reported to result in reduced potential clinical activity [73, 74], and improving this is therefore a cornerstone of ongoing investigations. Milone *et al.* showed that the CARs containing the 4-1BB co-stimulatory domain have superior antileukaemic efficacy and improved persistence in a primary human ALL xenograft model [81]. This was supported by another study again showing greater persistence but this time with a mesothelin targeting CAR [118]. CARs containing the 4-1BB co-stimulatory domain have also been associated with clinical success targeting CD19 [76, 89] and a recent publication by Long *et al.* provides a biological explanations for the increased persistence of 4-1BB incorporating constructs compared to those incorporating a CD28 co-stimulatory domain [119]. They show that the amelioration of ex-

haustion correlates to a unique transcriptional profile. Several key genes described to contribute to exhaustion were differentially expressed between cells transduced with a CD28 co-stimulatory domain containing construct compared to 4-1BB. Their results suggest that quantitative reductions in exhaustion-associated molecules may contribute to the improved persistence. In third-generation CARs, multiple co-stimulatory domains are placed in tandem, however limited data is published of the clinical experience using these constructs [120]. Pre-clinical *in vitro* studies exhibited superior proliferation, interferon-γ secretion and cytotoxicity [121], compared to second generation CARs transduced with a CD28 co-stimulatory domain.

In view of the complex cellular, signalling, and metabolic status in tumour lesions, there is considerable interest in understanding the impact of CAR-mediated costimulation on T cell performance. An interesting study on specific metabolic pathways by Kawalekar *et al.* addresses the impact of costimulation on metabolic plasticity of human engineered $CAR^{+}T$ cells, through different signalling pathways and towards different maturation stages. Inclusion of 4-1BB as co-stimulatory molecule promoted the outgrowth of CD8+ central memory T cells that had significantly enhanced respiratory capacity, increased fatty acid oxidation and enhanced mitochondrial biogenesis. In contrast, CAR T cells with CD28 domains yielded effector memory cells with a genetic signature consistent with enhanced glycolysis [122, 123]. The study on the impact of CAR costimulation on the metabolic reprogramming of CAR T cells advances the understanding how to manage T cell metabolism and to balance the redirected response toward long-lived memory cells [123]. The constructs used in all the experiments conducted for this thesis incorporated a 4-1BB costimulatory domain, with the anticipation of accomplishing enhanced T cell persistence.

1.3.3.2 Spacer and transmembrane domain

It can be difficult to mimic the structural and spatial elements of T cell recognition that has evolved to very closely regulate the interaction between the T cell and its target. During formation of the immunological synapse, the 15-nm distance between a T cell and an APC is dictated by the structures of the TCR and pMHC

[124]. This close proximity is important to exclude the phosphatases CD45 and CD148, which have large ectodomains, from the synapse to allow TCR-induced tyrosine phosphorylation to be initiated in the absence of these negative regulators [124]. Unlike a T cell receptor contact with peptide-loaded HLA class I or II, CARs adapt to a different dimensional connection and the synapse between a CAR and target cell is influenced by the scFv's epitope location and the spacer region, relative to the distance from the tumour cell's plasma membrane. CARs do not form a traditional synapse, showing differences in Lck and actin distribution. The LFA-1 integrin is known to mediate adhesion between T cells and antigen-presenting cells and CAR T cells exhibit reduced accumulation of LFA-1 in the synapse, which may contribute to reduced adhesion and facilitate detachment from tumour cells [125].

Moritz *et al.* designed a CAR that, in contrast to earlier reported versions that attached the scFv directly to the CD3ζ domain [126], added a flexible hinge motif derived from the membrane proximal portion of CD8 and laid the foundation for several transmembrane domains tested. The connecting sequence between the antigen recognition domain and the transmembrane domain directly influences the orthogonal synapse distance and flexibility between CAR T cell and target cell. Examples of spacer regions include immunoglobulin domains such as the Fc region of IgG or the immunoglobulin-like extracellular regions of CD4 and CD8. There are somewhat conflicting results as to what would be the optimal design of the spacer or hinge region. Guest *et al.* compared CARs targeting carcinoembryonic antigen (CEA), neural small adhesion molecule (NCAM), 5T4 and CD19, investigating the influence of adding an IgG derived hinge region on CAR T cell functionality. While 5T4- and CD19-specific CAR-T cells with a hinge had enhanced effector function, CEA- and NCAM-specific CAR-T cells had optimal activity without [127]. Similarly, Hudecek *et al.* compared the effect of different lengths of hinge regions on ROR1 CAR T cells, showing an improved functional outcome in ROR CAR T cells containing a short hinge region [128]. Targeting CD30 however, a different research group had found that the inclusion of an Fc hinge region reduced cellular activity upon encounter of antigen, compared to CAR T cells without any spacer domain

[129]. Thus where in some cases no spacer or very short hinge regions seemed to result in an optimal functionality of the CAR transduced cells, others have reported that a more flexible spacer may be required to permit the efficient binding of epitopes residing closer to the cell membrane [127–131]. These results clearly illustrate that the choice for a spacer region is target dependent and that modifying this region is likely to significantly impact the receptor stability and substrate binding affinity, depending on the location of the target epitope. In addition, detrimental effects of the hinge region have also been described. Cross-activation can occur between IgG1 Fc-hinge-containing CAR T cells and Fcγ-receptor-positive cells, resulting in unspecific innate immune activation and AICD [132, 133].

When comparing the effect of the spacer region in the CD19 trials, potent antitumour activity has been shown against chronic lymphocytic leukaemia, using a short spacer region derived from the human CD8α-chain [76, 77]. Limited reports of persistence and clinical efficacy have been published with a longer spacer domain, derived from the IgG1 hinge and fc [113], thought to be caused by the endogenous immune response against the murine component [90]. In the context of this thesis the hinge and transmembrane region of the human CD8α-chain were cloned in-frame between the scFv and the signalling domains, identical to the CAR construct taken forward for clinical evaluation in the CARPALL trial.

1.3.3.3 Antigen binding domain

An immunoglobulin is a 4 chain-structure consisting of two identical heavy and light chains (V_H & V_L), as shown in figure 1.5. Antigen recognition is mediated by a combining site in the variable fragments (Fab) that requires contributions from both the V_H and V_L. Within these two domains are three hypervariable regions termed complementarity determining regions (CDRs) between flanking framework regions, which are more highly conserved. CDRs can interact and determine binding to the antigen.

As indicated earlier, the binding domain most commonly incorporated into a CAR is an scFv, consisting of the immunoglobulin light chain variable region (V_L) and the heavy chain variable region (V_H) linked by a peptide linker sequence, retain-

ing its specificity and affinity and enabling MHC-independent antigen recognition [134]. Individual scFvs targeting a surface molecule are either derived from murine or humanized antibodies or synthesized and screened via phage display libraries. A major challenge in CAR design is ensuring specificity to the tumour, whilst sparing healthy cells.

A wide array of antigens has been exploited to target with a CAR. There are 6 hybridomas producing murine monoclonal anti-human CD19 specific scFvs available [96, 135–139]:

- SJ25C1, Mouse IgG1
- FMC63, Mouse IgG2a
- 4G7, Mouse IgG1
- HD37, Mouse IgG1
- CAT-13.1E10, Mouse IgG1
- B43, Mouse IgG1

Of these, 4 have been used in clinical CD19 CAR studies to date. Studies performed by the NIH and University of Pennsylvania have used an scFv, derived from the FMC63 hybridoma, whereas studies at the Memorial Sloan Kettering Cancer Center used an scFv derived from the SJ25C1 hybridoma [79, 89, 140]. Studies performed at UCL have used FMC63, 4G7 and CAT. The amino acid sequence alignments of the variable domains (V_H & V_L) are shown in table 1.4. The use of murine scFv sequences can induce immunogeneicity resulting in a potential advanced reactivity against and early evanescence of the CAR-transduced cells [73, 74]. Humanizing the foreign sequences of the scFv or using a fully human scFv can render them less immunogenic. However one could still develop anti-idiotype antibodies that may be inhibitory.

1.3.3.4 Impact of CAR T cell receptor affinity on T cell function

The upper limit of natural TCR affinity correlates to a dissociation constant (K_D) of around 1 - 50 μM [142, 143]. This is considerably weaker than reported affinities for protein-protein interaction and the antibodies used for CARs. Although higher affinity interactions increase specificity for a ligand, a quick dissociation

Table 1.4: The amino acid sequence alignment of the variable domains (VH and VL) of scFv FMC63, 4G7, HD37, CAT, B4 & SJ25C1 are shown with framework regions (FR) and complementarity determining regions (CDR) using Kabat numbering [141] .

Heavy chain

scFv	FR1	CDR1	FR2	CDR2	FR3	CDR3	FR4
KABAT	31 35		50 65		95 102		
HD37	QVQLQQSGAELVRPGSSVKISCKASGYAFS	SYWMN	WVKQRPGQGLEWIG	QIWPGDGDTNYNGKFKG	KATLTADESSSTAYMQLSSLASEDSAVYFCAR	RETTTVGRYYYAMDY	WGQGTTVTVSS
B4	QVQLQQPGAEVVKPGASVRLSCKTSGYTFT	SNWMH	WVKQRPGQGLEWIG	EIDPSDSYTNYNQKFKG	KAKLTVDKSSSTAYMEVSSLTSEDSAVYYCAR	GSNPYYYAMDY	WGQGTSVTVSS
FMC63	EVKLQESGPGLVAPSQSLSVTCTVSGVSLP	DYGVS	WIRQPPRKGLEWLG	VIWGSETTYYNSALKS	RLTIIKDNSKSQVFLKMNSLQTDDTAIYYCAK	HYYYGGSYAMDY	WGQGTSVTVSS
CAT	QVQLQQSGPELVKPGASVKISCKASGYAFS	SSWMN	WVKQRPGKGLEWIG	RIYPGDEDTNYSGKFKD	KATLTADKSSTTAYMQLSSLTSEDSAVYFCAR	SLLYGDYLDY	WGQGTTLTVSS
4G7	EVQLQQSGPELIKPGASVKMSCKASGYTFT	SYVMH	WVKQKPGQGLEWIG	YINPYNDGTKYNEKFKG	KATLTSDKSSSTAYMELSSLTSEDSAVYYCAR	GTYYYGSRVFDY	WGQGTTLTVSS
SJ25C1	QVQLLESGAELVRPGSSVKISCKASGYAFS	SYWMN	WVKQRPGQGLEWIG	QIYPGDGDTNYNGKFKG	QATLTADKSSSTAYMQLSGLTSEDSAVYSCAR	KTISSVVDFYFDY	WGQGTTVTVSS

Light chain

scFv	FR1	CDR1	FR2	CDR2	FR3	CDR3	FR4
KABAT	24 34		50 56		89 97		
HD37	DIQLTQSPASLAVSLGQRATISC	KASQSVDYDGDSYLN	WYQQIPGQPPKLLIY	DASNLVS	GIPPRFSGSGSGTDFTLNIHPVEKVDAATYHC	QQSTEDPWT	FGGGTKLEIK
B4	QIVLTQSPAIMSASPGEKVTMTC	SASSGVNYMH	WYQQKPGTSPKRWIY	DTSKLAS	GVPARFSGSGSGTSYSLTISSMEAEDAATYYC	HQRGSYT	FGGGTKLEIK
FMC63	DIQMTQTTSSLSASLGDRVTISC	RASQDISKYLN	WYQQKPDGTVKLLIY	HTSRLHS	GVPSRFSGSGSGTDYSLTISNLEQEDIATYFC	QQGNTLPYT	FGGGTKLEIT
CAT	QIVLTQSPAIMSASPGEKVTMTC	SASSSVSYMH	WYQQKSGTSPKRWIY	DTSKLAS	GVPDRFSGSGSGTSYFLTINNMEAEDAATYYC	QQWNINPLT	FGAGTKLELK
4G7	DIVMTQAAPSIPVTPGESVSISC	RSSKSLLNSNGNTYLY	WFLQRPGQSPQLLIY	RMSNLAS	GVPDRFSGSGSGTAFTLRISRVEAEDVGVYYC	MQHLEYPFT	FGAGTKLELK
SJ25C1	ELVLTQSPKFMSTSVGDRVSVTC	KASQNVGTNVA	WYQQKPGQSPKPLIY	SATYRNS	GVPDRFTGSGSGTDFTLTITNVQSKDLADYFY	FCQYNRYPYT	SGGGTKLEIK

rate has been described to be of particular importance, as T cell functional avidity can be detrimentally affected when dissociation is prolonged [31]. As described earlier, in contrast to the natural TCR, CARs employ a different mechanism by which they recognize antigens in an MHC-independent manner. CARs, through their binding domains, recognize membrane-bound cell surface antigen, typically with a higher affinity (K_D= 80-1 nM) compared to TCR-pMHC affinity. However, because CAR transduced cells bind to antigens independent of MHC, the increased avidity through co-receptor engagement might be less distinct compared to wild type TCR and the difference in overall avidity between wild type TCR and CAR is therefore unidentified and possibly not as considerable as formerly thought.

Avidity of CAR-transduced cells is co-determined by the density of CAR on the cell surface and the antigen expression density. Whether differences in the affinities of the CD19 targeting domain, when significantly different, could affect CAR-mediated T cell functionality has not been evaluated, while previous studies, investigating different targets and CARs have to some extent been contradicting. A functional and dynamic balance between CAR expression density and TAA density has been described, showing that high levels of CAR expression lead to T cells being triggered by both low and high expressed TAAs, whereas low levels of CAR expression lead to CAR T cells being unable to lyse and produce cytokines in response to low expressed TAAs. There appears to be a window within which the level of CAR expression does not seem to impact T cell activation [144], however exceeding this level of expression, transduced cells are susceptible to AICD following engagement to its target [145]. The threshold for complete T cell activation is readily met, regardless of CAR affinity, due to high numbers of simultaneous CAR-antigen binding events [146].

Different studies showed there is a functional threshold affinity beyond which no improvement in T cell function is achieved, defined as ”the affinity ceiling”. Chmielewski *et al.* described a threshold of $1.6x10^{-8}$M and Haso *et al.* compared 2 CARs with binding domain affinities of $5.8x10^{-9}$M and $2.3x10^{-9}$M showing no significant differences between the two [147, 148]. Transduced cells, binding with a

strength above this window, are susceptible to activation induced cell death (AICD) following engagement to its target [149], as well as non-specific target recognition [150]. When the expression levels of CAR and/or antigen are low however, the optimal affinity remains elusive [146, 147, 151, 152]. Variances in outcome could be attributed to stability of the binding domain and mechanisms by which affinity of binding domains were altered, affecting either on- or off-rate.

1.4 Aims & Objectives

The overarching aim of this project is to investigate the impact of scFv affinity, and in particular the off rate, on CAR-mediated T-cell function both *in vitro* and *in vivo*.

Specifically, my objectives are:

- To generate 6 CARs that are identical in backbone other than their CD19-targeting domain, incorporating the 6 different CD19 binding scFvs;
- To compare the affinity of the 6 scFvs;
- To phenotypically characterize T cells transduced with the different affinity CD19 CARs;
- To characterise the effect of affinity on CAR+ T cells by investigating functional responses *in vitro*, studying proliferation, differentiation, target cell killing, and the production and secretion of effector cytokines;
- To perform live cell imaging, to investigate the impact of differences in CAR affinity on interactions between CAR T cells and their targets on a microscopic level; and
- To study the anti-tumour response of different affinity CARs in a clinically relevant xenograft NSG model of disseminated leukaemia.

Chapter 3 details the experiments, investigating the affinity of the different anti-CD19 binding domains. Chapter 4 sets out the phenotypic characterisations and CAR^+ T cell functional responses, using various *in vitro* techniques. Lastly, the anti-tumour response in several subsequent *in vivo* studies, using a xenograft NSG model of disseminated leukaemia, are being discussed in chapter 5.

Chapter 2

Materials and methods

2.1 Materials

2.1.1 Blood samples, cell lines, buffers, media and solutions

Cell line	Description	Distributor
Raji	Burkitt Lymphoma cell line	ATCC
NALM6	B cell precursor leukaemia, ffLuc-eGFP-expressing	Gift from Hilde Almasbak
SupT1	T cell lymphoblastic lymphoma cell line	ATCC
SupT1 CD19	T cell lymphoblastic lymphoma cell line transduced to express CD19	Gift from Martin Pule
MP23021 SupT1 CD19	T cell lymphoblastic lymphoma cell line transduced to express CD19 at a low level (CD19 expression = 150x lower than supT1 CD19)	Gift from Martin Pule
K562 CD19	Chronic myeloid leukaemia cell line transfected to express human CD19-rabbit IgG1 recombinant protein	Gift from Martin Pule
HEK293 T cells	Human embryonic kidney cell line	ATCC

Table 2.1: Cell lines

Peripheral blood was taken from healthy volunteers after their informed consent. All cell lines used in this report were validated by PCR to be free from Mycoplasma (MycoAlert Mycoplasma Detection Kit, Lonza). Raji, K562 and 293T cell lines were obtained from ATCC. SupT1 cells were purchased from ECACC and transduced with an SFG vector to express human CD19 (SupT1-CD19) and single cell selected by flow cytometry to generate a cell line, this work was done my members of Martin Pule's lab. K562 cells were transduced to express human CD19-rabbit IgG1 recombinant protein. NALM6 cells expressing GFP and firefly luciferase were kindly provided by Dr.Hilde Almasbak. Unless otherwise stated, all culture medium was Roswell Park Memorial Institute (RPMI)1640 plus 10% heat inactivated fetal

calf serum (FCS) (R10). K562 and 293T cells were cultured in Dulbeccos Modified Eagle Medium (DMEM) supplemented with 10% FCS (D10). All cell lines were kept in 5% CO_2 humidified incubators at 37°C. Adherent cell lines were routinely cultured to 70-80% confluency, then passaged 1:10 following dissociation with 0.05% Trypsin-EDTA (Gibco).

Stock solutions:

10mM PEI - Adjust 50ml PBS to pH4.5 using HCl. Weigh 10.3g polyethylenimine (Sigma-Aldrich 40872-7) into a 50ml falcon tube, add 31ml PBS pH4.5, place in a 75C water bath and vortex every 10 min until completely dissolved. Aliquot and store at -80C.

2.2 Methods

2.2.1 Molecular biology techniques

2.2.1.1 Generation of plasmids

Lentiviral vector

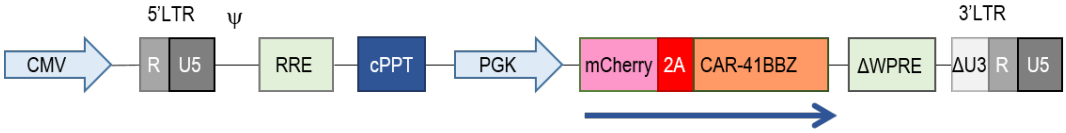

Figure 2.1: Schematic representation of the self-inactivating lentiviral transfer vector used in this thesis.

CMV	Heterologous CMV transcriptional promotor
LTR	Long terminal repeat: controls gene expression
R	R region: start of transcription
U5	5′ untranscribed region, involved in reverese transcription
Ψ	Packaging signal: required for encapsidation of viral genome
RRE	Rev response element
cPPT	Central polypurine tract: provides increased transduction
PGK	Human phosphoglycerate kinase promotor
ΔWPRE	Mutated woodchuck hepatitis virus post-transcriptional response element: improves nuclear export of mRNA
ΔU3	3′ untranscribed region, functional HIV-1 promotor and contains transcriptional enhancers, which have been mutated so the vector is self inactivating

The pCCL-aCD19 scFv-41BBZ lentiviral vector encodes the pCCL lentiviral backbone, in which the enhancer and promoter of CMV are joined to the R region of HIV-1 and the aCD19 scFv-41BBZ CAR. A schematic representation of the vector is given in figure 2.1. The CAR consist of an anti-CD19 scFv de-

rived from available mouse hybridomas, a portion of the human CD8 stalk and 41BB molecule, and the intracellular component of the human TCR-ζ molecule. The compact marker/suicide gene RQR8 was coexpressed with CAR by cloning it upstream of the CAR separated by an in-frame 2A ribosomal skipping sequence. [153]. RQR8 was later replaced by genes encoding for the marker gene mCherry.

To encode the anti-CD19 scFv components, previously published DNA sequences were used [96, 135–139]. The generated sequence encoded the following components: a NcoI site, a signal peptide, the variable heavy chain, a serine/glycine linker, the light chain and a BamHI site. All constructs were generated by gene synthesis using polymerase chain reaction (PCR) assembly of overlapping oligos, see chapter 2.2.1.2.

Soluble single chain fv-Fc

For affinity measurements the different aCD19 scFvs were fused to mouse IgG2a-Fc and generated in a secreted format. MP13227(SFG.dCD19-mIgG2aFc.I2.eBFP2) was used as the parental construct and cut with NcoI and BamHI after which the correspondingly digested scFvs were ligated into this plasmid.

Cloning of truncated CD19 isoforms

We constructed the full length peptide and three variants with increasing truncation of CD19 ($\Delta 2$, $\Delta 2-3$, $\Delta 2-3-4$) as displayed in figure 3.4, including a V5 tag (template from MP14479) under the signal-peptide. The cDNA fragments for CD19 (template dCD19-MluI MP14012) and the truncated isoforms were ordered as GBlocks (IDTDNA) with NcoI/MIuI restriction sites and the constructs were cloned into the retroviral vector SFG.I2.eGFP (MP3279) with NcoI/MluI restriction enzymes, followed by ligation. For completeness we included a full length (ecto) CD19 in the same format.

2.2.1.2 Oligo assembly

Oligonucleotides were purchased from IDTDNA. By PCR assembly of overlapping oligos, short stretches of DNA are synthesized. To amplify the full length product, forward and reverse primers were used. The oligos were reconstituted at 100µM.

10µl of each oligo was pooled in an eppendorf. To perform the assembly PCR, three dilutions of the oligo pool were prepared at 25 µM, 12.5 µM and 6.25 µM. With each of these dilutions as a template the PCR was then set up using: 36.5µL Nuclease-free water, 10µL Phusion HiFid buffer (NewEngland Biolabs), 2µL of pool template, 1µL of Deoxynucleotide (dNTP) Solution Mix (NewEngland Biolabs) and 0.5µL of Phusion hot-start polymerase (NewEngland Biolabs). The PCR thermocycles were as follows: 98°*C* for 2 minutes, 98°*C* for 1 minute,65°*C* for 45 seconds, 72°*C* for 1 minute, repeat cycle 2 35x, 72°*C* for 10 minutes and then 4°*C* until sample is retrieved.

To perform the amplification PCR, the PCR product was purified using the Qiagen PCR clean up kit and eluted in nuclease free water. The PCR was then set up as follows: 35.5µL Nuclease-free water, 10µL Phusion HiFid buffer (NewEngland Biolabs), 2µL of cleaned-up template, 1µL of forward primer, 1µL of reverse primer, 1µL of dNTP Mix (NewEngland Biolabs) and 0.5µL of Phusion hot-start polymerase (NewEngland Biolabs). The PCR thermocycles are described above. The product was then purified again and, after determining its size using agarose gel electropheresis, digested with restriction endonucleases.

2.2.1.3 Agarose gel electropheresis

Agarose gel electrophoresis was used for separation of DNA fragments by size. Migration rates are dependent on the pore size of the gel, which is determined by the agarose concentration. Optimal resolution of the fragments of interest was achieved by using 1% agarose, which ensures 0.25 - 12kb range of separation. Excised bands were purified using a gel extraction kit (QIAGEN) following manufacturers protocol.

2.2.1.4 Triple ligation

The construct pCCL.PGK.RQR8-2A-aCD19-4g7-HL-CD8STK-41BBZ (MP20151) was produced prior to the commencement of this PhD and was used as the parental construct. NcoI is not a unique cutter for this construct and since the newly generated scFvs have NcoI/BamHI restriction sites, a triple ligation strategy was set up. Two different digestions with MP20151 were set up as seen in table 2.2. CAR

insert and lentiviral backbone were identified as DNA fragments by agarose gel electrophoresis and stained with ethidium bromide for visualization under ultraviolet light exposure. Bands were excised and purified (Qiaquick Gel Extraction kit, Qiagen), and then ligated at a molar ratio of MP20151 I 1: MP20151 II 4.5: scFv 4.5.

	MP20151 I	**MP20151 II**	**scFv**
NEB3.1 (µl)	10	10	10
H_2O (µl)	75	75	75
Enzyme I (5µl)	SalI	SalI	BamHI
Enzyme II (5µl)	BamHI	NcoI	NcoI
DNA (µg)	5	5	5
Fragmentsize (bp)	7771bp	541bp	approx. 800bp

Table 2.2: Triple ligation for CD19 CAR

2.2.1.5 Restriction enzyme digestion

DNA digestion and restriction patterns were used to accurately verify successful cloning and presence of inserts. The mixture for digestion is set up as follows: 1 µg DNA, 2 µL NEB Buffer, 0.5 µL Enzyme 1, 0.5 µL Enzyme 2, 1 µL 1 in 10 diluted BSA, filled up to a total volume of 20 µL with nuclease free water. This mixture was then incubated for a minimum of 1 hour at $37°C$.

2.2.1.6 Transformation of plasmid DNA from *E.Coli*

Heat shock transformation of NEB5α competent bacteria (C2987H, high efficiency, New England Biolabs) allows the introduction of a circular DNA plasmid which confers resistance to a particular antibiotic granting later selection with that antibiotic. It was done by, after thawing, carefully adding 1 µl plasmid and incubating the bacteria on ice for 30 minutes, after which bacteria were incubated at $42°C$ for 35 seconds and subsequently incubated on ice for 5 minutes. Following addition of 250µL SOC media, samples were shaken at 200 rpm for at least 40 minutes at $37°C$. Transformed bacteria were then spread onto antibiotic-containing agar plates (the antibiotic used for selection was dependent upon the plasmid being amplified) cultured at $37°C$ for 12-16 hours and bacteria clones positive for the backbone were then identified.

2.2.1.7 Mini/Midi-prep of plasmid DNA

Twelve clones were selected for mini-culture in LB media with antibiotic selection at $37°C$ for 16 hours. Preparation of DNA from minipreps was done via MiniPrep kit (Qiagen) and subsequent analytical digestion with restriction enzymes and analysis of fragment size by agarose gel electrophoresis identified clones positive for the construct. Positive clones were then checked by sequencing to confirm successful cloning. A correct clone was then inoculated into large culture in TB media with antibiotic selection and cultured on shaker at $37°C$ for 16 hours, until log-phase growth was achieved. DNA was isolated from bacteria using EndoFree Midi Prep kit (Qiagen). Spectrophotometer analysis of DNA verified purity by OD260/280 reading between 1.8 and 2.0.

2.2.1.8 Quantification of DNA

The absorbance of the final midiprep solution was measured on a spectrophotometer set to record at 260/280 nm wavelength. To determine the purity of DNA a ratio of A260/280 $>$ 1.8 was pursued.

2.2.1.9 Sequencing

All the new constructs were sent for sequencing to confirm successful cloning (Beckman Coulter). The results were analysed and sequence alignment was performed using Snapgene software.

2.2.2 Cell culture techniques

2.2.2.1 Lentiviral vector production

Vectors were produced by transient transfection into 293T cells. 293 T cells were chosen as the packaging cell line for the production of the lentiviral particles due to its ease of transfection. The day before transfection 20-25 x 10^6 293T cells were in 20ml D10 per 15cm dish - they should be 85-95% confluent on the day of transfection - the growth rate of 293Ts can be variable so this cell number may need adjustment. A full prep required 20 plates. On the day of transfection, for each dish of 293Ts 5ml of Optimem containing 50 µg vector plasmid, 17.5 µg pMD2.G plasmid (VSV-G envelope), and 32.5 µg pCMV-dR8.74 (Gag/pol packaging) plasmid

was prepared and sterilised using a 0.22 µm filter. In separate flasks 1µl 10mM PEI to 5ml Optimem was added for each dish and filtered. The DNA and PEI solutions were combined in a 1:1 volume ratio (mixing continuously) and incubated at room temperature for 20min to form transfection complex solution. 10ml of transfection complex was added dropwise into the complete DMEM in each flask containing 293Ts and incubate at 37C 5% CO_2 for 4h, after which the the PEI:DNA complex was removed and replaced with D10. The following morning media was replaced with 12mls of fresh media per plate and 48 hours after transfection the virus containing supernatant was harvested and concentrated by ultracentrifugation. This step was then repeated at 72 hours.

2.2.2.2 Vector titration

Vector titre was assessed using 293T cells, seeded at $1x10^5$ cells per well in 1ml D10 per well in a 12-well plate. Cells were incubated in 5% CO_2 humidified incubators at $37°C$ for 6 hours.Following incubation, polybrene (MILLIPORE UK LTD) was added to each well of 293T cells at a concentration of 5µg/ml. Vector sample was thawed on ice and serially diluted in D10. From the resultant dilutions; 100 µl of the serially diluted vector was added gently dropwise to each well of 293T cells. Cells were incubated in 5% CO_2 humidified incubators at $37°C$ between 60-72 hours. Following incubation, the vector transduced 293T cells and negative controls were gently harvested off the 12-well plates using Cell Dissociation Solution (Sigma-Aldrich) and washed in phosphate-buffered saline (PBS; Sigma-Aldrich). Percentage transduction efficiency was assessed by expression for mCherry and titre was standardised against an in-house lentiviral vector control of known titre. Vector titre can be estimated across a range of vector volumes (2- 0.00064ul), but the estimate of stable transducing units was considered most accurate when between 5-20% of 293T cells were transduced.

2.2.2.3 Expression soluble scFv-fc

For expression of soluble scFv-fc 293T cells were transfected, by using Genejuice transfection reagent (EMD Millipore). In short 293T cells were plated 24 hours prior to transfection. Number of cells seeded was dependent on growth rate of cell

line. Generally 1.5x10^6 cells per entire plate were seeded (either 6,12 or 24 well plate). When 60% confluency was achieved, transfection was performed. See table 2.3 for amount of media, genejuice and DNA per well. First genejuice and plain medium were mixed and incubated for 5 minutes. The DNA was then added and incubated at room temperature for 15 minutes to allow formation of liposomes. The mix was then carefully added to each well and gently agitated to allow appropriate mixing.

Well type	Genejuice	Plain medium	DNA
100mm plate	30 µl	470µl	12.5 µg
6-well plate	5 µl	95 µl	2 µg
12-well plate	2.5 µl	47.5µl	1µg
24-well plate	1.25µl	23.75µl	0.5µg

Table 2.3: Genejuice mix

2.2.2.4 Expression CD19 truncated isoforms

The truncated CD19 isoforms were expressed on 293T cells by transient transfection using PEI, described in section 2.2.2.1. In short 293T cells were plated 24 hours prior to transfection. Number of cells seeded was dependent on growth rate of cell line. Generally 20x10^6 cells per 15cm plate were seeded in 10ml D10 . For transfection 5ml of plain Optimem was needed per plate to which 1µl of 10mM PEI was added. Another 5ml of plain Optimem was prepared per plate to which 30 µg of plasmid DNA was added. The two were then mixed and incubated for 20 minutes at room temperature. Without removing the cell-culture medium, the 10ml transfection mix was then added dropwise to each plate.

2.2.2.5 Human peripheral blood mononuclear cell isolation

Peripheral blood mononuclear cells (PBMCs) were isolated by density gradient centrifugation using FicollPaque Plus (GE Health,UK) at 750g for 25 minutes. Mononuclear cells were aspirated using a Pasteur pipette into phosphate buffered saline (PBS) and centrifuged at 220g for 10 minutes. Cells were counted and again centrifuged at 300g for 5 minutes. The PBMCs were then re-suspended in R10 at a density of 1 x10^6 cells/ml.

2.2.2.6 Activation of human T-cells

PBMCs were initially activated with Dynabeads® Human T-Expander CD3/CD28 (Life technologies) at 1:1 ratio. bead:cell ratio, exogenous Interleukin-2 (Proleukin ®, Novartis) at 100 IU/ml was supplemented to the media throughout the activation/transduction and expansion phases. Following further optimisation by Dr. Sara Ghorashian, it was decided to change this protocol to an activation with Dynabeads at 3:1 ratio, without further addition of cytokines. This proved to result in better transduction efficiencies whilst retaining an early memory phenotype.

2.2.2.7 Lentiviral transduction of human T-cells

Twenty-four hours after activation, T cells were transduced in a 24 well plate. Activated T cells were counted using trypan blue exclusion and 1ml of viable cells at a concentration of 1 x 10^6/ml in R10 was added to each well. Cells were transduced at varying multiplicities of infection (MOI, the average number of virus particles infecting each cell) and were subsequently incubated for 24 hours, after which the cells were topped up with an additional 1ml of R10, to a total volume of 2ml/well. The cells were recovered, counted and resuspended at 1 x 10^6/ml in fresh R10 72 hours following transduction. Anti-CD3/ CD28 beads were removed by magnetic separation on day 5 post-transduction, after which the transduction efficiency was determined by expression of mCherry and binding to a recombinant CD19 tagged with a rabbit IgG1 fc domain. CAR expression was then read out by staining with a secondary anti-rabbit fc antibody.

2.2.2.8 CD56 depletion

To preclude non-specific target cell killing, proliferation or cytokine production by natural killer cells (NK cells) in the PBMC preparation used for transduction due to MHC-I mismatch, cultures were depleted for CD56 expressing cells using CD56 MicroBeads (Miltenyi Biotec), according to manufacturer's protocol. CD56 is expressed by essentially all human NK cells and is increased on the cell membrane after activation. Depletion was performed one day prior to set up of further *in-vitro* functional testing, corresponding to 6 days post-transduction.

2.2.2.9 Culture methods for larger scale production of CAR T cells

Larger numbers of cells were cultured and transduced in G-rex culture vessels (Wilson-Wolf), a gas permeable rapid expansion culture technology. G-Rex10 gas permeable surface area = 10 cm^2 and therefore $10x10^6$ cells were activated on day 0 in 10ml of R10. Activation protocol was identical to the protocol in plates, i.e. 3:1 bead: cell ratio, without addition of cytokines. The next day (24 hours after activation) cells were transduced with MOI of 1, based on day 0 count. Twenty-four hours after transduction, the medium was topped up to a total volume of 40ml R10. If necessary, medium can be refreshed by carefully replacing 20ml of medium with 20 ml of fresh R10. Beads were removed 6 days following transduction, after which the cells were transferred to a MACS GMP Cell Differentiation Bag - 100 (Miltenyi) at $1x10^6$ /ml R10. We validated to ensure the distribution of memory subsets following culture in Grex was idential to that obtained in plates.

2.2.3 Affinity determination

2.2.3.1 Biacore

Experiments were performed on a Biacore T200 instrument using 0.01 M HEPES pH 7.4, 0.15 M NaCl, 3 mM EDTA, 0.005% v/v Surfactant P20 (HBS-EP) as running and dilution buffer (GE Healthcare Bio-Sciences). Prior to experimental setup recombinant CD19 protein (sino biologicals or Acro biosystems) was reconstituted according to the manufacturers instructions and dialysed against HBS-EP at 4°C to reduce observed bulk refractive index changes. For binding kinetics, goat anti-mouse IgG (GE Healthcare) was covalently coupled to a CM5 Sensor Chip (GE Healthcare). Anti CD19 scFv-Fc (mIgG2a) constructs were then captured at a target density of 100 response units (RU) and various concentrations of CD19 protein injected over the flow cell at a flow rate of 30 µl/min. Bulk refractive index differences were subtracted using a blank control flow cell in which capture antibody had been immobilized to the same level as the active surface. A double reference subtraction was performed using buffer alone in place of CD19 protein, to account for system baseline drift. BIAevaluation software Version 2.0 (GE Healthcare) was

used for data processing. Kinetic rate constants were obtained by curve fitting according to a 1:1 Langmuir binding model.

2.2.3.2 Cellular affinity by flow cytometry

After production of the soluble scFv-fc an ELISA was performed to quantify the amount of protein in the supernatant. A 96 well plate (Maxisorp) was coated with 100 µl per well of 1 µg/ml anti-mouse IgG2a in PBS. A second plate was coated with 100 µl PBS alone. The plates were then incubated for 1hr at room temperature or at $4°C$ over night. After decanting the plates they were blocked with 200 µl of 3% BSA/PBST (PBS containing 0.1% Tween 20) per well for 1 hour at room temperature and washed twice afterwards. 100 µl of the scFv-fc supernatant or standards (e.g. purified mouse IgG2a scFv-Fc) were then added at several dilutions to each plate and incubated at room temperature for 1 hr, after which the plates were washed 3 times with PBST and once with PBS. A hundred µl of 1/4000 anti-mouse IgG-HRP (GE Healthcare) diluted in 1% BSA/ PBST was then added and incubated for 1 hour at room temperature, after which the plates were again washed 3 times with PBST and once with PBS. A 100 µl of OPD substrate (one OPD (o-Phenylenediamine dihydrochloride) tablet (Sigma) was dissolved in 25ml of phosphate-citrate buffer with sodium perborate immediately prior to use) was then added to each well and incubated for 5 minutes, after which the reaction was stopped by the addition of 50µl of 4M HCl. The adsorbance at 490 nm was then read on a plate reader.

To determine optimal number of Raji cells we performed the experiment in a serial 1:2 dilution starting at $1x10^6$ Raji cells/well. The cells were pelleted the supernatant was discarded. A 100 µL of scFv-fc (5x serially diluted 1:2 in DMEM + 10%FCS) was then to each corresponding well. The samples were incubated at room temperature for 1 h and placed on ice for 5 minutes afterwards.The decrease in temperature greatly decreases the off-rate. The cells were then again pelleted and carefully remove supernatant for ELISA assay (in case needed) The samples were washed with 200 µL of ice-cold PBS, and resuspended in 100 µL of a 1:100 dilution of secondary aMuIgG FITC antibody. Cells were incubated on ice for 30 minutes

after which they were washed and finally resuspended in a 100 µl of cold fixation buffer before they were analysed by flow cytometry. In the Raji morphology gate 5,000 events were recorded and the statistical information from the FITC MFI was collected. Autofluorescence of non-stained Raji cells was subtracted before the MFI against the concentration of cells was plotted. A Scatchard analysis, a method of linearizing data from a saturation binding experiment in order to determine binding constants, was performed to fit the curve and determine K_d (Graphpad Prism v7.02). The first step was to perform a Non-linear Regression (Curve Fit) analysis, specifically the One site binding (hyperbola) assay. The data can then be transformed to a Scatchard line. Select Analyze and Data manipulations, then Transforms. In the next dialog, Parameters: Transforms, choose Pharmacology and biochemistry transforms from the Function List drop-down box, then set the Scatchard radio button.

The following equation was used: $y = m1 + m2 * m0/(m3 + m0)$ where m1 = MFI of no antigen control, m2 = MFI at saturation, and m3 = K_D. The slope of the straight line equals $-1/K_D$ from which K_D can be calculated.

2.2.4 Western Blot

Twenty micrograms of each cell lysate was loaded and separated by 4-20% SDSpolyacrylamide gradient gel electrophoresis and then transferred to 0.45-µm polyvinylidene fluoride membranes (200 V, 50 min). After blocking for 1 h in Phosphate buffered saline with tween 20 (PBST) (10 mM sodium phosphate, 0.9% NaCl, and 0.1% Tween 20) containing 5% skimmed dry milk, blots were incubated either for 1 hour at room temperature overnight at 4°C with the primary antibodies in PBST containing 5% skimmmed milk. The blots were washed three times with PBST (40 min) and incubated for 1 h with horseradish peroxidase-conjugated secondary antibody (Santa Cruz Biotechnology, Santa Cruz, CA, USA) in PBST containing 5% skimmed dry milk. Immunoreactivity of the protein bands were detected by enhanced chemiluminescent autoradiography (ECL kit, Amersham Pharmacia Biotech, Piscataway, NJ).

2.2.5 *In-vitro* functional assays

For direct comparison of different CAR constructs, normalization for transduction efficiency was accomplished by the addition of untransduced T-cells from the same donor to a transduction level of 20% in all constructs, or corresponding to the lowest percentage of the constructs compared in al *in-vitro* assays, as per published protocols[154].

2.2.5.1 ^{51}Cr release cytotoxicity assay

Standard ^{51}Cr release assays were performed to determine cytotoxic activity of CD19-CAR T cells against CD19^{+} cell targets, Raji and SupT1CD19 as well as a CD19^{-} target, supT1NT. Three x 10^6 target cells were labeled with 100 µCi ^{51}Cr (Perkin Elmer) for 1 hour, during which cells were intermittently agitated to improve the uptake of ^{51}Cr. On washing, 5 x 10^4 targets per well were coincubated for 4 to 5 hours with effector T cells at various effector to target (E:T) ratios, starting from 32:1 to 2:1. Untransduced cells, which had been activated using an identical method, served as a negative control. Target cells in complete media or lysed with 1% TritonX-100 (SigmaAldrich) were used to determine spontaneous and maximum release, respectively. Assay supernatants were counted for ^{51}Cr release using High Binding Isoplate-96 HB (Perkin Elmer) and a 1450 MicroBeta TriLux (Perkin Elmer). Specific lysis was calculated as follows: % Lysis = (experimental lysis - spontaneous lysis) / (maximum lysis - spontaneous lysis) x 100.

2.2.5.2 Long term cytotoxicity assay by flow cytometry

Effector and target cells (NALM6, SupT1-CD19 and SupT1CD19LO) were co-cultured in triplicates in a 96-well round-bottom plate at a 1:1, 4:1 or 10:1 ratio (total number of cells $1x10^5$) without further addition of cytokines. At 24 hours triplicate wells were harvested and merged into single FACS tubes for flow cytometric analysis. Cells were stained for expression of CD2 and a live dead marker was included, as an assessment of viability. Countbright beads (Thermo Fisher) were added to allow a standardized acquisition on the flow cytometer. After the addition of Fixation buffer, cells were stored at 4°C in the dark until analysis. Target

cells were identified by GFP expression (NALM6) or CD2 expression (negative in SupT1CD19 & SupT1CD19LO).

2.2.5.3 ^{3}H-thymidine proliferation assay

The ^{3}H-thymidine incorporation assay employs a method wherein a radioactive nucleoside, tritiated thymidine (^{3}H-thymidine), is incorporated into new strands of chromosomal DNA during mitotic cell division. The amount of radioactivity incorporated into DNA in each well is measured with a betacounter and is proportional to the number of proliferating cells. The readout is counts per minute (cpm) per well.

On day 6 after transduction, 1 x 10^5 transduced and untransduced effector cells were co-cultured at a 1:1 ratio with irradiated target cells (Raji & SupT1NT) in R10 medium, without addition of IL-2 in 96-well round bottomed plates. The cells were allowed to proliferate for a further 48 hours at 37°C in a humidified CO_2 tissue culture incubator. ^{3}H-thymidine was diluted in RPMI+10% FCS to a concentration of 10 µl /ml = 10 µCi /ml. 100 µl of medium was carefully removed from each well, so as not to disturb the cell layer as far as possible, and replaced with the ^{3}H-thymidine solution, resulting in a final concentration of 1 µCi/well for the final 18 hours of culture.

Cells were harvested with a Tomtec Harvester 96 MACH 3M, according to the manufacturer's protocol. In the harvesting step the cell material including genomic DNA is captured into 96-format glass-fiber filtermats, using water as wash buffer. Meltilex, a solid scintillator was then added on top before reading the samples in the 1450 MicroBeta TriLux (Perkin Elmer).

After determining the mean of the triplicate wells, specific proliferation was calculated as CPM (effectors+targets) - CPM effectors only - CPM targets only.

2.2.5.4 Cytokine production

Cytokine levels were determined by analysing supernatants from triplicate wells after 48-hours of coculture of 1 x 10^5 effector cells with 1 x 10^5 target cells using a BD ^{TM} cytokine bead array according to manufacturer's protocol. The CBA Human Th1/Th2/Th17 Cytokine Kit can be used to measure Interleukin-2 (IL- 2),

Interleukin-4 (IL-4), Interleukin-6 (IL-6), Interleukin- 10 (IL-10), Tumor Necrosis Factor (TNF), Interferon-γ(IFN-γ), and Interleukin-17A (IL-17A) protein levels in a single sample. The kit performance has been optimized for analysis of physiologically relevant concentrations (pg/mL levels) of specific cytokine proteins in tissue culture supernatants. Data were analysed using FCAP Array (Softflow, Inc.). Mean and SEM are reported.

2.2.6 Flow Cytometry

Flow cytometry acquisition was performed using a BD LSR II (BD Biosciences) or Aria, and data analyis was performed using FlowJo vX (Tree Star, Inc., Ashland OR). Expression of CAR was detected by binding to recombinant CD19-rabbit IgG1 protein that was fluorescent labelled with an aRabbit-fc secondary antibody, or on the basis of mCherry expression. The transduced population was identified using the following strategy: 1) FSC-A vs. FSC-W to eliminate doublets based on FSC 2) SSC-A vs SSC-W to eliminate doublets based on SSC 3) FSC-A vs SSC-A for a morphologic lymphocyte gate 4) Live dead vs CD3 to gate on the live CD3 cells 5) finally the CD3+ transduced+ cells, using non-transduced cells as negative control. All FACS plots presenting CAR T cell phenotype data were pre-gated on gated CAR+ cells. For non-transduced T cells, whole T cell populations were used for analysis.

2.2.6.1 General staining protocol

Immunostaining of between $2x10^5$ to $1x10^6$ cells was performed with monoclonal conjugated antibodies at certain dilutions stated in table 2.4.

When staining of intracellular proteins was required, the Biolegend Fix&Perm protocol was followed.

Binding of soluble scFv-Fcs

To detect binding of soluble scFv-Fcs to tumour and T cells by flow cytometry, supernatants were harvested from 293T cells transiently transfected with constructs encoding the soluble CD19 scFv-Fcs. Target cells were incubated with harvested supernatants, washed, and then stained with an anti-mouse IgG F(ab)2 secondary.

Binding to truncated CD19 isoforms

FMC63 and CAT scFv-fc (as described earlier) were added as primary layer and incubated for 20mins at room temperature. A secondary layer of amuIgG2a-PE (biolegend) was added. Binding was identified as double positivity for transgene expression (GFP) and scFv-fc (PE)

2.2.6.2 PE QuantiBRITE CD19 expression quantification

QuantiBRITE PE tubes are designed for use with PE-labeled monoclonal antibodies for the purpose of estimating expression levels by flow cytometry. When the QuantiBRITE PE tube is run at the same instrument settings as the assay, the PE axis can be converted into the number of PE molecules bound per cell. This assay was set up according to the manufacturers protocol. Anti-CD19 PE Antibodies (BD, Miltenyi, Biolegend) were first compared and titrated, to determine the concentration to saturate the cell lines. Miltenyi CD19 PE (130098068) was used at a concentration of 1/10.

2.2.7 Live cell imaging

CAR^+ T cells were selected for mCherry expression by cell sorting using FACSAria III (BD) to exclude non-transduced cells affecting confocal analysis. GFP^+ NALM6 cells were used as targets. Effectors and targets were co-cultured at a 1:8 ratio (total number of cells=$9x10^4$) in R10-HEPES (Life Technologies) in triplicate wells using a 96 well microplate with a glass base (Greiner Bio-One Ltd). DAPI was added to the solution at a concentration of 500ng/ml, allowing identification of dead cells.

Live cell imaging was performed for 20hrs at controlled environmental conditions (5% CO_2 at $37°C$) on a Zeiss axiovert with Ludl motorised stage and a 10x NA 0.25 CP-Achromat objective and Hamamatsu Orca ER camera. Multi-point (2 points per well) 4 channel timelapse imaging was run with Volocity software. Fluoroscence was captured with minimal excitation power and high camera gain to minimise phototoxicity.

ImageJ (Fiji) software was used to score contact between target and effector cells. Green and red channels were converted to binary images using extended minima thresholding. Thresholded regions were extended by 2 pixels with binary

dilation, and clusters split with a watershed. Regions of overlap between the thresholded images were scored as contact points, and a new image produced showing these contact points. The macro for image thresholding and production of the contacts points image will be available upon publication of the paper.

The resulting image was then analysed in ICY (Open source) to assess the frequency and duration of interactions between effectors and targets using the Spot Tracking Plugin. Motility of the cells was measured by the Motion Profiler, including min/max/avg/total displacement in pixels. Statistical analysis was performed using SPSS Statistics 22 (IBM).

Following live imaging, cells were harvested and analysed by flow cytometry, permitting quantification of cell death in both control and experimental groups, determining differences in number of DAPI- NALM6+ cells, normalized against spontaneous cell death in negative control wells. The number of cells acquired was standardized by the addition of counting beads.

2.2.8 *In vivo* anti tumour activity

2.2.8.1 Animals

All animal studies were approved by the University College London Biological Services Ethical Review Committee and licensed under the Animals (Scientific Procedures) Act 1986 (ASPA). Non-obese diabetic/ severe combined immunodeficiency/ common γ-chain knockout (NSG,female, aged 6-10 weeks) were obtained from Charles River Laboratory (Wilmington, MA) and raised under pathogen free conditions.

2.2.8.2 Irradiation

Unless otherwise stated, mice were sublethally irradiated at 2.8 Gy 1 day prior to intravenous inoculation with tumour cells.

2.2.8.3 Intravenous injection of mice

Mice were heated for 15 minutes in a warming box to encourage vasodilatation of the tail veins. Intravenous inoculation with $1x10^6$ NALM6 engineered to express firefly Luciferase (F-Luc), as described earlier [133], was done in a volume

of 0.2ml. Engrafted mice received CAR^+ T cells in a single injection with a volume of 0.2ml (dose specifically stated for each individual experiment), 7 days post NALM6 injection, depending on experimental outline. CAR^+ T cells were analysed by FACS for CAR expression one day prior to injection and were generally injected as bulk (transduced and untransduced populations). If transduction efficiencies were $> 10\%$ different, they were corrected by the addition of untransduced cells to match the lower expressing construct.

2.2.8.4 Bioluminescent imaging of mice

To assess engraftment and antitumor activity of genetically modified human T cells, tumour growth was evaluated by bioluminescent imaging (BLI) using the IVIS Imaging Sytem. By intraperitoneal injection, anesthetized mice were given 150 µg D-Luciferin Potassium Salt (Hichrom). Mice were anesthetized with isoflurane and imaged 10 minutes after D-luciferin injection, with an exposure time of 60 seconds, unless images were saturated, in which case the software was set to automatically determine the exposure time. Luciferase activity was analyzed using Living Image Software and the photon flux analyzed as photons/s/cm^2/sr (Perkin Elmer).

2.2.8.5 Monitoring

Mice were closely monitored every 1-3 days for signs of xenogeneic graft-versus-host disease and other toxicities and their weights were recorded 3 times per week. End point predetermined by length of experiment or if animal becomes ill (evidence by piloerection, hunched posture or loss of response to the environment). In addition, a loss in weight by 15% over 48 hours would result in the animal being culled. To help prevent excess suffering the mouse grimace scale was used to determine levels [155]. The 5 facial expressions, orbital tightening, nose bulge, check bulge, ear position and whisker change were coded on a scale of 0-2. If any animal exceeded the score of 2 on any one of 5 conditions for 48 hours, it would be culled according to the Protection of Animals Act, after which bone marrow and spleen were investigated for presence of disease and CAR+T cells.

2.2.8.6 Spleen & Bone Marrow preparation

After sacrifice, single cell suspensions were made of spleen and bone marrow by maceration through a cell strainer. Red blood cells were lysed using ACK lysing buffer (LONZA) and the cells were re-suspended in 2ml PBS.

Bone marrow was harvested from both a single femur and tibia from each animal. The ends of the bone were removed and the contents of the bone marrow were flushed with PBS and through a cell strainer, harvested in a 50ml falcon. Cells were pelleted by centrifugation at 300G for 5 minutes. Red blood cells were lysed using ACK lysing buffer (LONZA) and the cells were re-suspended in 1ml PBS.

Results were presented as disease free survival, phenotype, and absolute cell counts.

2.2.9 Statistical analyses

All statistical analyses were performed in GraphPad Prism v7.02. Unless otherwise stated, data were expressed as mean $\pm$ SEM. Statistical analyses of in vitro assays were undertaken by 2-way ANOVA with donor matching and Tukey post-test for multiple comparisons or 2-tailed Student t-test, as indicated in figure legends. Statistical significance was indicated as follows in the figures: ***P $<$ 0.001; **P $<$ 0.005; *P $<$ 0.05; and NS, nonsignificant (P $>$ 0.05).

Specificity	Clone	Isotype	Manufacturer	Fluorochrome	Dilution
CD3	UCHT1	Mouse IgG2a	Biolegend	PerCPCy5.5	2:100
CD3	OKT3	Mouse IgG2a	Biolegend	FITC	1:100
CD4	OKT4	Mouse IgG2b	Biolegend	APC	1:100
CD4	M-T466	Mouse IgG1	Miltenyi	PE-Vio770	1:100
CD8	HIT-8a	Mouse IgG1	Biolegend	PE	1:100
CD8	HIT-8a	Mouse IgG1	Biolegend	FITC	1:100
CD8	SK1	Mouse IgG1	Biolegend	BV605	1:100
CD19	HIB19	Mouse IgG1	Biolegend	BV605	1:100
CD34 Qbend10	4H11	Mouse IgG1	Sigma-Aldrich	APC	1:100
CD45RA	H100	Mouse IgG2b	Biolegend	BV605	1:100
CD69	FN50	Mouse IgG1	Biolegend	APC	1:100
CD95	DX2	Mouse IgG1	Biolegend	BV421	1:100
CD127	A019D5	Mouse IgG1	Biolegend	BV711	1:100
CD197 (CCR7)	G043H7	Mouse IgG2a	Biolegend	APC/APC-Cy7	1:100
CD223 (LAG3)	3DS223H	Mouse IgG1	eBioscience	APCeFluor 780	2:100
CD279 (PD1)	EH12.2H7	Mouse IgG1	Biolegend	BV421	2:100
CD366 (TIM3)	F38-2E2	Mouse IgG1	Biolegend	BV711	1:100
anti-BCl-2	100	Mouse IgG1	Biolegend	BV421	5:100
anti TNFα	MAb11	Mouse IgG1	Biolegend	BV421	5:100
anti IL-2	MQ1-17H12	Rat IgG2a	Biolegend	BV605	5:100
anti IFNγ	4S.B3	Mouse IgG1	Biolegend	APC	5:100
Anti-Rabbit IgG	polyclonal	Goat F(ab')$_2$	Jackson Immunoresearch	FITC	1:100
Anti-Rabbit IgG	Poly4064	Donkey	Biolegend	BV421	1:100
Anti-V5 tag	polyclonal	Rabbit	Abcam	PerCP	5:100
Fixable viability dye			Life technologies	Aqua	0.5:1000
Fixable viability dye			eBioscience	APCeFluor 780	0.2:100

Table 2.4: Antibodies

Chapter 3

Determination of binding characteristics of anti-CD19 single chain variable fragments

3.1 Introduction

A large number of CARs have been described and the antigen binding domains have most often been formed out of monoclonal antibodies derived from specific anti-human hybridomas. The majority of these antibodies have a high affinity for their target, binding cognate ligand with nM affinity [111, 156–158].

In the context of antigen-antibody interactions, binding affinity is the strength of the monomeric reversible binding between an epitope and an antibody's antigen binding site, typically described by the equilibrium dissociation constant (K_D). The (K_D) can further be described by the association rate, or the on-rate (k_a), and the dissociation rate, the off-rate (k_d) and measures the propensity of an immune-complex to fall apart into its component molecules an antibody and antigen and can be described by the following equations:

$$K_D = \frac{k_\mathrm{d}}{k_\mathrm{a}} = \frac{k_\mathrm{off}}{k_\mathrm{on}} = M \tag{3.1}$$

$$k_{\mathrm{a}} = Msec^{-1} \tag{3.2}$$

$$k_{\mathrm{d}} = sec^{-1} \tag{3.3}$$

The half life ($t_{1/2}$) for the interaction is derived from the off-rate:

$$t_{1/2} = \frac{ln(0.5)}{-k_{\mathrm{d}}} \tag{3.4}$$

k_d and k_a are reciprocally related and can alternatively be calculated from the following:

$$k_a = \frac{[\mathrm{AbAg}]}{[\mathrm{Ab}]\,[\mathrm{Ag}]} = \frac{k_{\mathrm{on}}}{k_{\mathrm{off}}} = \frac{1}{K_D} = M^{-1} \tag{3.5}$$

Thus, is it possible for two antibodies to have the same affinity, but for one to have both a high on- and off-rate constant, while the other may have both a low on- and off-rate constant.

To understand the affinity of the interaction between the different scFvs and CD19, Biacore surface plasmon resonance (SPR) measurement was used to determine the binding kinetics between these two proteins. SPR biosensors, such as the Biacore T200, monitor the reversible interactions of proteins and detects in real time the kinetics of the association and dissociation as the protein absorbs and desorbs (fig 3.1). The soluble scFv-fc, derived from the anti human CD19 mAb, is immobilized onto the surface of the chip and soluble CD19-antibody is flown over the surface at a constant rate.

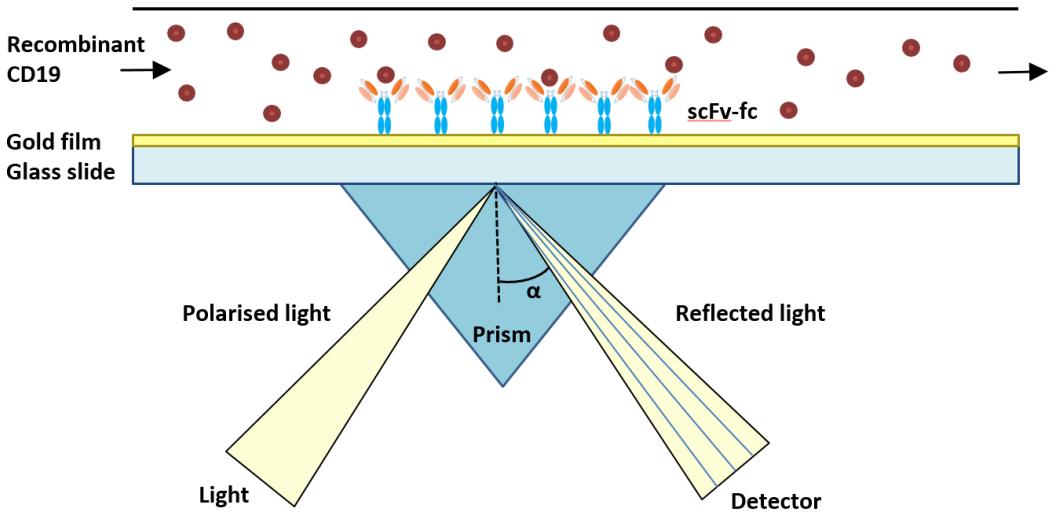

Figure 3.1: **SPR Biacore**

The instrument measures the mass bound to the surface by a spectroscopic phenomenon. The chip is covered by gold, and covalently coupled to goat anti-mouse IgG, onto which the CD19 scFv-fc is then linked. After immobilisation, the target - soluble recombinant CD19 - applied in the solution forms a complex with the scFv. Upon binding, the local refractive index will change and this has an effect on the plasmon waves, resulting in a shift of the resonance angle (α). This change in angle is proportional to the mass bound to the chip's surface.

The instrument measures the mass bound to the surface by a spectroscopic phenomenon. The chip is covered by gold, and covalently coupled to goat anti-mouse IgG, onto which the CD19 scFv-fc is then linked. After successful immobilisation, the target - soluble recombinant CD19 - is applied in the solution and will then form a complex with the scFv. Upon binding, the local refractive index will change and this has an effect on the plasmon waves, resulting in a shift of the resonance angle. This change in angle is proportional to the mass bound to the chip's surface.

Published clinical studies use T cells expressing CARs specific for CD19 incorporating antigen binding domains that are derived from different anti-human CD19 hybridomas. The choice for a specific hybridoma has been pragmatic and potentially economically driven, as a new binder is patentable. The influence of the affinity of different CD19-targeting CARs on the downstream functionality of T cells in responses against $CD19^{+}$ targets has not yet been clearly delineated.

In 10% to 20% of cases of paediatric B-ALL treated with CD19-directed immunotherapy treatment failure occurs due to relapse associated with epitope loss [86]. *De novo* genomic alterations in the CD19 gene found to primarily affect exon 2, leading to a N-terminal truncated CD19 Δex2 isoform [95]. This mutant bypasses recognition by CAR T cells and was reported in studies using different CD19-targeting CARs with different binding domains and different costimulatory domains, and seemed to be independent of expansion or clinical protocol [85, 88, 97, 159, 160]. The binding site on CD19 of our binder derived from CAT hybridoma, has not yet been identified.

3.1.1 Aims

- To characterise the equilibrium dissociation constant, determined by on- and off-rate of 6 hybridoma derived murine anti-human CD19 scFvs
- To identify the epitope binding site of CAT scFv on CD19

3.2 Results

3.2.1 Kinetic properties of aCD19 binders varied and are predominantly determined by off-rate

We set out to compare 6 different anti human CD19 binders derived from different hybridomas, of which 4 are taken forward in clinical trials:

- CAT
- SJ25C1
- FMC63
- B4
- 4G7
- HD37

All 6 CD19 binders were cloned in an scFv-fc format, as illustrated in figure 1.5. This allowed linking to goat anti-mouse IgG, covalently coupled to the surface of the Biacore chip. Soluble protein was expressed and quantified by ELISA. To date we have not been able to express SJ25C1 as a CAR or scFv-Fc. This is most likely caused by an error in the published sequence, showing a repeated tyrosine-phenylalanine insertion before the conserved cysteine in framework 3 of the light chain (see table 1.4). It is unusual to see an amino acid insertion at this framework position, so we believed that it was an error in the sequence from the original paper.

SPR analyses for binding to CD19 were performed to assess the 5 different aCD19 binders. In this system, binding curves associated with different concentrations of CD19, injected in subsequent measurement cycles, are normalized to the same baseline. Two individual experiments were conducted, resulting in very similar data, one representative experiment is described in table 3.1 and displayed in figure 3.2. Figure 3.2 visualises the k_a and k_d on its respective axes. The CAT scFv-fc showed substantially lower (> 100 fold) binding affinity. A higher K_D(0.116μM) was the result of a much quicker off-rate ($7.07x10^{-2}$ $M^{-1}s^{-1}$) (table 3.1). Interestingly the on-rate of CAT scFv-fc was comparable to the strongest binder FMC63. HD37, B4 and 4G7 scFv-fcs all have relatively high affinities based on their low K_d values, but all three show a slower on-rate.

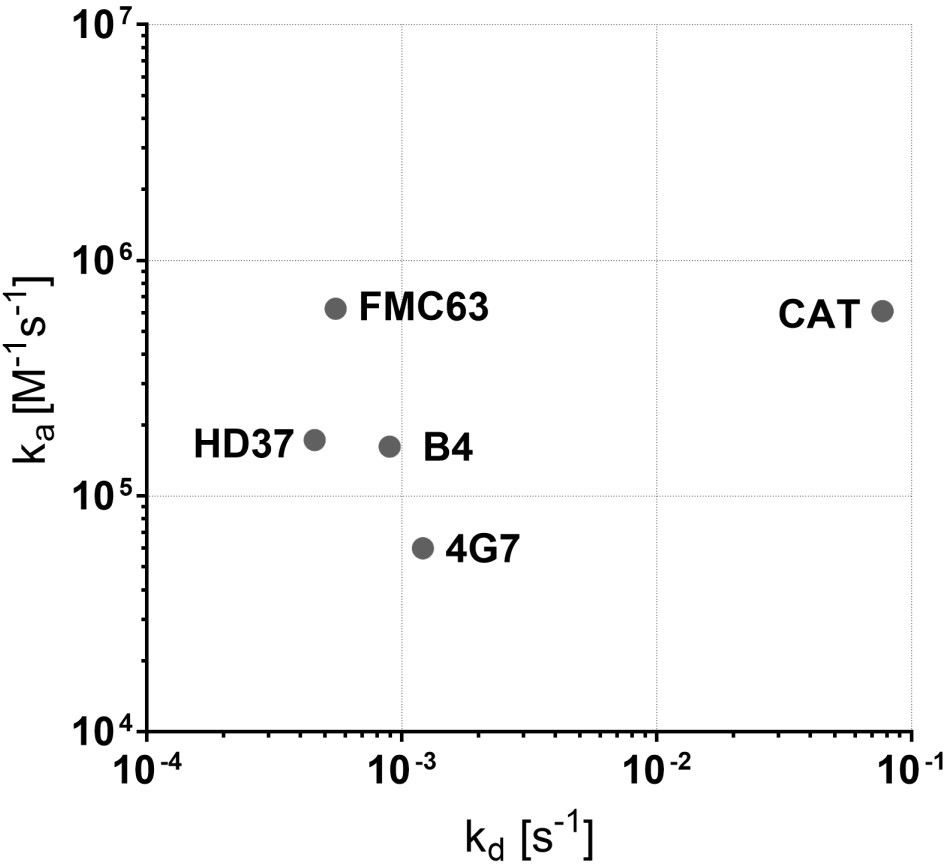

Figure 3.2: **Kinetic binding constants of anti-CD19 scFv-fcs determined by SPR Biacore**

Constants plotted on a k_a versus k_d plot, showing the interactions of the different scFvs, derived from anti-CD19 hybridomas, with recombinant soluble CD19 protein. K_D values were calculated according to equation 3.1 and ranged from 8.8e-10 to 1.1e-7

scFv	**On-rate k_a** ($M^{-1}sec^{-1}$)	**Off-rate k_d**(sec^{-1})	**Dissociation constant K_D** (nM)
HD37	$1.73e^{+05}$	$4.55e^{-04}$	2.63
B4	$1.62e^{+05}$	$8.96e^{-04}$	5.52
FMC63	$6.24e^{+05}$	$5.50e^{-04}$	0.881
CAT	$6.09e^{+05}$	$7.07e^{-02}$	116
4G7	$6.01e^{+04}$	$1.21e^{-03}$	20.1

Table 3.1: **Kinetic binding variables of anti-CD19 scFv-fcs determined by Biacore kinetic screening**

Kinetic and equilibrium dissociation constants of the CD19 binders derived from HD37, B4, FMC63, CAT & 4G7 hybridomas

3.2.2 Investigation of the affinity of FMC63, 4G7 and CAT scFv-fc by Scatchard analysis

Since SPR assays are based on recombinant protein binding, we sought to cross-reference the binding data of FMC63, 4G7 and CAT in scFv-fc format by flow cytometry, based on their distinct kinetic properties. For this experiment the affinity against target cells that naturally express CD19 on their cell surface (Raji) was measured. The conventional method for measuring the affinity of an antibody for a surface antigen is by Scatchard analysis. Scatchard analysis is a method of linearizing data from a saturation binding experiment in order to determine binding constants. One creates a secondary plot of specific binding/free ligand concentration (y-axis) vs. specific binding (x-axis). The slope of this line equals -1/K_D. Scatchard analysis revealed an affinity of the different scFv-fcs to $CD19^+$ Raji cells that reflected our SPR results, again showing a $>$ 100 fold reduction in binding strength of CAT scFv-fc compared to FMC63 scFv-fc (fig 3.3 B-D).

$CD19^+$ target cells, Raji cells ($1x10^6/ml$) were serially diluted and incubated with different concentrations of anti-CD19 scFv-Fc, and allowed to equilibrate, prior to flow cytometric analysis of scFv-Fc binding to the cells. The Scatchard analysis, as shown in figure 3.3, showed that FMC63 scFv-Fc bound to CD19 on Raji cells at significantly lower concentrations ($< 5x10^{-10}M$) than 4G7 and CAT. For FMC63 and 4G7 binding plateaued at $2.5x10^{-9}M$ and $1x10^{-8}M$ respectively. No such saturation of binding was seen with CAT, which is indicative of a high K_D value or low affinity. A non-linear regression analysis was performed to fit the curve and determine K_D values.

Although the absolute K_D values obtained using either SPR Biacore of Scatchard methods, are not directly comparable, having been derived differently measuring the binding between different compounds, these results do confirm that the relation between the affinities of the different scFv-fcs, showing a $>$ 100 fold difference between FMC63 and CAT, as measured by Biacore, seems to be similar, when targeting an antigen on the cell surface (FMC63 scFv-fc SPR 0.88 nM vs

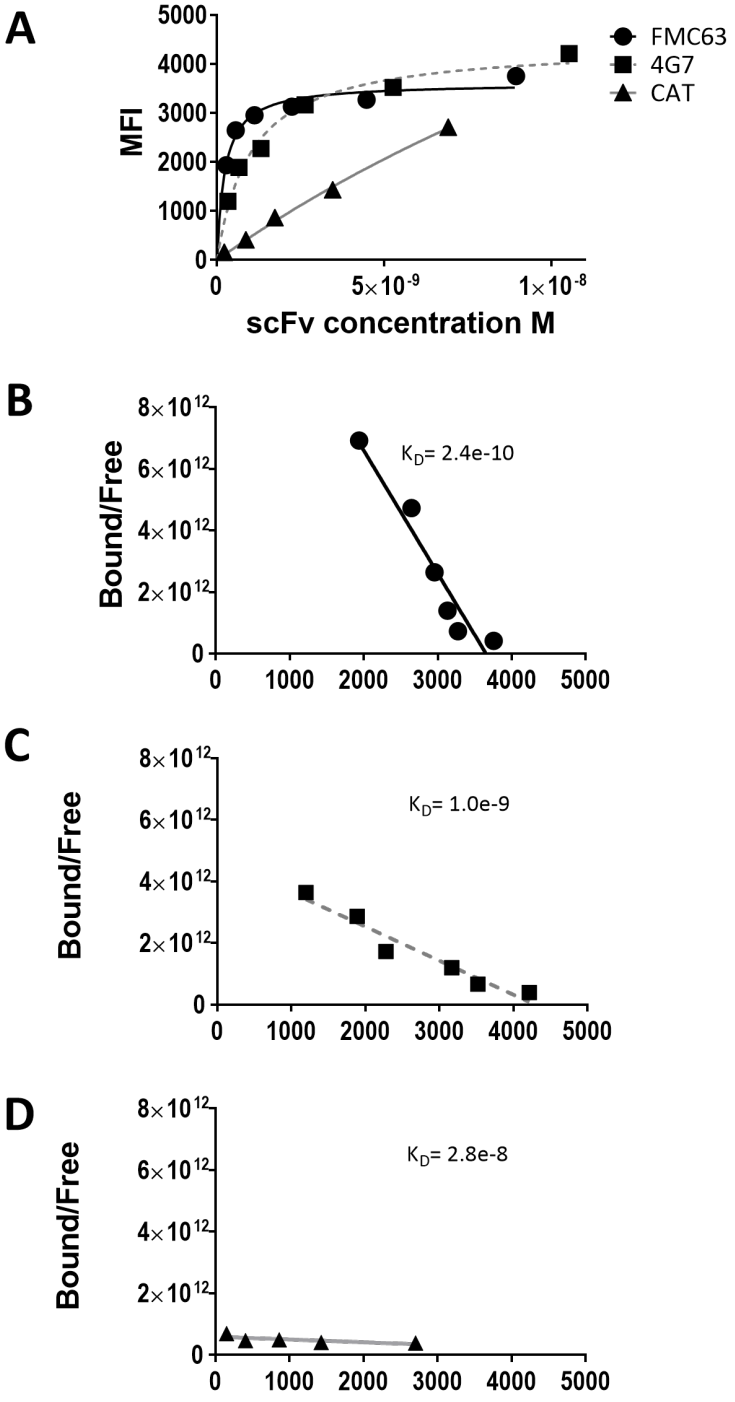

Figure 3.3: **Determination of affinity of FMC63, 4G7 and CAT scFv-fcs for cell-bound CD19 using Scatchard analysis**

Scatchard analysis is a method of linearizing data from a saturation binding experiment in order to determine binding constants. The slope of the straight line equals $-1/K_D$ from which K_D was calculated.(A) Saturation Binding Curves. Scatchard of (B)FMC63 scFv-Fc (C) 4G7 scFv-Fc (D) CAT scFv-Fc

Scatchard 0.2nM, 4G7 scFv-fc SPR 20nM vs Scatchard 1nM and CAT scFv-fc SPR 116nM vs Scatchard 28nM).

3.2.3 Binding of CAT and FMC63 scFv-fc to truncated protein isoforms of CD19

The distance between the CAR-bound epitope and the target cell membrane influences the synapse formation between the CAR-expressing T cell and target. CD19 is a 95-kDa transmembrane glycoprotein of the immunoglobulin superfamily containing two extracellular immunoglobulin(IgG)-like domains and an extensive cytoplasmic tail. We constructed the full length peptide and three variants with increasing truncation of CD19 (Δ ex2, Δ ex2-3, Δ ex2-3-4), including a V5 tag under the signal-peptide (Fig. 3.4). The V5 tag allowed us to verify if the protein was expressed on the cell surface, which had to be confirmed prior to study potential binding of our different scFv-fcs to the truncated isoforms of CD19. The truncated CD19 isoforms were expressed on 293T cells by transient transfection. In addition, transgene expression was identified by GFP expression.

In the study by Sotillo *et al.* two isoforms were described, Δ ex2 and Δ ex5-6. Δ ex5-6 is completely cytosolic, lacking both transmembrane and extracellular domains. In addition, they reported that the Δ ex2 CD19 isoform is also largely cytosolic, unlike full-length CD19, which localizes exclusively to the plasma membrane [95], but based on confocal microscopy protein/cell membrane co-localization scoring a small fraction (less than 10% of total) did appear to make it to the cell membrane.

By flow cytometry we were unable to detect any of the truncated isoforms expressed on the cell membrane, despite demonstration of successful transfection on the basis of GFP expression, as shown in the upper row of figure 3.6. Western blot analysis of the total cell lysates expressing the different isoforms confirmed presence of the protein (Fig. 3.5). We therefore repeated the staining for V5, this time on permeabilized cells and, albeit at low levels, were able to detect V5, as shown in the lower row of figure 3.6. This was important for further analysis of the binding of FMC63 and CAT scFv on the truncated isoforms of CD19, because it

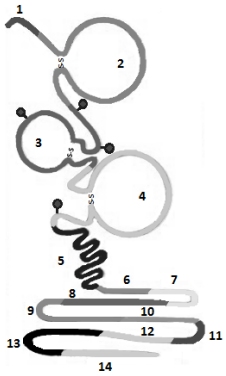

(a)

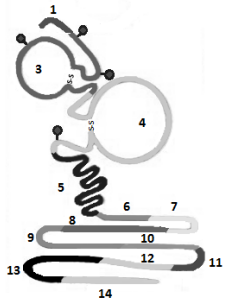

(b)

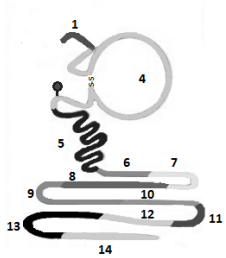

(c)

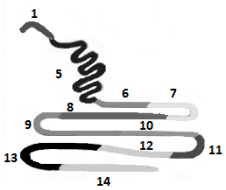

(d)

Figure 3.4: **CD19 truncated isoforms**

The truncated CD19 variants were expressed by 293T cells in order to investigate the binding epitope location of FMC63 and CAT scFvs. The predicted CD19 proteins encoded by the full-length (FL) (A) and the truncated Δex2(B), Δex2-3(C), Δex2-3-4(D) isoforms of CD19. The epitope recognized by CD19-CAR T cells is encoded by a sequence contained within exons 1-4. The transmembrane domain is encoded by exons 5 and 6.
Adapted from [95]

confirmed presence of the protein at least in the cytosol. The 293T cells were again permeabilized and we performed binding studies on truncated variants of CD19. By a secondary staining, targeting the murine Fc component of the scFv-Fcs, binding of both FMC63 and CAT scFv-fc to wild type CD19 showed 16.8% and 16.1% dual positivity respectively (exon 2, Fig. 3.7). Of note, the higher MFI of FMC63 scFv (MFI 3651, in figure 3.7 as compared to CAT scFv (MFI 1372) is in line with the previous Scatchard analysis discussed in section 3.2.2, confirming higher levels of binding of FMC63 to CD19 and consistent with its higher affinity. No binding of either FMC63 or CAT scFv-Fc to exon 2 truncation mutants was seen, suggesting both bind this region of CD19.

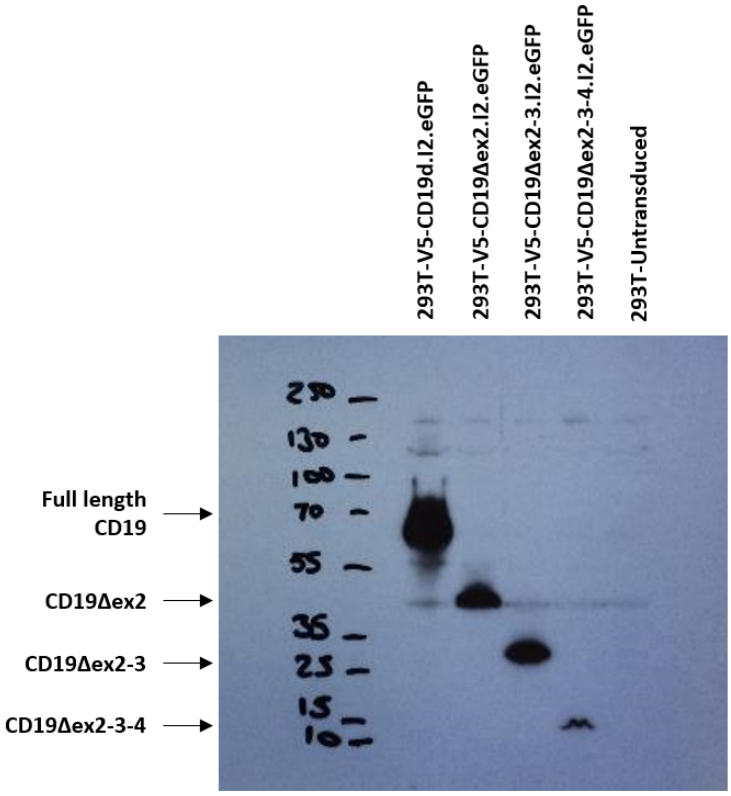

Figure 3.5: **Western Blot of CD19 truncated isoforms transiently expressed on 293T cells.**

Western blot analysis of lysed 293T cells confirmed presence of the different truncated isoforms of CD19. Bands represent detection of protein by binding of aV5 antibody. Sizes corresponded to expected length of glycosylated protein [95]

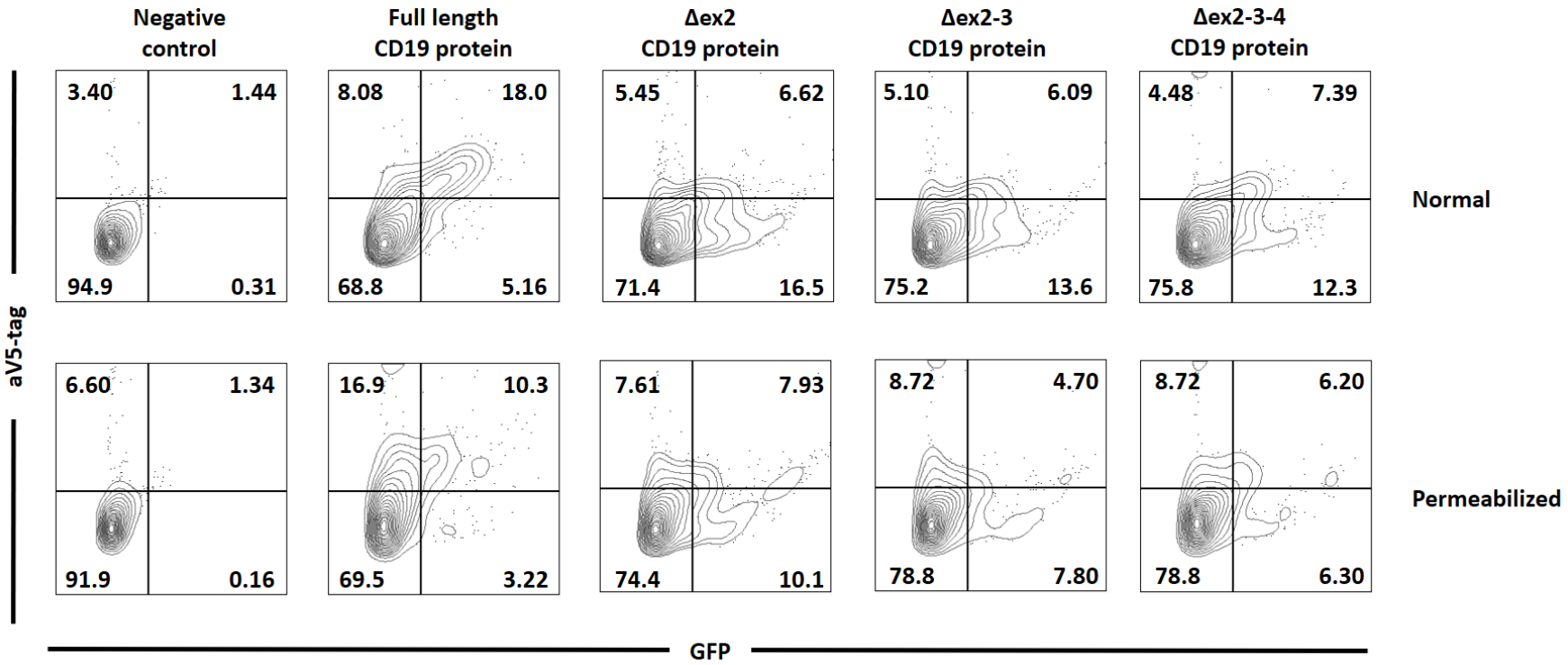

Figure 3.6: **Expression of CD19 truncated isoforms by 293T cells**

Expressed are the full length peptide and three variants with increasing truncation of CD19 (Δ ex2, Δ ex2-3, Δ ex2-3-4), including a V5 tag under the signal-peptide. The V5 tag allowed verification of cell surface expression of the protein had, necessary to study potential binding of our different scFv-fcs to the truncated isoforms of CD19. In addition, transgene expression was identified by GFP expression.

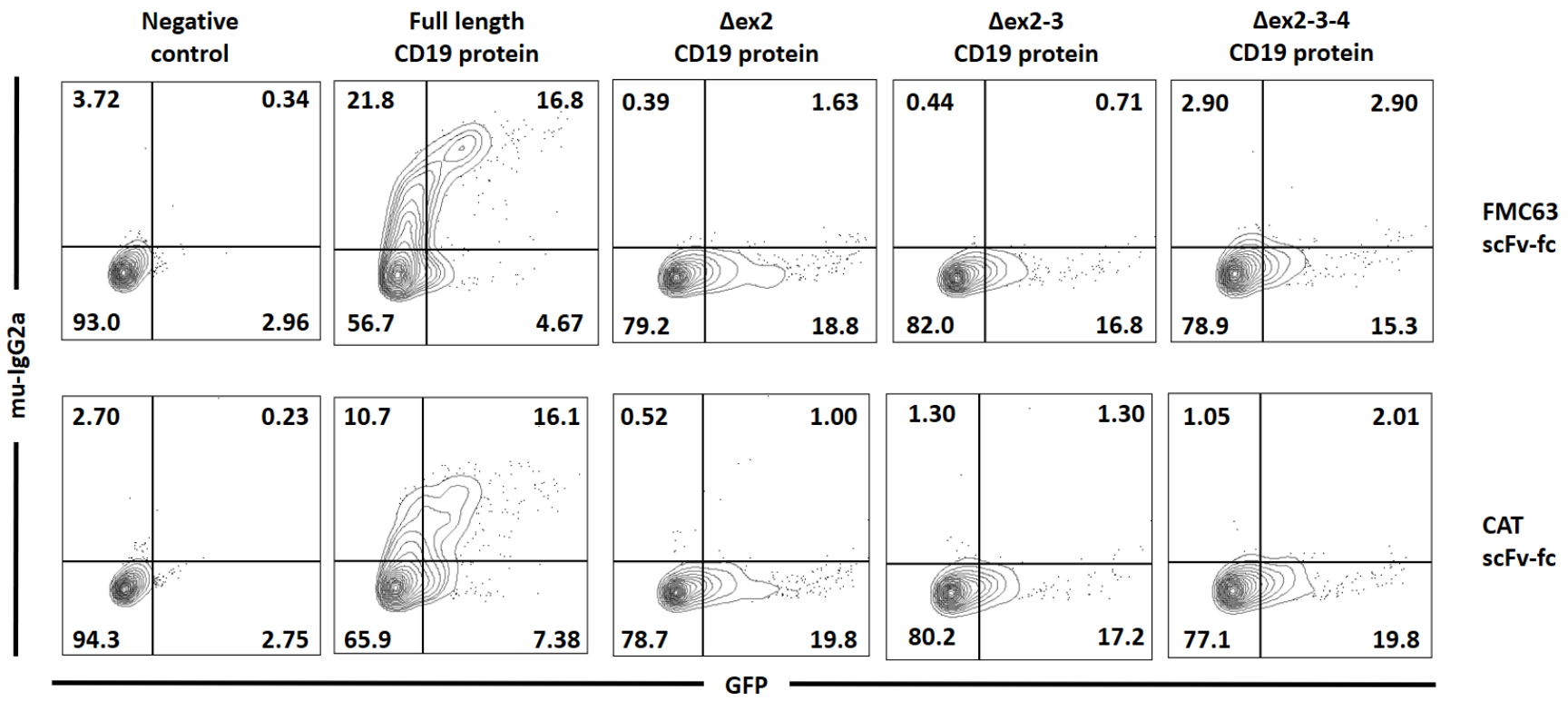

Figure 3.7: **Binding of FMC63 and CAT scFv to CD19 truncated isoforms as determined by intracellular staining with scFv-fcs and detection with a secondary anti-murine fc antibody**

Binding of FMC63 and CAT scFv to CD19 truncated isoforms as determined by intracellular staining with scFv-fcs and detection with a secondary anti-murine fc antibody.

3.3 Discussion

In chapter 1, we highlighted that in natural T cell interactions the binding and interaction of the TCR with a specific pMHC is pivotal in regulating the activity and specificity of the T cell. Although higher affinity interactions increase specificity for a ligand, a threshold of affinity has been described, as T cell functional avidity can be detrimentally affected when dissociation is prolonged [31]. In contrast to the natural TCR, CARs employ a different mechanism by which they recognize antigens in an MHC-independent manner. CARs, through their scFv, recognize membrane-bound cell surface antigen typically with a much higher affinity (KD= 80-1 nM) compared to TCR-pMHC affinity (KD=10-1 μM) [143], and are commonly derived from high affinity monoclonal antibodies (mAbs) cloned from hybridomas.

To date, different scFvs targeting CD19 have been used in CARs taken forward in clinical trials. Relative to the previously published affinities of different binding domains used in CAR design, typically ranging between 1-10nM, 4 out of 5 of our CD19 binding domains show similar binding strengths, ranging between 0.8-20nM. We have generated a novel CD19-CAR, derived from a different murine anti-human CD19 hybridoma (CAT CAR) [161]. CAT scFv has a fast on-rate, forming a similar amount of complexes per second with CD19 compared to FMC63, however displaying a much quicker off-rate, releasing off its target in only a matter of seconds, resulting in a much lower affinity of 118nM.

Although some studies have addressed the impact of binding domain affinity on CAR T cell functionality [146, 147, 151, 152], none of these binding domains were reported to have such a quick off-rate. In addition, the fact that CAT scFv on-rate is very similar to FMC63 scFv gives us the unique opportunity to specifically study the impact of the dissociation constant on CAR T cell functional avidity.

Binding of CAT and FMC63 scFv-fc to truncated protein isoforms of CD19 expressed by 293T cells show both bind to an epitope contained within exon 2. This suggests that differences in synapse width are unlikely to contribute to differences in response of T cells bearing the FMC63 or CAT CARs.

We were unable to stably express the CD19 truncated isoforms on the cell surface, but instead showed these proteins were located in the cytosol. After personal communication with Elena Sotillo [95], one possible explanation for their observed "expression" of CD19 truncated isoforms on the cell surface was the use of an expression vector that resulted in unphysiological high expression levels, that may have resulted in leakage of the protein from the cytosol to the cell surface. This has significant clinical relevance, as the frameshift mutations clustered in the non-constitutive exon 2 eliminate full-length CD19, but allow expression of the Δ ex2 isoform in the cytosol, as a result, the mutated CD19 cannot be effectively targeted by CAR T cell immunotherapy because of its general restriction to targeting of cell surface molecules.

Chapter 4

In vitro characterization of FMC63-CAR$^+$ and CAT-CAR$^+$ T cells

4.1 Introduction

In chapter 3 we characterised the binding affinities of scFvs derived from 5 anti-CD19 hybridomas (FMC63, CAT, 4G7, HD37, B4). The influence of the affinity and differing binding kinetics of different CD19-binding domains on the downstream CAR T cell functionality in response to CD19$^+$ targets has not yet been delineated. We next sought to investigate the impact of scFv affinity, on CAR T cell function *in vitro* and in particular of the off rate, by incorporating different anti-CD19 scFvs into an identical second generation 41BBZ CAR backbone, as illustrated in figure 4.1. We focused particularly on FMC63 and CAT as we have shown that these bind epitopes expressed on exon 2 of CD19 with distinct affinities and binding kinetics (Figure 3.7 and section 3.2.3). The fact that the difference in affinity between CAT and FMC63 (K_D FMC63 0.881nM and CAT K_D 116nM) is solely contributed to by an increased off rate (k_d FMC63 $5.5x10^{-4}$ and k_d CAT $7.07x10^{-2}$) in the setting of a near identical on rate (k_a FMC63 $6.24x10^5$ and k_a CAT $6.09x10^5$) provided an opportunity to dissect the relative contributions of these binding variables to downstream CAR T cell function.

4.1.1 Aims

- To investigate the impact of scFv affinity, and in particular of the off rate, by incorporating FMC63 and CAT anti-CD19 scFvs into an identical second generation 41BBZ CAR backbone.
- To phenotypically characterize T cells transduced with the different affinity CD19 CARs.
- To investigate CAR^+ T cell functional responses, using *in vitro* functional assays, studying proliferation, differentiation, target cell killing, and the production and secretion of effector cytokines.
- To perform live cell imaging, to investigate the impact of differences in CAR affinity on interactions between CAR T cells and their targets on a microscopic level.

4.2 Results

4.2.1 Expression of Chimeric Antigen Receptor is identified by transgene expression and binding to recombinant CD19 soluble protein.

Second generation CARs differing only in their aCD19 scFv, from either the FMC63 or CAT hybridoma, linked to a CD8 transmembrane domain, a CD137 (4-1BB) costimulatory domain, and a CD3 ζ-signalling domain were expresssed in primary human T cells by lentiviral transduction after activation with CD3/CD28 beads (detailed description in section 2.2.2.7). Figure 4.1 shows the schematic representation two different anti-CD19 scFvs into an identical second generation 41BBZ CAR backbone.

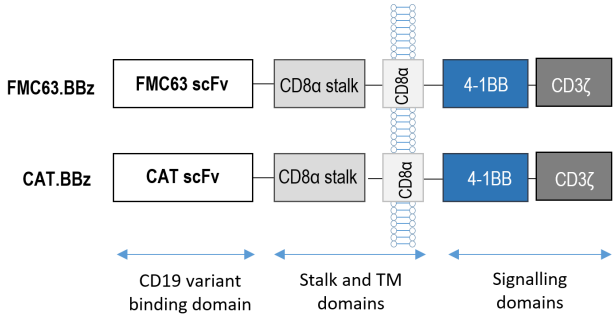

Figure 4.1: **Schematic representation of anti-CD19 CAR**

Both constructs contain an aCD19 scFv, from either the FMC63 or CAT hybridoma, a CD8 transmembrane domain, a CD137 (4-1BB) costimulatory domain, and a CD3 ζ-signalling domain.

We first sought to evaluate the surface expression of CAR on T cells after transduction using the pCCL.PGK lentiviral vector. The pCCL-aCD19 scFv-41BBZ lentiviral vector encodes the pCCL lentiviral backbone, in which the enhancer and promoter of CMV are joined to the R region of HIV-1 and the aCD19 scFv-41BBZ CAR. A schematic representation of the vector is given in figure 2.1. The mCherry gene was coexpressed with CAR by cloning it upstream of the CAR separated by an in-frame 2A ribosomal skipping sequence.

Transduction efficiency was found to be donor dependent, ranging from 20-60% as assessed by mCherry expression. Representative FACS plots illustrating the two detection methods used to determine transduction efficiency of FMC63 and

CAT CAR constructs are displayed in figure 4.2. CAR expression was detected by binding to a recombinant CD19 protein-Fc construct and correlated well at a 1:1 ratio with mCherry consistent with the presence of an in-frame 2A ribosomal skipping sequence [162]. As expected, the mean fluorescence intensity (MFI) for FMC63 was higher than for CAT with the tagged CD19 protein, whereas mCherry expression was similar.

In order to ensure differences seen resulted only from the differing binding kinetics of the CARs, we corrected the number of CAR transduced T cells, taking into account relative transduction efficiency when the difference between constructs exceeded 10%. Donor-matched non-transduced cells were therefore added, to normalise transduction efficiency to the lowest transduction level in all constructs in all *in-vitro* assays, as per published protocols [154]. Transgene expression levels were comparable between the two constructs, showing no significant difference in mCherry MFI (fig. 4.3) (MFI FMC63 2476, MFI CAT 2132 in representative FACS plot), but a lower MFI for rCD19 in CAT CAR, in accordance with its lower affinity for CD19 (MFI FMC63 7680, MFI CAT 4831). As CAR T cell avidity is influenced by the receptor expression density, it was critical to establish comparable levels of CAR expression in both constructs compared.

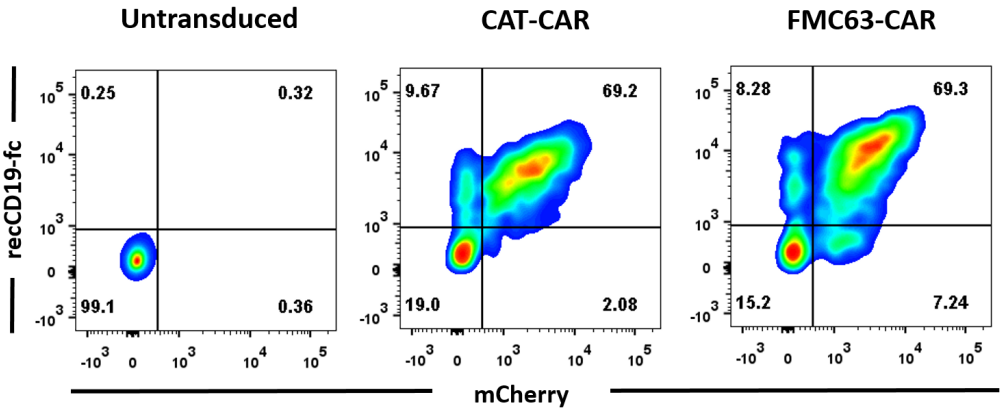

Figure 4.2: **Transduction efficiency of activated CD3/CD28 bead-expanded human T cells**

Transduction efficiency of PBMCs lentivirally-transduced to express FMC63 and CAT CAR constructs. The panel shows detection of CAR using mCherry transgene expression and a recombinant CD19 protein with an Fc tag construct. Data are representative of >20 independent experiments. (Median fluorescence intensity (MFI) of mCherry FMC63 2476, CAT 2132. MFI for rCD19 FMC63 7680, MFI CAT 4831 in representative FACS plot).

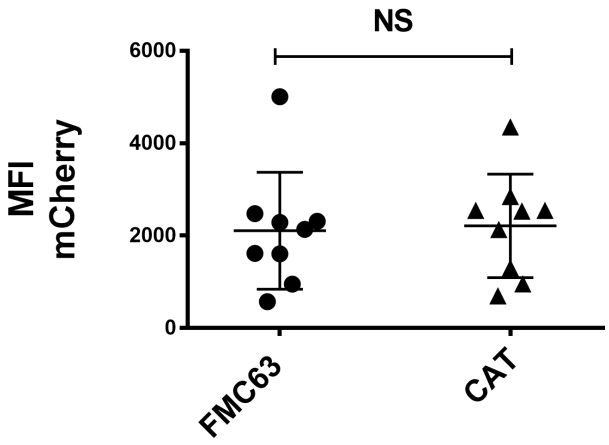

Figure 4.3: **mCherry transgene expression levels of FMC63 and CAT CAR-transduced T cells measured by flow cytometry**

MFI of mCherry transgene expression levels of FMC63 and CAT CAR-transduced T cells was determined 7 days-post transduction by flow cytometry,statistical comparisons were made with a two-tailed paired Student t-test, NS = not significant, n=9

4.2.2 Phenotype of T cells transduced with FMC63 and CAT CAR

To determine if the different affinity binding domains impacted T cell phenotype, we analysed CAR transduced T cells for their expression of CD45RA and CCR7 as markers for differential memory subsets, as illustrated in figure 4.4. Human T cells can be divided into at least four different subsets, based on their phenotype and functions: naive (T_{naive}, CCR7+ CD45RA+) and central memory (T_{CM}, CCR7+ CD45RA-) T cells display high proliferative potential and lack of an immediate effector functions whereas effector memory (T_{EM}, CCR7- CD45RA-) and $CD45RA^+$ effector memory (T_{EMRA}, CCR7- CD45RA+) T cells have low proliferative capacities but produce cytokines and exert cytotoxic activity, respectively [163]. $CD45RA^+$ effector TEMRA cells represent the most differentiated type of memory cells and have a high susceptibility to apoptosis. From a TCR perspective it is known that TCR affinity and $t_{1/2}$ of the pMHC-TCR interaction influence memory fate [164] and effector memory T cells are favoured by strong TCR signalling [165]. It has recently been shown that the proliferative capacity of memory $CD8^+$ T cells following antigen clearance progressively increases with time both in the T_{CM} and T_{EM} subpopulations, but is most prominent among T_{CM} cells [166]. Which T cell subsets should be utilized for adoptive immunotherapy has been debated for many years. T_{CM} however have been associated with long-term CAR^+ T cell therapeutic efficacy due to their ability to achieve long-term persistence *in vivo* and a greater proliferative capacity upon antigen-reencounter[166].

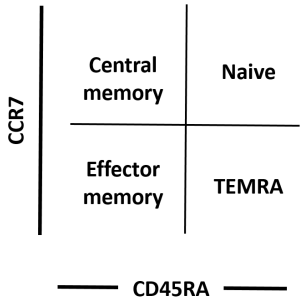

Figure 4.4:
Characterization of T cell memory compartments

We hypothesized that prolonged antigen ligation in FMC63 CAR transduced T cells could lead to a more pronounced differentiation into T_{EM} cells and potentially T_{EMRA} cells. To investigate this, T cells were rested for 8 days following transduction, after which they were stimulated with irradiated $CD19^+$ target cells (Raji) at a 1:1 ratio and kept in culture for another 7 days, without further addition

of cytokines. Representative FACS plots of the different memory compartments identified are displayed in figure 4.5. The difference in scFv did not result in an alteration of the proportion of effector memory and central memory T cells found after *in vitro* expansion in the presence of antigen, as shown in figure 4.6. To determine the effect of proliferation on the different memory compartments after antigen specific stimulation, T cells transduced with FMC63 or CAT CAR were compared by absolute number in each compartment (T_{CM}: FMC63 $5.6x10^5 \pm 1.9x10^5$, CAT $6.4x10^5 \pm 2.0x10^5$; T_{EM} $3.6x10^5 \pm 1.2x10^5$, CAT $3.9x10^5 \pm 9.2x10^4$). In contrast, there was limited persistence and proliferation of untransduced T cells following stimulation. Collectively, these data suggest that FMC63 and CAT CAR^+ T cells, co-cultured with $CD19^+$ targets, demonstrate proliferation upon antigen specific stimulation and equivalent proportions of central and effector memory phenotype T cells, suggesting that prolonged binding of FMC63 CAR T cells to CD19 target *in vitro* does not lead to differentiation into a more terminally differentiated phenotype.

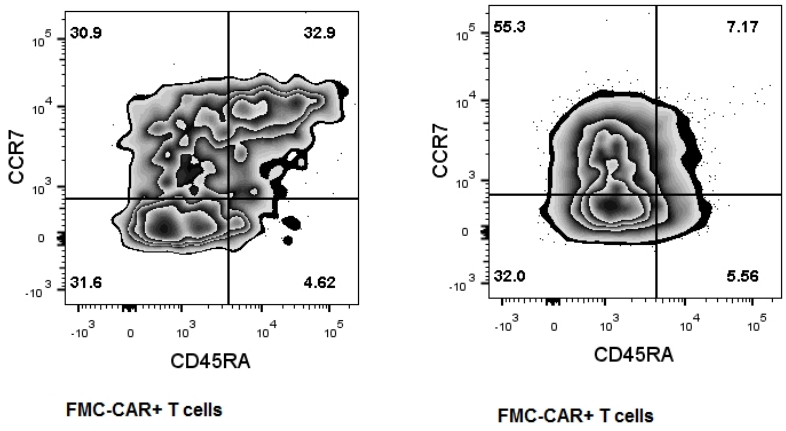

(a) (b)

Figure 4.5: **Representative FACS plots of CAR^+ T cell memory compartments analysed by flow cytometry**

Distribution of CAR^+ T cells between the different memory T cell subsets at 7 days post activation with irradiated $CD19^+$ target cells (Raji) at a 1:1 ratio. Representative FACS plots of 3 independent experiments in 5 different donors show (A) CAR^+ T cell phenotype eight days post-transduction without antigen stimulation (B)$CD19^+$ antigen stimulated CAR^+ T cell phenotype, 7 days after stimulation, without any further addition of cytokines.

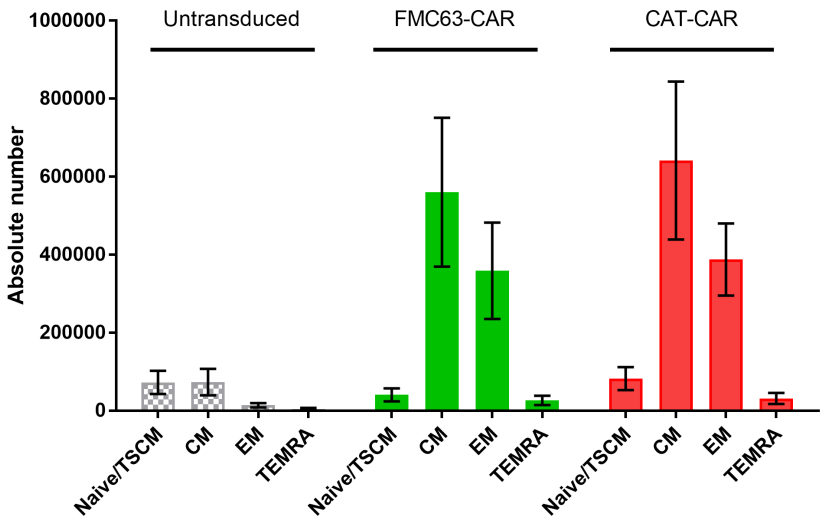

Figure 4.6: **Distribution of absolute numbers of CAR$^+$ T cells within different memory subsets 7 days post stimulation**

Eight days post transduction $1x10^5$ CAR$^+$ T cells and untransduced T cells were stimulated with irradiated Raji cells at a 1:1 ratio and left in culture for another 7 days, without addition of cytokines. Absolute number of T_{CM}: FMC63 $5.6x10^5 \pm 1.9x10^5$, CAT $6.4x10^5 \pm 2.0x10^5$; T_{EM} $3.6x10^5 \pm 1.2x10^5$, CAT $3.9x10^5 \pm 9.2x10^4$. Data represented as mean $\pm SEM$, n=4

4.2.3 Antigen induced receptor downregulation

The serial triggering model of TCR stimulation is based on the assumption that one pMHC sequentially engages several TCR molecules to obtain a threshold for T cells activation [31]. Rapid downregulation of the endogenous TCR can occur during the process of activation, within the time scale of $1/k_{off}$, and is considered a parameter for TCR occupancy and serial triggering, which is influenced by the strength of TCR binding and relates to biological response [34, 167, 168]. CAR downregulation has also been described, but the effect of affinity on CAR downregulation is unknown [77, 145].

On the assumption that the quick off rate of CAT-CAR$^+$ T cells would benefit serial triggering we sought to determine the propensity for antigen-induced CAR downregulation. To investigate this, CAR$^+$ T cells were co-cultured with CD19$^+$ Raji cells and CD19$^-$ SupT1 NT and CAR expression was analysed 7 days after the start of co-culture. Density of CAR expression, represented by MFI, was measured by flow cytometry as shown in figure 4.7. Our data show that whereas expression of the two CARs was comparable following stimulation with CD19$^-$ SupT1 NT cells, following stimulation with Raji, T cells expressing CAT CAR demonstrated a reduction in MFI at 7 days post-co-culture relative to FMC63 CAR transduced T cells, (MFI anti-rabbit Fc FITC following Raji stimulation: CAT transduced cells 1164 $\pm$ 181.2, FMC63 transduced cells 1981 $\pm$ 263.6). These results suggest that the greater receptor (CAR) downregulation in T cells expressing CAT CAR compared to FMC63 may reflect a greater propensity for serial triggering, which we would hypothesise may be related to its faster off-rate. In contrast, CAR expression after co-culture with a CD19 negative target remains unchanged and was not significantly different between the CAR T cell populations demonstrating this effect is dependent on interaction of the scFv domain with of CAR with CD19$^+$ antigen.

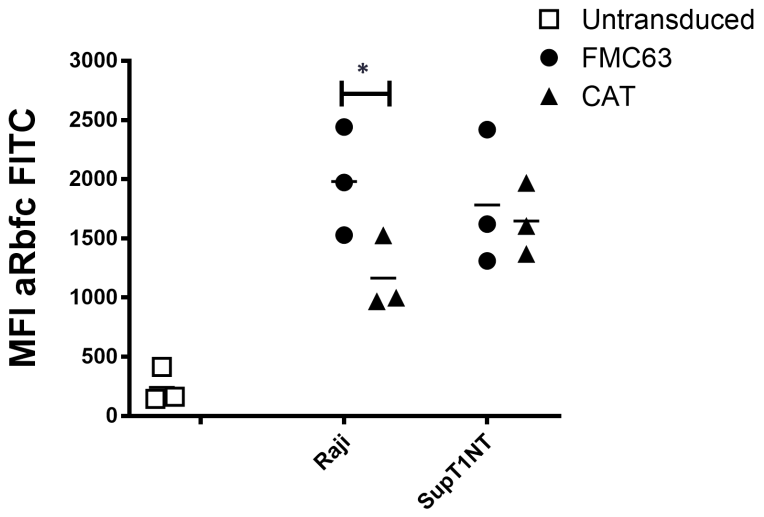

Figure 4.7: **CAR T cell surface expression of FMC63 and CAT CAR following CD19 antigen positive and negative stimulation**

CAR surface expression levels on T cells was determined following co-culture with $CD19^{+}$ and $CD19^{-}$ targets (Raji & SupT1 cells at 1:1 effector:target ratio) as determined by binding to rec-CD19-Rbfc protein, followed by a secondary anti-rabbit fc staining. MFI aRbfc FITC following Raji stimulation: CAT transduced cells 1164 $\pm$ 181.2, FMC63 transduced cells 1981 $\pm$ 263.6, Student t-test, n=3, * $p < 0.05$

4.2.4 Lower CAR affinity in the context of a faster off-rate does not result in reduced antigen-specific responses and is associated with enhanced proliferation

To investigate whether lower CAR affinity in the context of a faster off-rate would result in reduced antigen specific responses, we studied antigen specific proliferation of FMC63 and CAT CAR transduced T cells, and their production and secretion of effector cytokines.

4.2.4.1 Cytokine production

Differences in cytokine production may have important consequences both for the functionality of the CAR^+ T cells and toxicity when used clinically. To compare their functionality supernatants were harvested 48 hours after 1:1 stimulation of FMC63 and CAT CAR transduced T cells from the same donors (n=4) with Raji cells and analysed by cytokine bead array analysis. There was a significantly greater production of TNF-alpha (Mean concentration $\pm$ SEM: CAT CAR T cells: 750.7 $\pm$ 103.3 pg/ml, FMC CAR T cells: 292.1 $\pm$ 36.51 pg/ml, n=4, $p<0.01$) and a trend towards greater production of IL-2 in CAT CAR transduced T cells (Mean concentration $\pm$ SD CAT CAR T cells: 11156 $\pm$ 2777 pg/ml, FMC63 CAR T cells: 5501 $\pm$ 1285 pg/ml, n=4, p=0.11) (Fig. 4.8). T cell activation is associated with the release of pro-inflammatory cytokines. Following activation with CD3/CD28 dynabeads the CAR T cells have matured towards a Th1/Tc1 phenotype, as identified by the production of TNF-alpha, IFN-gamma and IL-2 [169]. This was seen in both CARs after CD19 specific activation by Raji cells. The greater production of TNF-a lpha and IL-2 may reflect enhanced activation as a result of serial triggering in CAT CAR transduced T cells.

4.2.4.2 ^{3}H-thymidine proliferation assay

To further investigate the impact of CAR binding affinity on the effector functions of the CAR T cells, we compared the antigen specific proliferative response, measured by ^{3}H-thymidine uptake after stimulation of CAR expressing T cell populations with two different cell lines that naturally express CD19 (Raji and NALM6)

in 5 donors. As illustrated in figure 4.9, 3 days after antigen stimulation, in the absence of exogenous cytokines, CAT CAR transduced T cells showed a significantly greater proliferative response to both $CD19^+$ targets (Mean CPM $\pm$ SEM: Raji: CAT CAR T Cells 63158 ± 7159, FMC63 CAR T cells 27582 ± 2776, n=4, $p<0.01$; NALM6: CAT CAR T cells 49237 ± 14006, FMC63 CAR T cells 13097 ± 4047). Taken together with the greater Th1 cytokine production observed this suggests T cells transduced with the low affinity CAT CAR may show enhanced functional avidity in response to $CD19^+$ targets.

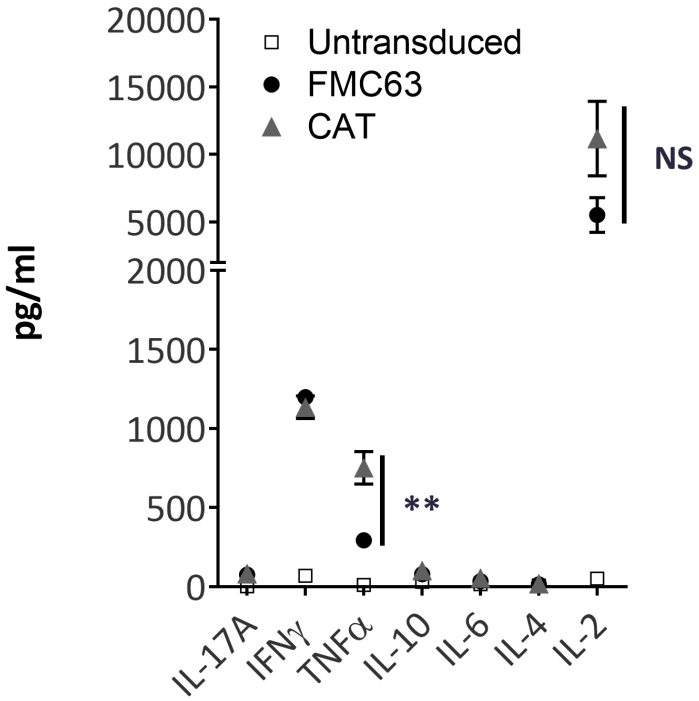

Figure 4.8: **Quantification of cytokine production by Cytokine Bead Array of FMC63 and CAT CAR$^+$ T cells following CD19$^+$ stimulation**

Production of cytokines in response to 1:1 co-culture with irradiated Raji cells measured by Cytokine Bead Array of culture supernatants taken at 48 hours. Data, mean ± SEM, n=4; **, P<0.01; NS, non= significant, statistical comparisons were made with a two-tailed paired Student t-test.

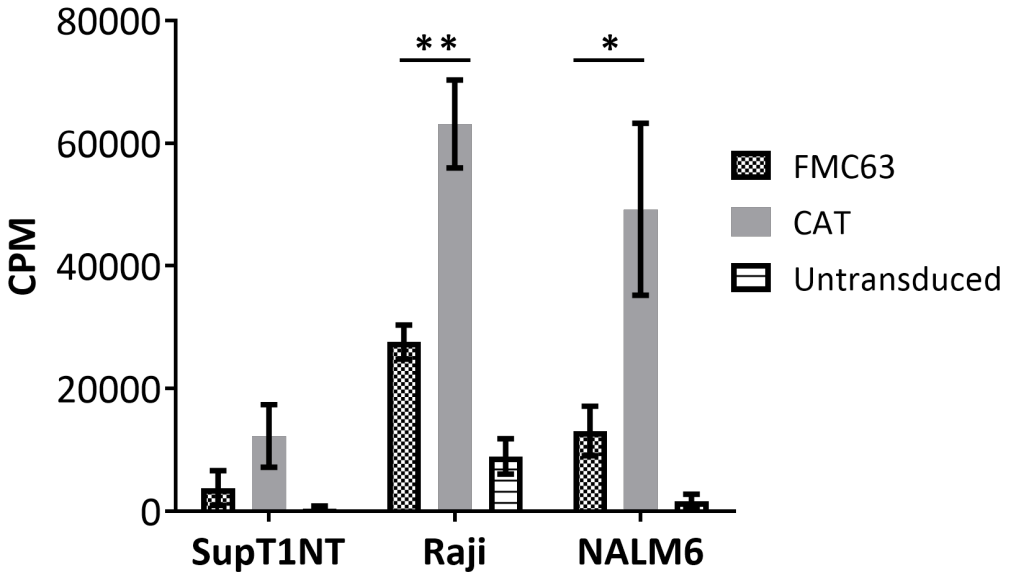

Figure 4.9: **CAT+ CAR transduced T cells exhibit enhanced functional avidity compared to FMC63 transduced T cells determined by proliferative response following CD19+ stimulation**

Proliferation, as measured by the incorporation of ^{3}H-thymidine following a 72 hour 1:1 co-culture with irradiated CD19 positive (Raji & NALM6) and CD19 negative (SupT1) cell lines. Data, mean $\pm$ SEM, n=5; *, $P<0.05$, ** $p<0.01$, statistical comparisons were made with a two-tailed paired Student t-test

4.2.5 Neither FMC63 nor CAT CAR transduced T cells exhibit an exhausted phenotype following CD19 specific stimulation

Although functional effector T cells can transiently express inhibitory receptors during activation, prolonged and/or high expression of multiple inhibitory/activation receptors is a key feature of the exhaustion of $CD8^+$ and $CD4^+$ T cells [170]. To assess the effect of CAR binding affinity on T cell exhaustion, we compared the expression of PD-1 and TIM3 on FMC63 vs CAT CAR transduced T cells from 5 donors 7 days after the start of a 1:1 co-culture with irradiated Raji cells. As shown in figure 4.10, the pattern of inhibitory-receptor co-expression was comparable between both FMC63 and CAT CAR transduced T cells. There was a small proportion of T cells expressing both PD1 and TIM3, which as a combination is indicative of exhaustion (FMC63 4.4% $\pm$ 1.3, CAT 7.4% $\pm$ 3.3, n=4). Single expression of both PD1 and TIM3 was also comparable (FMC63 PD1+ 17.2% $\pm$ 11.6, CAT PD1+ 19.3% $\pm$ 10.6; FMC63 TIM3+ 45.8% $\pm$ 24.3, CAT TIM3+ 37.8% $\pm$ 21.0). Singular expression of either PD1 or TIM3 alone may reflect activation of the CAR^+ T cells, following antigen specific stimulation.

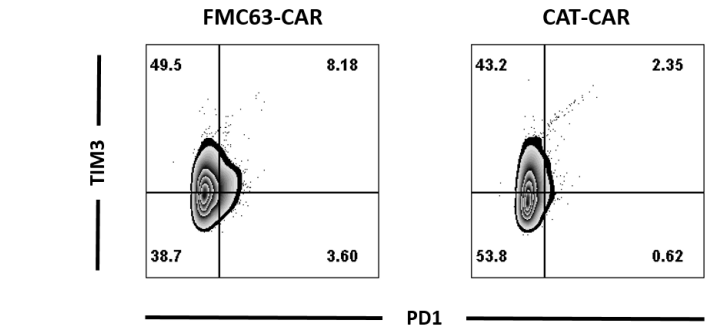

(a)

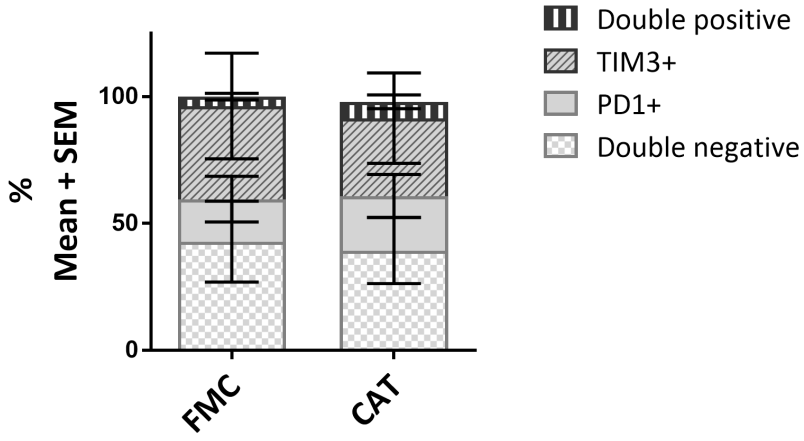

(b)

Figure 4.10: **Expression of activation/exhaustion markers on CAR transduced T cells following CD19⁺ stimulation**

Expression of activation & exhaustion markers 7 days after 1:1 stimulation with irradiated Raji cells measured by flow cytometry for PD1 and TIM3 gated on CAR+ T cells. (A) Representative FACS plots of PD1 and TIM3 expression on FMC63 and CAT CAR transduced T cells (B)Cumulative data on exhaustion marker expression analysed by flow cytometry. Data represented as mean $\pm$ SEM,$n = 5$

4.2.6 T cells transduced with a lower affinity anti-CD19 CAR demonstrate a greater cytotoxic capacity

To further characterize the antitumour activity of CARs, we assessed their ability to kill different tumour cell lines *in-vitro* using a standard 4hr ^{51}Cr release cytotoxicity assay in 5 donors. The target cell lines employed were a T cell lymphoma cell line (SupT1) that was engineered to express CD19 and Raji, a Burkitt lymphoma cell line that naturally expresses CD19. Resting transduced and non-transduced T cells were used as effector cells.

We observed CD19 specific cell lysis induced by both the FMC63 and CAT CAR$^+$ T cells, as shown in figure 4.11. However at all E:T ratios, the relative cytolysis of T cells bearing CAT CAR against SupT1 CD19 was greater than those bearing FMC63 CAR. This effect was more apparent at low E:T ratios (at 0.8:1 11% in FMC63 CAR T cells vs 20% in CAT CAR T cells).

The relatively small difference between the observed maximal lysis at an E:T of 0.4:1 (13%) and that observed at E:T of 0.8:1 (20%) may indicate that CAT+ T-cells lyse more than one target cell, and could potentially explain an improved ability to serially kill as compared to the high affinity binder FMC63. No lysis was observed with non-transduced T cells and similarly neither FMC63 nor CAT transduced T cells killed SupT1NT cells, demonstrating the antigen-specific nature of cytotoxicity.

A similar trend was seen against Raji cells, however unexpectedly, the cytotoxic activity of T cells transduced with both CARs against this cell line was significantly lower than anticipated. We have tried, by using freshly thawed cells and changing the passaging schedule of the cell line, to increase the chromium uptake of these cells, but this did not result in any improvement. As the cytotoxic activity was consistently low, after having repeated the assay multiple times, we hypothesized that the 4 hour incubation is insufficient for CAR T cells to effectively lyse the Raji cells. In a separate experiment where we co-cultured effectors and targets for 24 hours we showed that indeed CAR T cells transduced with either construct were able to effectively lyse Raji cells (data not shown).

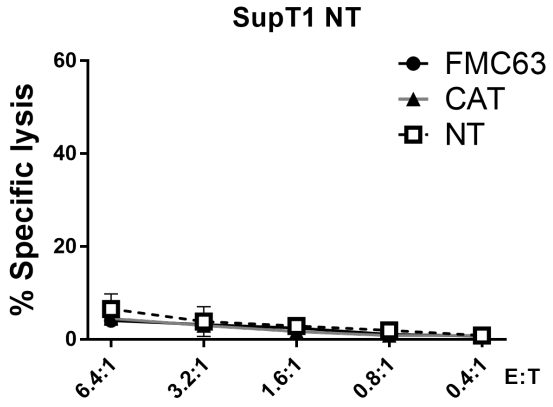

(a)

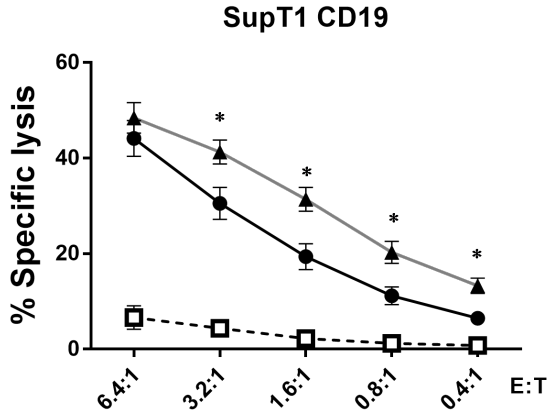

(b)

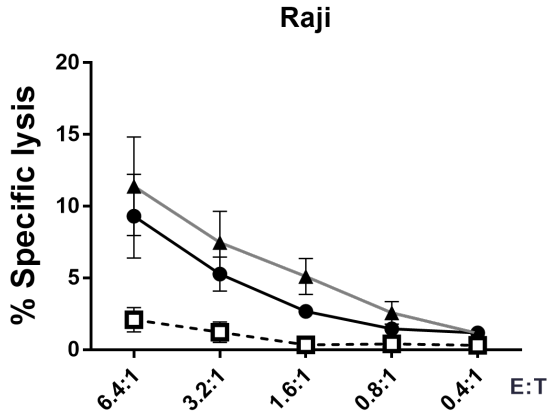

(c)

Figure 4.11: **CAR$^+$ T cells demonstrate efficacious and antigen-specific killing of CD19$^+$ tumour cells measured by standard 4-hour ^{51}Chromium release assay.**

CAR$^+$ T cell cytotoxic activity against (A) Target antigen negative supT1NT (B) SupT1 cells that are engineered to express CD19 (SupT1CD19) (C) Raji cells, a Burkitt lymphoma cell line that naturally expresses CD19 . Plots show mean % lysis SE, n= 5; *, P<0.05,statistical comparisons were made with a 2-way ANOVA.

4.2.7 Long term cytotoxicity assay

Given our findings of receptor downregulation, as an indicator of potential serial triggering in CAT CAR transduced T cells (as described in section 4.2.1), and the results of the ^{51}Cr release cytotoxicity assay, we hypothesised that changes in CAR affinity may not only result in serial triggering but also serial killing.

Indeed CAR T cells have been shown to serially kill multiple targets [171]. Davenport *et al.* show that at low E:T ratios the tumour cell killing rate was similar via TCR or CAR ligation over the first 20 hours of coincubation. However, from 20 to 50 hours, tumour cell death mediated through CAR became attenuated. They do not provide data on the binding affinity of the TCR or CAR compared in this study. We hypothesize though that the capacity of CAR transduced T cells to undertake serial killing may also be dependent on interaction half-time.

To test this hypothesis in the CAR transduced T cells, we set up a flow cytometry based cytotoxicity assay against two different cell lines: (i) NALM6, naturally expressing CD19, (ii) SupT1CD19LO, a cell line engineered to express CD19 at very low levels. Experimental parameters were altered by reducing the E:T ratio to 1:10, in order to uncover serial killing activity of multiple targets by CAR T cells, which might not otherwise be determined under standard conditions for cytotoxicity assay.

First, the absolute levels of CD19 expression on several cell lines were quantified, as displayed in figure 4.12. CD19 expression levels on SupT1CD19 LO cells are approximately 150-fold lower than the naturally expressing cell lines, NALM6, Raji and B-cells (Absolute CD19 mAb bound/cell: Raji 3014, NALM6 2285, B cells 3018, SupT1 CD19LO cells 140).

Next, FMC63 and CAT CAR transduced T cells were incubated with SupT1NT, SupT1CD19LO and NALM6 targets at a 1:1 and 1:10 E:T ratio for 24 hours, as illustrated in figure 4.13. Target cells were not irradiated, to try and mimic the natural situation where target cell proliferation may affect the CAR T cell cytotoxic capacity. As previously observed in the ^{51}Cr release assay, there was no killing of SupT1NT cells. Interestingly at a 1:1 ratio, both CAT and FMC

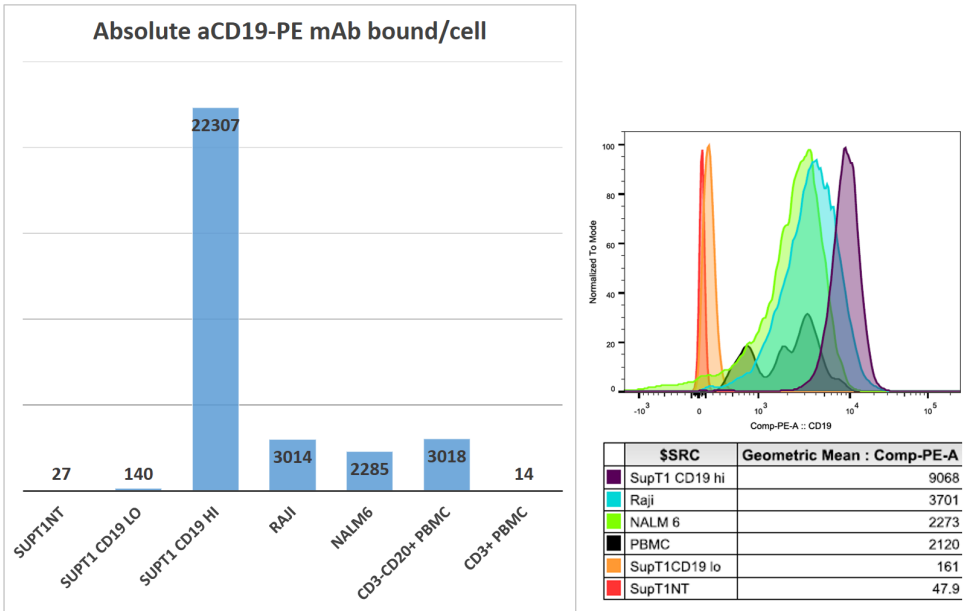

Figure 4.12: **PE-QuantiBRITE CD19 expression quantification of different cell lines**

CD19 expression levels were quantified, by the use of a PE-QuantiBRITE kit, on the following cell lines: SupT1NT: a CD19 negative T cell lymphoma cell line, SupT1CD19LO: a T cell lymphoma cell line engineered to express CD19 at very low levels, SupT1CD19HI: a T cell lymphoma cell line engineered to express CD19 at high levels, Raji: a naturally expressing Burkitt Lymphoma cell line, NALM6: a naturally expressing Acute Lymphoblastic Leukaemia cell line, CD3-CD20+PBMC: PBMC gated on CD20+ B cells, CD3+ PBMC: PBMC gated on CD3+ T cells

CAR transduced cells are able to effectively kill the majority of the NALM6 (Mean % remaining live fraction $\pm$ SEM: CAT 26.77 $\pm$ 9.472, FMC63 26.82 $\pm$ 11.17, n=8, p=0.84, as assessed with a non parametric paired t-test). Under more challenging conditions of reduced antigen density and/or low E:T ratios, the remaining live target cell percentage was consistently lower after incubation with CAT CAR transduced T cells than with FMC63 CAR T cells, but these results did not reach statistical significance, which may reflect donor-donor variability (SupT1CD19LO cells at a 1:1 ratio Mean % remaining live fraction $\pm$ SEM: CAT 21.08 $\pm$ 5.015, FMC63 28.57 $\pm$ 6.621,n=8, p=0.16, SupT1CD19LO at 1:10 ratio Mean % remaining live fraction $\pm$ SEM: CAT 67.98 $\pm$ 7.286, FMC63 84.23 $\pm$ 8.429,n=8, p=0.13, NALM6 at 1:10 ratio Mean % remaining live fraction $\pm$ SEM: CAT 38.61 $\pm$ 7.007, FMC63 51.23 $\pm$ 9.161, n=8, p=0.16). Thus, our data do not provide evidence for enhanced cytotoxicity against low expressing targets or serial killing of CAT CAR transduced cells compared to FMC63 CAR T cells.

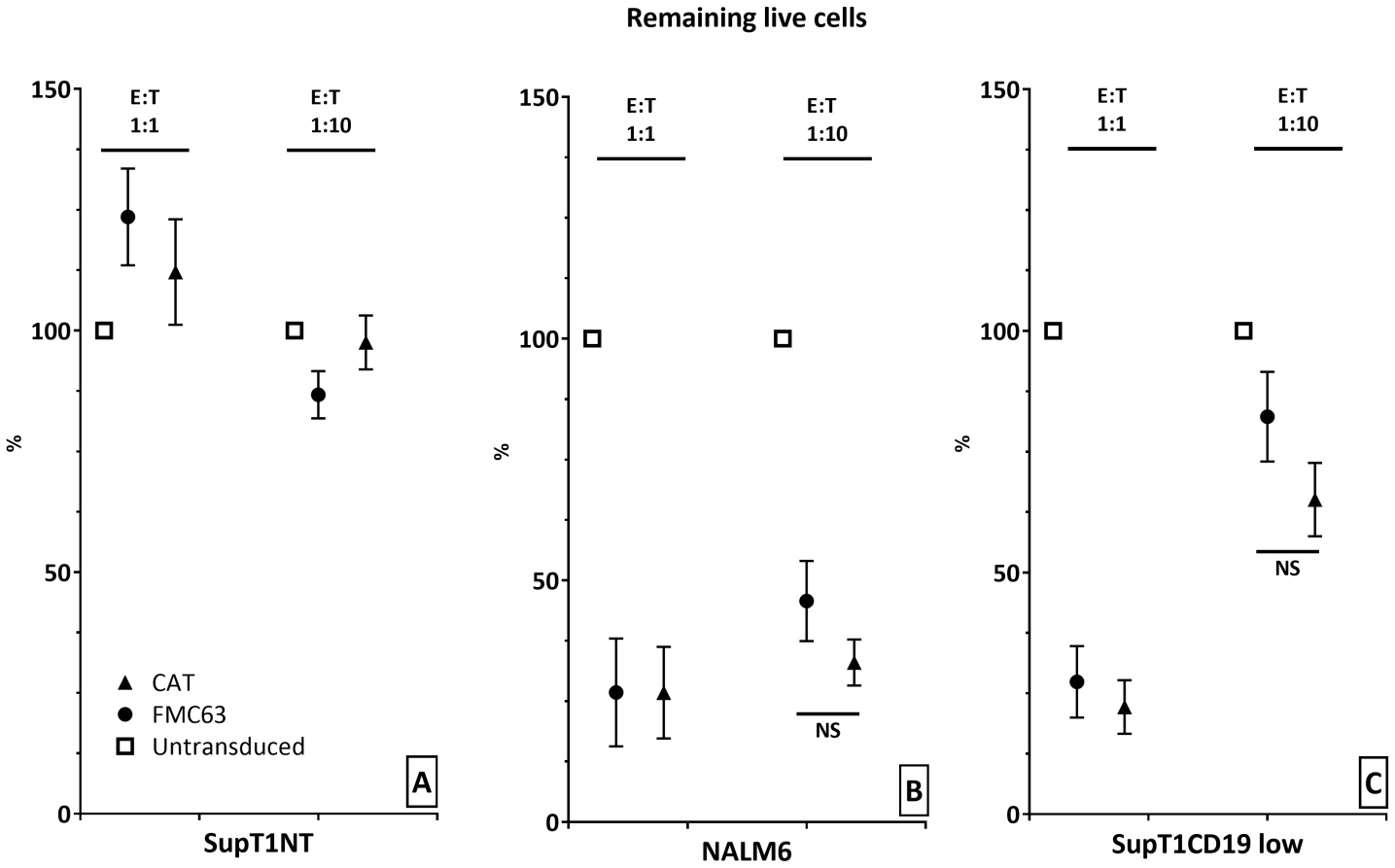

Figure 4.13: **24-hr Cytotoxicity assay by flow cytometry at 1:1 and 1:10 E:T ratio to investigate CAR T cell functional avidity**

CAR^+ T cells were incubated at 1:1 and 1:10 E:T ratios with non-irradiated target cells (SupT1NT, SupT1CD19LO and NALM6) for 24 hours. The remaining live cell fraction was calculated relative to the live cell fraction in the well co-cultured with non-transduced T cells. At a 1:1 ratio against NALM6 the Mean % remaining live fraction ± SEM was: CAT 26.77 ± 9.472, FMC63 26.82 ± 11.17, n=8, p=0.84. Against SupT1CD19LO the Mean % remaining live fraction ± SEM was: CAT 21.08 ± 5.015, FMC63 28.57 ± 6.621,n=8, p=0.16. At a 1:10 ratio against NALM 6 the Mean % remaining live fraction ± SEM was: CAT 38.61 ± 7.007, FMC63 51.23 ± 9.161,n=8, p=0.16. Against SupT1CD19LO the Mean % remaining live fraction ± SEM was: CAT 67.98 ± 7.286, FMC63 84.23 ± 8.429,n=8, p=0.13. Comparisons were analysed using Wilcoxon matched-pairs signed rank test (non-parametric paired t-test.)

4.2.8 Live cell imaging elucidates kinetic differences in effector-target interactions depending on CAR binding domain affinity

A study by Bousso and his group revealed that lower affinity pMHC-TCR interaction leads to a distinct kinetic profile and higher levels of motility of T cells, however when TCR stimulation reaches a certain threshold, T cells fully halt [172]. To investigate whether the low affinity interaction of CAT CAR resulted in differences in CAR T cell motility or the nature of effector:target interactions, FMC63 and CAT CAR T cells from the same donor were incubated with NALM6 cells at a 1:8 ratio and two-dimensional T-cell movement was captured by confocal microscopy over an interval of 20 hours (Fig. 4.14).

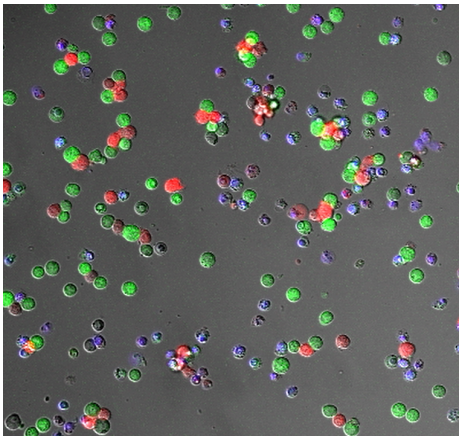

Figure 4.14:

Live cell imaging of CAR$^+$ T cells and NALM6 targets

Representative image of CAR$^+$ T cells expressing mCherry (red), NALM6 target cells expressing GFP (green) and dead cells having taken up DAPI (blue).

Real time assessment of cell death was performed after adding DAPI to the culture media. To be able to compare and quantify interactions between targets and different effector CAR T cells, we analysed comparable numbers of effectors and targets per image at t=0, as shown in figure 4.15.

We observed a significantly greater number of effector:target interactions with CAT CAR over 20 hours (mean no. of interactions $\pm$ SEM: CAT 80.6358.1, FMC63 57.73$\pm$37.5, n=752, $p<0.001$, table4.1). In addition, it appeared that CAT CAR T cells accumulated several contemporaneous interactions with targets cells. These were difficult to quantify, despite attempting to map overlapping effector/target cell membranes. Interestingly, the duration of these interactions were not significantly reduced compared to FMC63 transduced T cell (Mean duration (in frames) $\pm$ SEM: FMC63 17.46$\pm$22.0, CAT 17.75$\pm$26.1). However, we observed marked differences

in the motility of CAT transduced T cells, which showed greater displacement over time compared with FMC63 CAR T cells from the same donor (Mean displacement (pixel) $\pm$ SEM: CAT 130.86$\pm$10.53, FMC63 32.25$\pm$1.497, $p<0.001$, table4.1). The NALM6 cells displayed almost no movement or cell death when cultured independently. Interestingly, the number NALM6 quantified by flow cytometry by the use of counting beads, at the end of the experiment was much lower with CAT CAR than FMC63 CAR T cells (Absolute numbers of NALM6 targets remaining per well after 20 hours: CAT 3980, FMC63 32970, Non-transduced 89310), suggesting that the greater number of effector:target interactions and motility of CAT CAR T cells may enhance killing in this model. Further, the fraction of live CAR T cells after 20 hours was maintained compared to that plated out at time 0 in CAT whereas the number of FMC63 CAR T Cells after 20 hours of coincubation were much lower than at the initial set up (Live CAR T Cells: CAT 10920, FMC63 2870). We hypothesize this may reflect AICD, though this was not formally assessed.

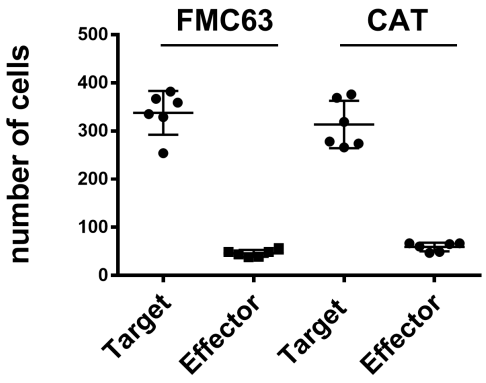

Figure 4.15: **Absolute numbers of CAR T cells and targets at t=0 under conditions of live cell imaging**

Two images per well, in triplicate wells were analysed over 20 hours. At time point zero the number of effectors and targets were quantified (Mean number of cells ±SEM. CAR T cells: CAT 59±9.042, FMC63 46±7.155, n=6, p=NS. NALM6 cells: CAT 313.7±49.18, FMC63 337±45.53, n=6, p=NS).

	CAR	Mean	SEM	p value
Number of Eff:Tg interactions in 20hrs/frame	FMC63 CAT	57.73 80.63	1.497 2.119	< 0.001
Total displacement effectors (pixel)	FMC63 CAT	32.25 130.86	11.50 10.53	< 0.001

Table 4.1: **Kinetic characteristics and absolute number of interactions between CAR T cell effectors and NALM6 target cells under conditions of live cell imaging**

Two images per well, in triplicate wells were analysed /over 20 hours. Absolute number of effector/target interactions were quantified over 20 hours (mean no. of interactions ± SEM: CAT 80.63 ± 2.119, FMC63 57.73± 1.497, n=752, $p<0.001$)

4.3 Discussion

There is a growing body of evidence indicating that a greater affinity of cognate T cell interaction does not always lead to greater T cell activation or specificity [31, 34, 167]. Kinetic models of TCR-ligand interaction propose that the duration of the TCR-pMHC interaction determines the functional potency. The kinetic proof-reading model and serial triggering hypothesis, discussed in section 1.2.4.2, are not mutually exclusive. Schmid *et al.* showed that that TCR/multimer off-rates directly correlated with functional avidity (as determined by the peptide concentration require to achieve half-maximal target lysis). TCR variants with the fastest off rates displayed poor or less efficient functional avidity (K_D 14.2 μM, off-rate $1.7x10^{-1}$), however TCR variants with the slowest off-rates (K_D 15 nM, off-rate $1.13x10^{-3}$) showed reduced killing of cognate tumour cell lines. In addition, increased TCR affinity to the nanomolar range was associated with the loss of target cell specificity [173].

The higher affinity of CARs as compared to TCR, leads to an interaction that can take minutes to hours, compared to the order of seconds. CAR T cells are therefore likely to require ligation of higher numbers of receptors simultaneously in order to become productively activated. Avidity of CAR-transduced cells is co-determined by the density of CAR on the cell surface and the antigen expression density. A window of CAR expression density has been described within which the level of CAR expression does not seem to impact T cell activation [144]. Below T cell activation is abrogated, however above this window, transduced cells are susceptible to activation induced cell death (AICD) following engagement to its target [145]. Seminal work on bi-specific T cell engagers suggested that mutated receptors with lower affinity to CD3, despite rapid dissociation, efficiently triggered T cell activation and cytotoxicity [174], and it was suggested that high affinity binding to CD3 would impede the mediation of serial killing [175]. We therefore rationalized that there are additional consequences of binding kinetics, which are more significant on the cell level, potentially influencing cluster formation with target cells and T cell effector motility.

The experimental data presented here support the model of improved functional avidity in T cells expressing CARs with a faster dissociation rate despite a concomitant lowering of measured affinity for soluble and cell-bound antigen. We showed that T cells transduced with CAT-CAR demonstrate a greater proliferative capacity following antigen specific stimulation, an increased capacity to produce cytokines in response to encounter with antigen, and higher cytotoxic responses in an antigen specific manner at low effector:target ratios. It should be noted that the greater capacity of CAT CAR T cells to produce IL-2 in response to activation by $CD19^+$ targets, acting in concert with signals through the TCR, may have differential effects on T cell survival and proliferation, and this paracrine effect may also contribute to the differences observed. In addition, using live cell imaging, we have demonstrated for the first time that there are significant differences in motility of high affinity compared to low affinity CAR-T cells, resulting in a greater ability to interact with targets.

Our data show no difference in exhaustion markers between CAT and FMC63 CAR T cells following a single round of antigenic stimulation but do not address this in the context of chronic antigen exposure. Loss of effector function during T cell exhaustion has first been identified during chronic LCMV infection. $CD8^+$ loss of function occurs in a hierarchical manner. Typically, functions such as IL-2 production, high proliferative capacity and ex vivo killing are lost first. Other properties, including the ability to produce TNF, are often lost at more intermediate stages of dysfunction. Severe exhaustion eventually leads to virus-specific cells that partially or, in some cases, completely lack the ability to produce large amounts of IFN-γ or to degranulate. The final stage of exhaustion is physical deletion of virus-specific T cells [170]. Because of induced apoptosis of the target cells, following irradiation, CAR^+ T cells were not chronically stimulated and we were therefore unable to investigate the effect of persistent antigen encounter. The *in vivo* studies discussed in chapter 5 were set up to give further insight into the effect of chronic antigen stimulation on CAR T cell exhaustion.

Chapter 5

In vivo efficacy

5.1 Introduction

In Chapter 4 we demonstrated that the reduced affinity of CAT CAR, by means of its quick off rate, paradoxically results in an improved functional avidity with increased proliferation, cytokine production, and cytotoxic responses *in vitro*. Interestingly, differences in motility of T cells transduced with the different affinity CARs were identified and the increased motility of CAT CAR T cells was associated with an increased number of effector to target interactions and therefore an increased capacity to serially engage and kill targets.

Previous studies have shown that $CD8^+$ expressing high-affinity TCRs, when given as adoptive T cell therapy, lose their cytotoxic effector properties, fail to infiltrate tumours and are rapidly deleted both in the tumour as well as the periphery [176–178]. To investigate whether CAR transduced T cells expressing different affinity receptors might show differences in anti-tumour efficacy, and whether our findings *in vitro* would be corroborated *in vivo* we compared CAT CAR to FMC63 CAR transduced T cells in a xenograft NSG model of established CD19 positive leukaemia. We hypothesized that, given the previously reported efficacy of FMC63 *in vivo* [140], in order to clearly delineate differences in functional avidity of CAT CAR transduced cells, we titrated T cell doses down to a level where T cell doses are purposefully lowered to only temporarily control leukaemia burden. We utilised a "stress test" model similar to that developed by Zhao *et al.* where differences in

the kinetics of NALM6 tumour control become apparent by lowering CD19 CAR T cell doses [179].

5.1.1 Aims

- To establish an *in vivo* model of B-ALL, investigating the tumour cell kinetics and number of tumour cells required for disease engraftment.
- To perform a dose finding experiment, titrating down the number of CAR T cells to subject these to an anti-tumour "stress test".
- To test efficacy and specificity of CAT and FMC63 CAR T-cells in a xenograft murine model of B-cell leukaemia

5.2 Results

5.2.1 Tumour cell kinetics and disease engraftment

We set up a xenograft model of NALM6 cells, to study anti-tumour efficacy of FMC63 and CAT CAR transduced T cells *in vivo*. These cells were modified to express firefly luciferase (ffLuc) and GFP [133, 180], allowing non-invasive serial imaging by bioluminescence (BLI) and flow cytometric analysis. Though Raji tumour cells have been described previously as a model to test CD19 CAR therapy efficacy [80, 115, 132], because they express several co-stimulatory ligands, such as CD80 (B7.1) and CD86 (B7.2), which could potentially deliver *in vivo* proliferative or anti-apoptotic signals to the infused T cells [101], we chose for the NALM6 model.

Initial tumour and CAR T cell dosing titration experiments were performed, informed by previously published model designs, that varied from $0.5x10^6$ NALM6 cells in combination with $1-4x10^5$ CAR T cells[179], to $1x10^6$ NALM6 cells combined with either $5x10^6$ [133], or $1x10^7$ CAR T cells [80]. We set up an optimisation experiment, to determine the optimal number of tumour cells to be given, as displayed in the experimental schema in figure 5.1. Different tumour cell doses were injected i.v. (0.5, 1 & 5x10^6 NALM6 cells). At day 7 following injection we found disease engraftment in all three cohorts compared to our negative control (Day 7: $0.5x10^6$ NALM6: $3.7x10^6 \pm 3.4x10^5$; $1x10^6$NALM6: $5.8x10^6 \pm 8.2x10^5$; $5x10^6$ NALM6: $5.6x10^7 \pm 4.3x10^6$ Mean Ph/sec/cm2/sr $\pm$ SEM). Evaluation of tumour burden by BLI is shown in figure 5.2. Signal localisation was seen in bone marrow, particularly femurs. Disease levels of the mice that received $5x10^6$ NALM6 cells were significantly higher than 0.5 and 1 x 10^6, as assessed by BLI, and we hypothesized this would potentially result in a too aggressive model. Hence, we decided to choose a lower dose and chose 1x 10^6 NALM6 cells, on the basis of a 5-fold higher BLI intensity compared to negative control, confirming disease engraftment in all animals, but also providing a suitable interval, based on the kinetics of the tumour growth so that recipient mice could be followed for a meaningful amount of time before necessitating sacrifice.

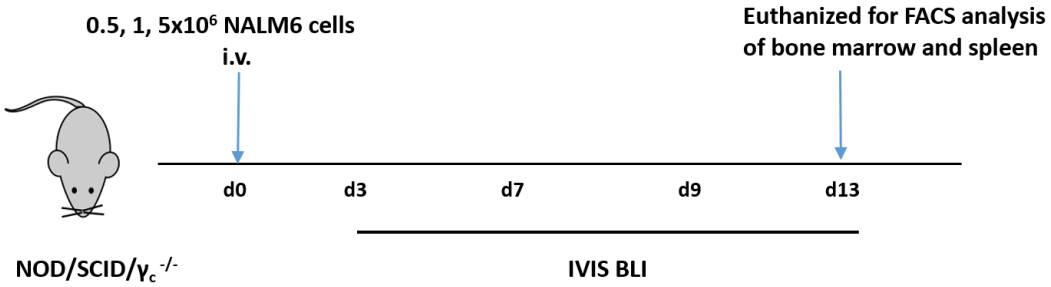

Figure 5.1: **Experimental schema of NSG NALM6 tumour model**

Mice were injected with $0.5, 1\&5x10^6$ GFP$^+$Fluc$^+$NALM6 cells. Disease engraftment was assessed at day 3, 7, 9 & 13. Tumour growth was evaluated using the IVIS imaging system. Photon emission from FLuc$^+$ NALM6 cells was quantified using Living Image software

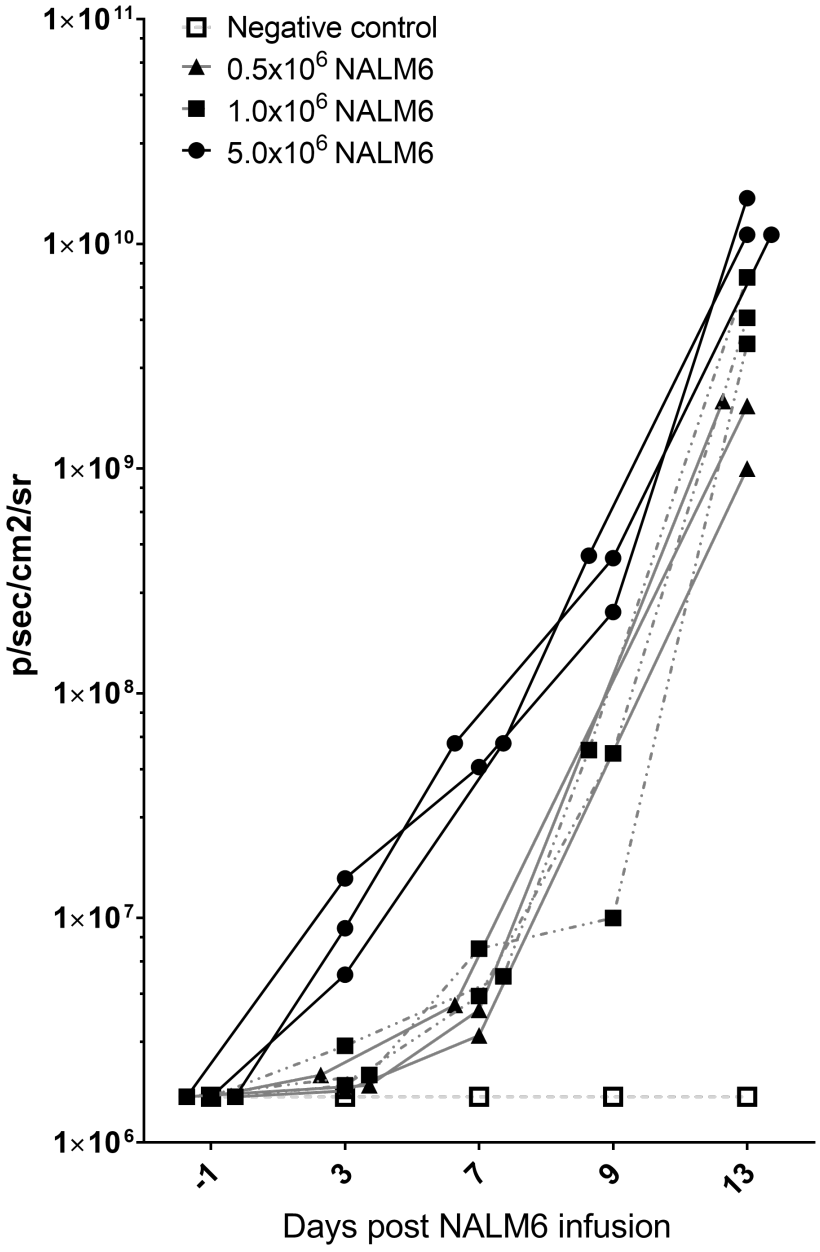

Figure 5.2: ***In vivo* NALM6 tumour cell kinetics and titration**

Different tumour cell doses were injected i.v. (0.5, 1 & 5x10^6 NALM6 cells) to study disease engraftment and determine optimal tumour cell dose. Each replicate is shown, n=3. Day 7: $0.5x10^6$ NALM6: $3.7x10^6 \pm 3.4x10^5$, $1x10^6$NALM6: $5.8x10^6 \pm 8.2x10^5$, $5x10^6$NALM6: $5.6x10^7 \pm 4.3x10^6$ Mean Ph/sec/cm2/sr $\pm$ SEM

5.2.2 CAR T Cell titration

To recapitulate a situation in which serial engagement of target cells and therefore, of killing was advantageous, CAR T cell dose was titrated in order to assess that with which a temporary control of tumour was achieved, rather than complete clearance.

Different CAR T cell doses were injected i.v. (1, 5 & 10x10^6 CAR T cells), 7 days following tumour cells were injected, to study response kinetics. Our aim was to subject the CAR T cells to a "stress test". The experimental schema is shown in figure 5.3. Mice were imaged prior to T-cell treatment to evaluate tumour burden and were stratified to evenly distribute tumour burden into four groups: mice receiving 5x10^6 untransduced T cells, 1, 5 or 10x10^6 CAR^+ T cells. Disease engraftment was assessed at day -1, 2, 6, 9, 13 & 16 post T cell dose injection. At day 6 following CAR T cell injection we found delayed tumour progression in all 3 CAR T cell treated cohorts, as compared to $5x10^6$ untransduced T cells, shown in figure 5.4 (Mean Ph/sec/cm2/sr $\pm$ SEM : $5x10^6$ Untransduced T cells $3.4x10^8 \pm 1.1x10^8$; $1x10^6$ CAR T cells: $3.7x10^6 \pm 3.4x10^5$; $5x10^6$CAR T cells: $5.8x10^6 \pm 8.2x10^5$; $10x10^6$CAR T cells: $5.6x10^7 \pm 4.3x10^6$). However, it appeared that doses of both 5 and 10x 10^6 CAR T cells resulted in very rapid disease clearance, where 1x10^6 did not show clearance but a more heterogeneous image of delayed tumour progression. Our objective to study differences in functional avidity would require temporary control of tumour growth and we therefore used a dose of 2-3x10^6 CAR T cells in subsequent experiments.

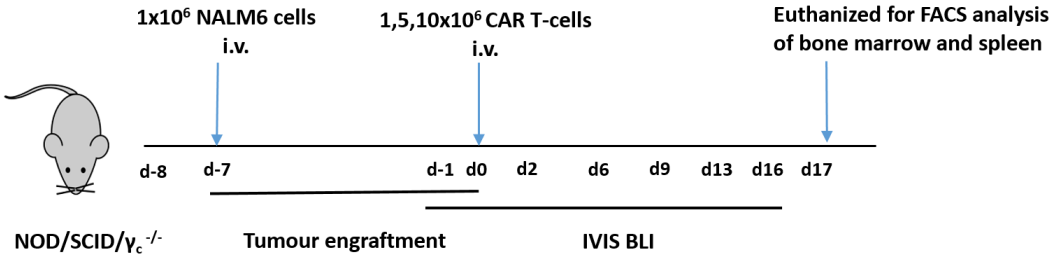

Figure 5.3: **Experimental schema of CAR T cell titration**

7 days following tumour injection, mice were injected with $1,5\&10x10^6$ CAR^+ T cells. Disease engraftment was assessed at day -1, 2, 6, 9, 13 & 16. Tumour growth was evaluated using the IVIS imaging system. Photon emission from $FLuc^+$ NALM6 cells was quantified using Living Image software

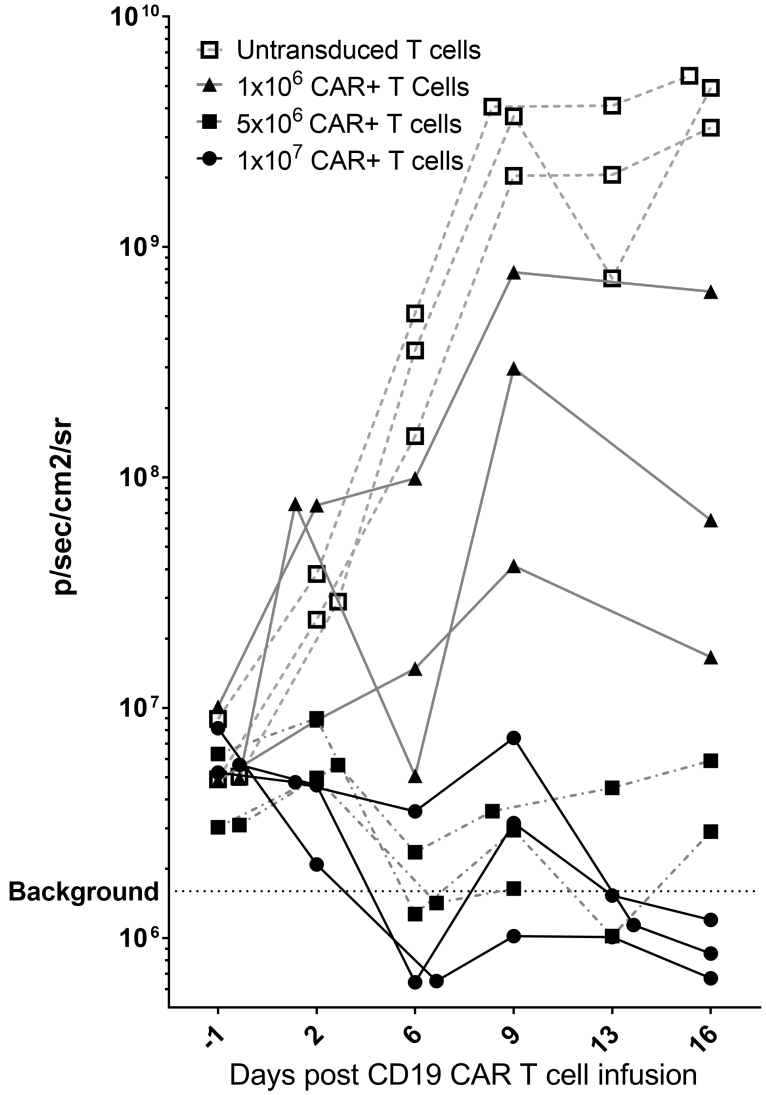

Figure 5.4: **Burden of NALM6 assessed after transfer of varying CAR T cell doses**

Different CAR T cell doses were injected i.v. (1, 5 & 10x10^6 CAR T cells) to study response kinetics. Each replicate is shown, n=3 mice per group. $5x10^6$ Untransduced T cells $3.4x10^8 \pm 1.1x10^8$, $1x10^6$ CAR T cells: $3.7x10^6 \pm 3.4x10^5$, $5x10^6$CAR T cells: $5.8x10^6 \pm 8.2x10^5$, $10x10^6$CAR T cells: $5.6x10^7 \pm 4.3x10^6$ Ph/sec/cm2/sr $\pm$ SEM

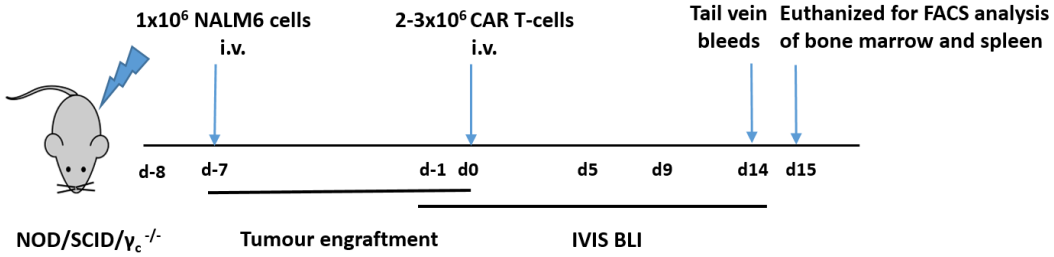

Figure 5.5: **Experimental schema of NSG NALM6 xenograft mice model**

To assess the ability of CD19 CAR T cells to kill NALM6 tumour in an established tumour model, mice were injected with $1x10^6$ GFP^+Fluc^+NALM6 cells 24 hours after sublethal irradiation and 7 days prior to T cell injection. Disease engraftment was assessed at day-1. Cohorts were randomized and recipients with similar tumour burdens were distributed evenly across the groups prior to CAR T cell injection or non-transduced T cells as negative control. Tumour growth was evaluated using the IVIS imaging system. Photon emission from $FLuc^+$ NALM6 cells was quantified using Living Image software. Post termination of the experiment the animals spleen and bone marrow were analyzed by flow cytometry.

5.2.3 Improved *in vivo* efficacy of low affinity CD19-CAR$^+$ T cells against ALL

Having established a tumour and T cell dose which would allow temporary disease control, we used this model to test the functional avidity of FMC63 and CAT CAR transduced T cells. The experimental model is shown in figure 5.5. In contrast to the previous experiments, we sub-lethally irradiated the animals with 2.8 Gy 24 hours prior to NALM6 tumour cell injection. This was based on previous engraftment rates of disease in $\pm$65% of the animals. To improve this and ensure engraftment in all animals, irradiation was used in an optimisation experiment and indeed proved to increase engraftment levels to 100%. Animals did not show any symptoms related to the irradiation.

Mice were imaged prior to T cell treatment to evaluate tumour burden and were stratified to evenly distribute tumour burden into four groups. One group was treated with untransduced T cells and served as control for xenogeneic T cell responses. The experimental arms received 2.5x10^6 CAR transduced T cells expressing either FMC63 CAR or CAT CAR.

Results of two independent experiments with comparable results are shown. Both CAT and FMC63 CAR transduced T cell products had a comparable distribution of CD4 and CD8 T cells prior to infusion as shown in figure 5.6. CAR expression levels were determined in both experiments and as in the *in vitro* experiments, where there were significant differences in transduction efficiency, non-transduced T cells were added to normalise the CAR$^+$ percentage in each groups.

All animals were followed for tumour burden by BLI (Fig. 5.7). Control mice receiving untransduced T cells showed rapid, disseminated tumour infiltration. Both the FMC63 and CAT cohorts were able to delay tumour growth, but CAT transduced T cells were more effective at inhibiting tumour growth compared to FMC63 expressing T cells from the same donor. On day 12 post T cell injection, substantial differences were seen in tumour burden as assessed by IVIS(Fig. 5.8 CAT CAR: $1.1x10^8 \pm 9.3x10^7$, FMC63 CAR $3.2x10^9 \pm 7.7x10^8$, Mean ph/sec/cm^2, n=18, $p<0.001$) .

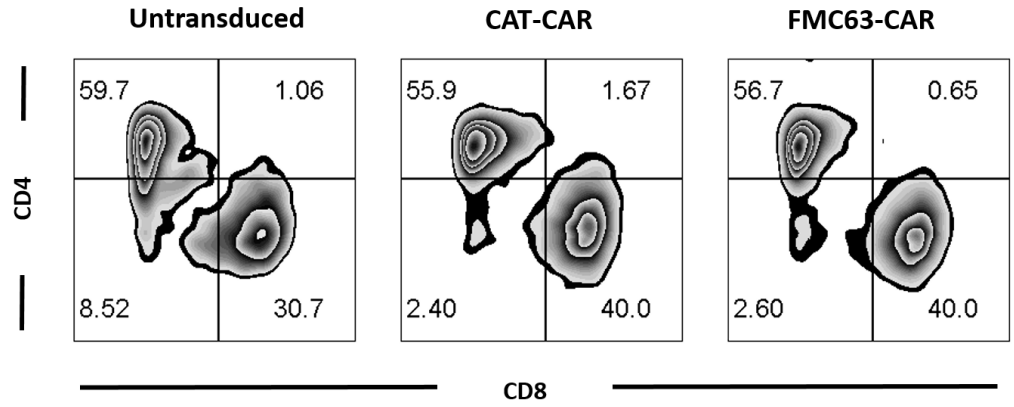

Figure 5.6: **CD4/CD8 distribution of FMC63 and CAT CAR$^+$ T cells prior to infusion**

FMC63 CAR$^+$ and CAT CAR$^+$ T cells were evaluated for CD4/CD8 ratio by flow cytometry. FACS plots show distribution of the T cell product 24 hours prior to infusion.

To test if our *in vitro* findings of a greater proliferative capacity of CAT CAR transduced T cells correlated with increased proliferation of CAR$^+$ T cells *in vivo*, we directly quantified the absolute number of FMC63 and CAT CAR transduced cells. Two weeks after infusion of CAR T cells peripheral blood samples were analysed, revealing a significantly greater absolute number of CAT CAR T cells in the circulation (Mean$\pm$SEM CAT 18743 $\pm$ 3127, FMC63 2843 $\pm$ 818.7CAR T cells/ml, n=9, $p<0.001$, Fig. 5.9c). This was associated with a lower number of NALM6 cells in the circulation of recipients of CAT CAR T cells (Mean$\pm$SEM 13.19 $\pm$ 5.494 CAT CAR, 594.5 $\pm$ 157.9 FMC63 CAR NALM6 cells/ml, n=9, $p<0.01$, Fig.5.10a). Similarly, FACS analysis of bone marrow after sacrifice, revealed a greater absolute number of CAR T cells in the CAT cohort compared to FMC63 (MeanSE cells/ml: $5.1x10^4 \pm 1.2x10^4$ CAT CAR; $2.0x10^4 \pm 4.6x10^3$ FMC63 CAR, n=9, $p<0.05$, Fig. 5.9a) and a higher number of NALM6 cells in recipients of FMC63 CAR T cells (Mean: 3x102 NALM6 cells/ml in CAT cohort, 2.8x105 NALM6/ml in FMC63 Cohort, n=9, $p<0.001$, Fig. 5.10b).

CAT CAR T cells accumulated greater at the disease site, as well as in the peripheral secondary lymphoid compartments, however a skewed distribution of CAR T cells into other organs can not be excluded, potentially explaining a difference in absolute number between FMC63 and CAT CAR transduced T cells, as these were not formally assessed. However such trafficking would be not be expected

given the comparable frequency of CAR T cells within distinct memory compartments (Mean % ± SEM; FMC63 CAR T cells: Naive 35.1±3.1, CM 8.4±1.9, EM 28.8±3.3, TEMRA 27.7±3.0, CAT CAR T cells: Naive 29.9±2.8, CM6.3±0.5, EM 36.7±3.2, TEMRA 27.1±0.9), determined by CCR7 and CD45RA expression (Fig. 5.11b), as well as their CD4/CD8 distribution (Fig. 5.11c, % $CD8^+$ ± SEM FMC63 43.6±1.0, CAT 41.7±3.9, NT 33.7±0.4).

The greater production of IL-2 *in vitro* as shown in section 4.2.4.1 may contribute to the greater proliferative capacity of CAT CAR transduced T cells. Similar to our findings *in vitro*, intracellular staining of Th1 like cytokines revealed that CAT CAR T cells at the tumour site show a greater ability to express TNF-α and again a trend towards greater expression of IL-2, 14 days following transfer to tumour bearing hosts (Fig. 5.12). When the expression of activation and exhaustion markers was investigated on CAR transduced T cells from the bone marrow, 15 days after infusion, we found comparable levels of expression of TIM3, LAG3 and PD1 in mice receiving FMC63 CAR transduced T cells as those treated with CAT CAR T cells(Fig. 5.13, MFI ± SEM of CAR transduced T cells in bone marrow 15 days following infusion. TIM3: FMC63 541.4 ± 121.7, CAT 512.8 ± 71.14, LAG3: FMC63 186.6 ± 25.95, CAT 203.2 ± 19.15, PD1: FMC63 86.04 ± 22.3, CAT 73.52 ± 7.703).

Several studies have suggested that the expansion and differentiation program is imprinted shortly after antigenic stimulation [181]. Virus-specific CD8 T cells generated during chronic, but not acute, LCMV infection expressed low levels of CD127 and CD122, the receptors for the homeostatic cytokines IL-7 and IL-15, respectively [182]. IL-7 is involved in maintaining memory populations and IL-7Rα signalling has an important function in T cell survival by increasing the expression of anti-apoptotic molecules (Bcl-2 and Bcl-XL)[183]. Van Leeuwen *et al.* describe that in chronic infections IL-7Rα^+ T cells express higher levels of Bcl-2 and show a superior recall response and enhanced proliferation in response to homeostatic signals [181]. Interestingly when we investigated IL-7Rα expression (CD127) on CAR transduced T cells, we found a significantly greater proportion of IL-7Rα^+

CAT CAR transduced T cells (Fig. 5.14, % CD127$^+$ CAR$^+$ T cells in BM: FMC63 22.96 $\pm$ 1.839, CAT 34.08 $\pm$ 1.944), as well as significantly higher expression levels (Fig. 5.14, MFI CD127 CAR$^+$ T cells in BM FMC63 201.7 $\pm$ 13.7, CAT 299.8 $\pm$ 11.9) compared to FMC63 CAR T cells. This directly correlated with an upregulation of the anti-apoptotic molecule Bcl-2, akin to results previously reported in chronic infections [183]. Over-expression of Bcl-2 inhibits the intrinsic apoptotic pathway, critical in regulating T cell survival, and is actively regulated in peripheral T cells, being upregulated in naive cells and memory cells and downregulated in the effector phase [184]. Intracytoplasmic flow cytometric analysis on the BM of treated mice (Fig. 5.15) showed both higher levels (MFI Bcl2 CAR$^+$ T cells in BM: FMC63 124 $\pm$ 26.27, CAT 337.6 $\pm$ 35.4), and a greater proportion of Bcl2$^+$ CAR T cells (Fig. 5.15, % Bcl2$^+$ CAR$^+$ T cells in BM: FMC63 10.24 $\pm$ 2.667, CAT 34.66 $\pm$ 3.345) in mice treated with CAT CAR T cells than FMC63 CAR T cells.

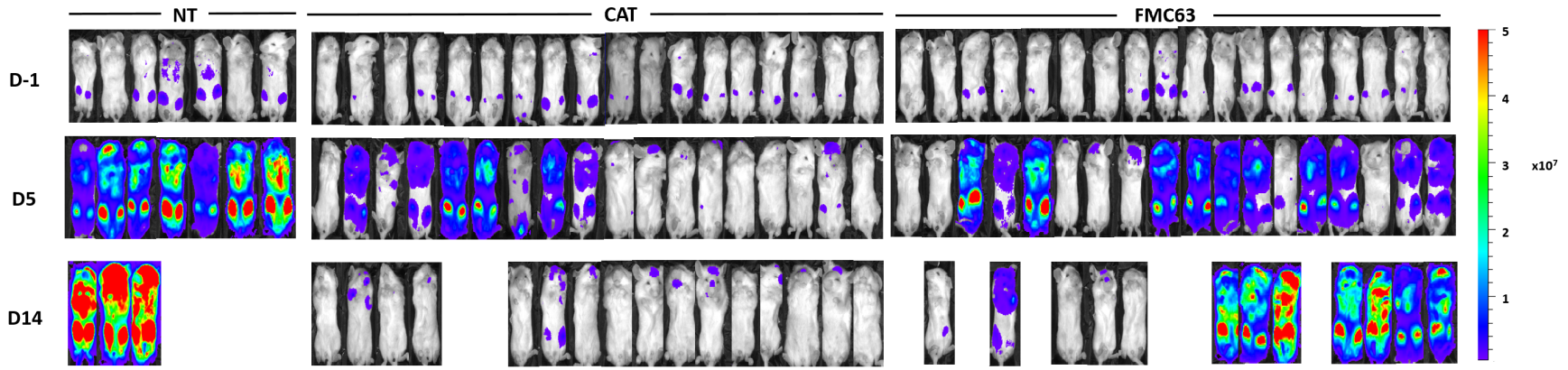

Figure 5.7: **Serial BLI assessment of NALM6 tumour growth *in vivo***

To assess the ability of CD19 CAR T cells to kill NALM6 tumour in an established tumour model, mice were injected with $1x10^6$ GFP$^+$Fluc$^+$NALM6 cells 24 hours after sublethal irradiation and 7 days prior to T cell injection. Disease engraftment was assessed at day-1. Cohorts were randomized and recipients with similar tumour burdens were distributed evenly across the groups prior to CAR T cell injection or non-transduced T cells as negative control. Tumour growth was evaluated using the IVIS imaging system. Photon emission from FLuc$^+$ NALM6 cells was quantified using Living Image software.

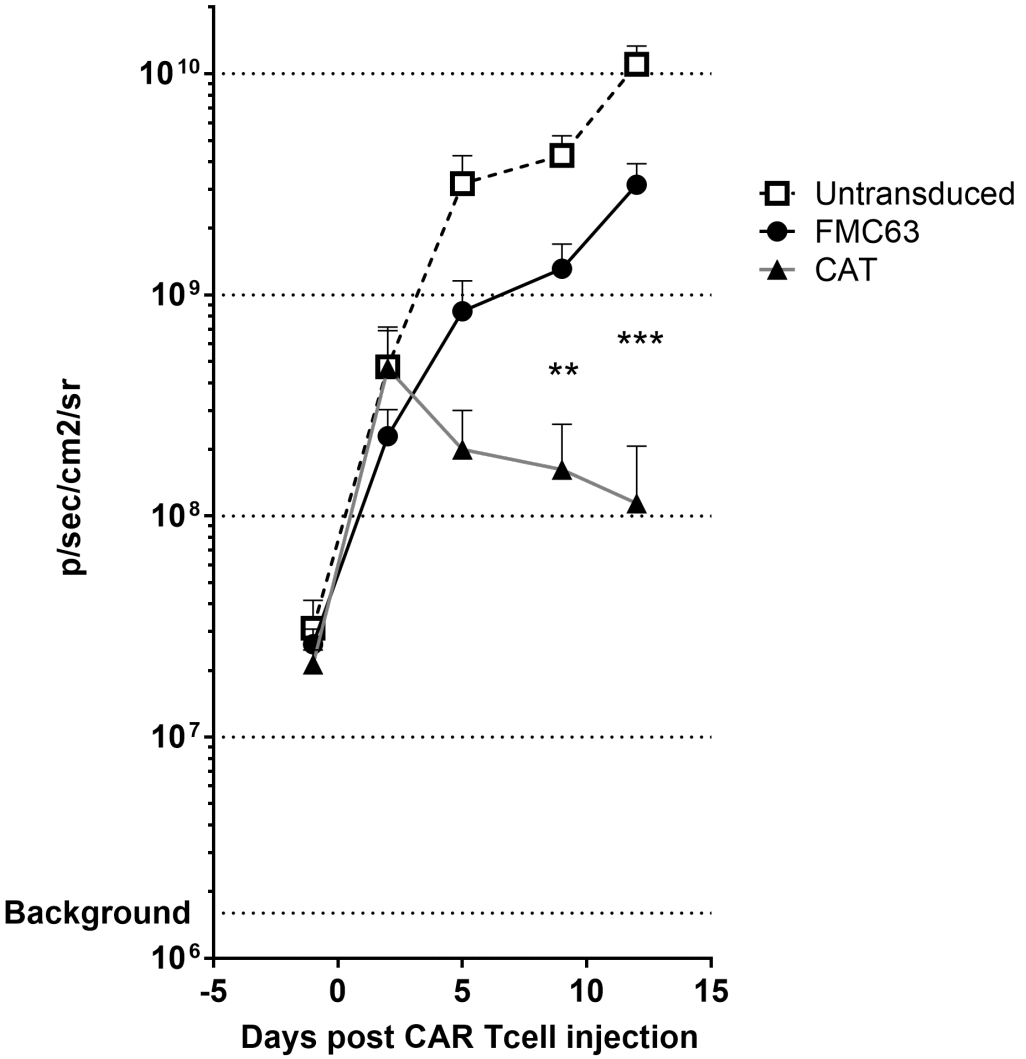

Figure 5.8: **CAT CAR$^+$ T cells show enhanced disease inhibition after transfer to tumour bearing hosts**

Mice were injected with $1x10^6$ GFP$^+$Fluc$^+$NALM6 cells 24 hours after sublethal irradiation and 7 days prior to T cell injection. Disease engraftment was assessed at day-1. Cohorts were randomized and recipients with similar tumour burdens were distributed evenly across the groups prior to CAR T cell injection or non-transduced T cells as negative control. Tumour growth was evaluated using the IVIS imaging system. The graph shows the kinetics of tumour growth. Photon emission from FLuc+ tumor cells was quantified and measured as maximum photon/sec/cm^2/steradian (p/s/cm^2/sr).Lines represent cumulative results of light emission values $\pm$ SEM bioluminescence signal determined in 2 separate experiments,n=18, Student t-test, **p$<$0.001, *** p$<$0.001.

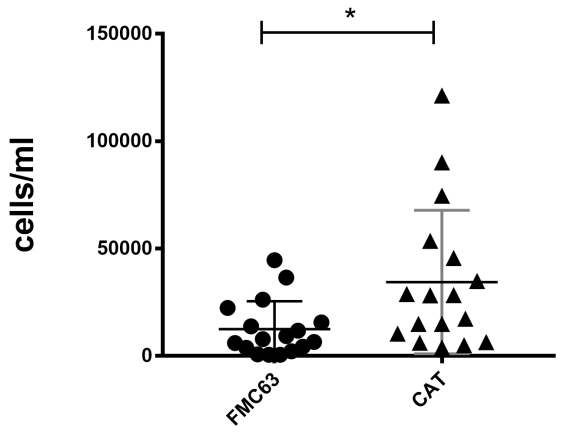

(a)

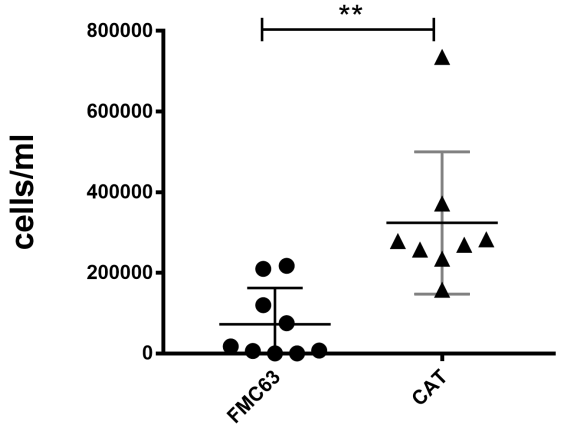

(b)

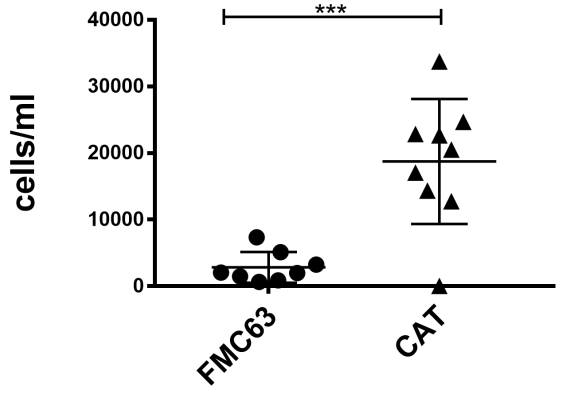

(c)

Figure 5.9: **CAT CAR⁺ T cells accumulate in greater number *in vivo***

After termination of the experiment 16days following infusion of CAR T cells, bone marrow, spleen and peripheral blood were investigated for presence of CAR T cells. Mean number ± SEM: (A) Bone marrow: CAT $3.4x10^4 \pm 8.1x10^3$, FMC63 $1.3x10^4 \pm 3.1x10^3$ n=18, $P<0.05$ (B) Spleen: CAT $3.2x10^5 \pm 6.2x10^4$, FMC $7.3x10^4 \pm 3.0x10^4$, n=9, $p<0.01$ (C) peripheral blood: CAT $1.9x10^4 \pm 3.1x10^3$, FMC63 $2.8x10^3 \pm 8.2x10^2$, n=9, $p<0.001$. Statistical comparisons were made using a two-sided student t-test.

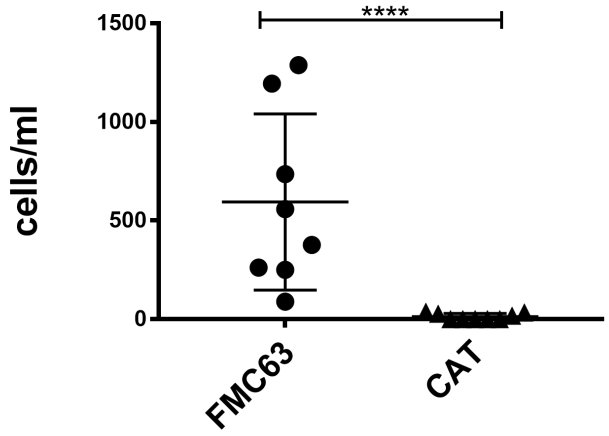

(a)

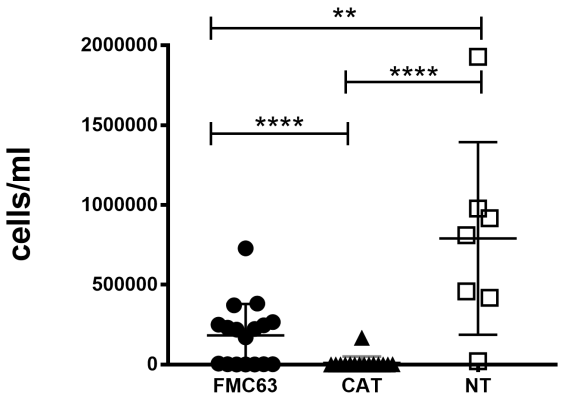

(b)

Figure 5.10: **NALM6 cell absolute numbers are reduced in cohort that received CAT CAR transduced T cells compared to FMC63 and non-transduced T cells**

Absolute numbers of NALM6 $^{+}$ cells were assessed in (A) peripheral blood and (B) bone marrow, n=18, statistical analysis was done by the use of a two-sided student t test; **, $P<0.01$, ***, $P<0.001$

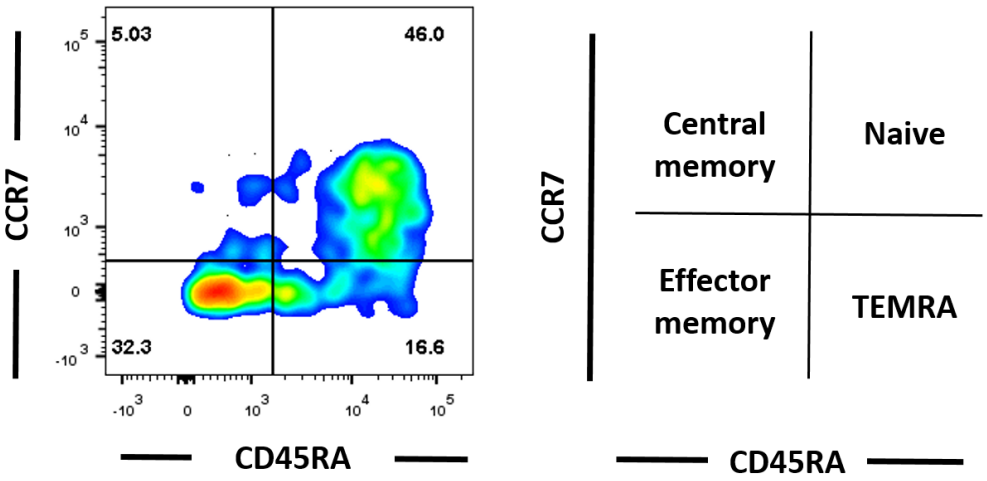

(a)

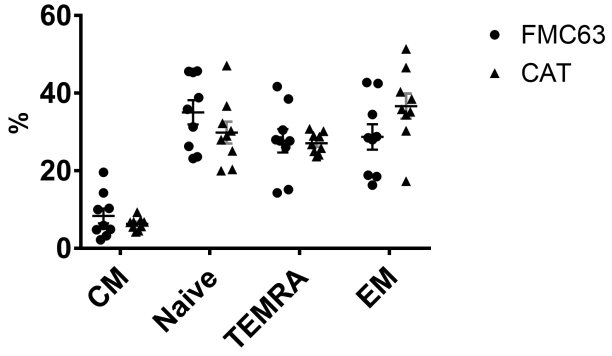

(b)

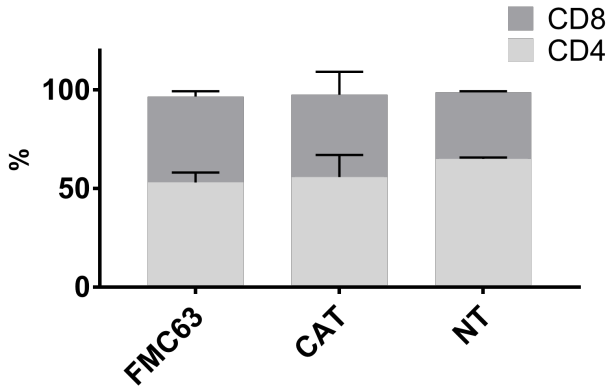

(c)

Figure 5.11: **The distribution of CAR T cells in the bone marrow between CD4 and CD8 as well as memory compartments was not significantly different 15 days after transfer to tumour bearing hosts**

(A) Representative FACS-plot of memory compartments, identified by CD45RA and CCR7 expression, gated on CAR+ T cells in bone marrow by flow cytometry, on day 15 post T cell injection. (B) Mean % ± SEM; FMC63 CAR T cells: Naive 35.1±3.1, CM 8.4±1.9, EM 28.8±3.3, TEMRA 27.7±3.0, CAT CAR T cells: Naive 29.9±2.8, CM6.3±0.5, EM 36.7±3.2, TEMRA 27.1±0.9), determined by CCR7 and CD45RA expression (C)% $CD8^+$ ± SEM FMC63 43.6±1.0, CAT 41.7±3.9, NT 33.7±0.4

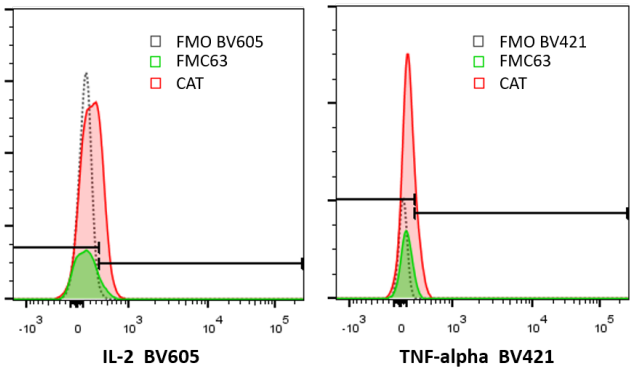

(a)

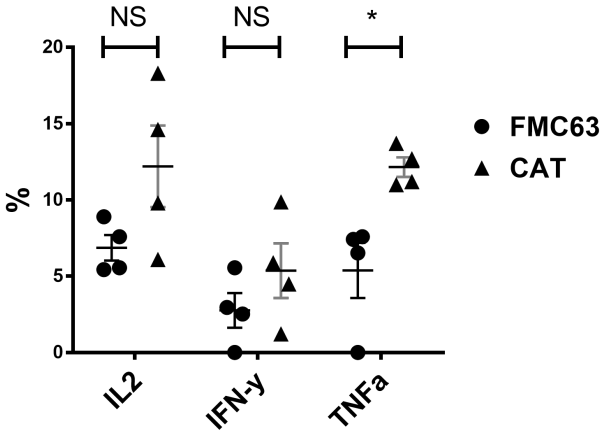

(b)

Figure 5.12: **CAT CAR T cells at the tumour site showed a greater ability to express TNF-αafter transfer to tumour bearing hosts**

Percentage of cytokine-producing CAR T cells in bone marrow was determined by flow cytometry after gating on CAR^+ T cells. Data, mean percent producing ± SD, n=4; two-sided student t test; *P $<$ 0.05

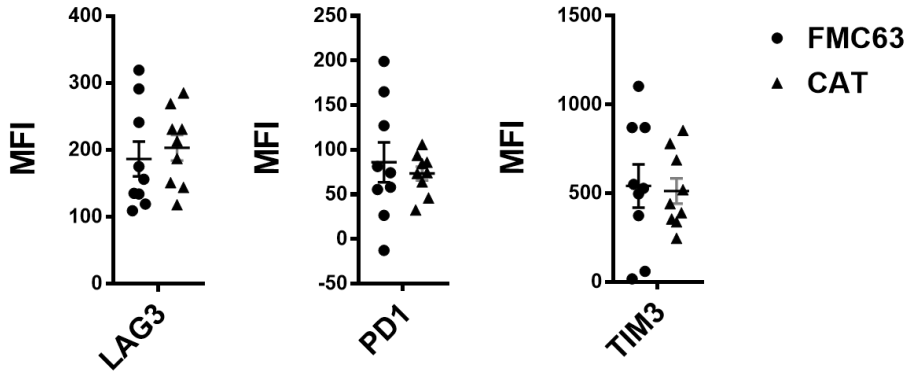

Figure 5.13: **Activation/Exhaustion marker expression levels of CAR$^+$ cells in bone marrow**

Mean fluorescence intensity of the expression levels activation/exhaustion markers LAG3, PD-1 and TIM3 on CAR T cells in the bone marrow was assessed by flow cytometry 15 days following infusion. MFI ± SEM TIM3: FMC63 541.4 ± 121.7, CAT 512.8 ± 71.14, LAG3: FMC63 186.6 ± 25.95, CAT 203.2 ± 19.15, PD1: FMC63 86.04 ± 22.3, CAT 73.52 ± 7.703. Data, mean ± SD, n=9

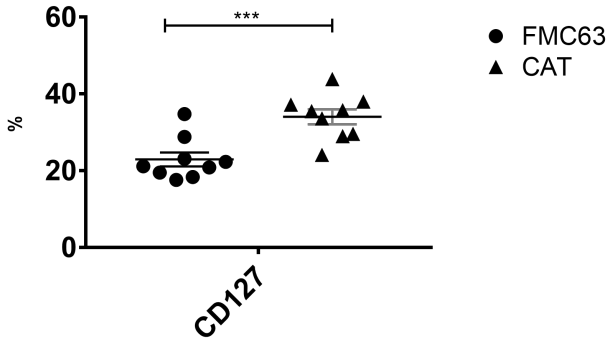

(a)

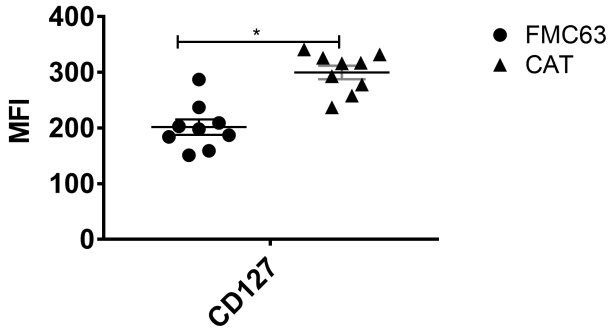

(b)

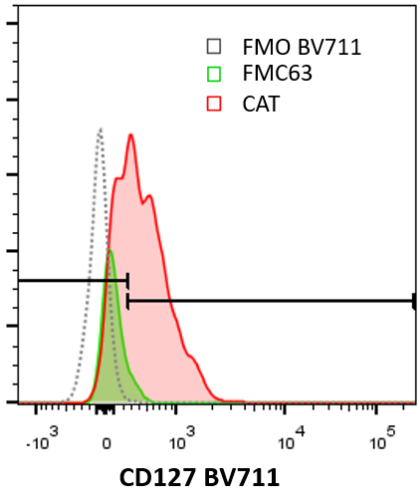

(c)

Figure 5.14: **A greater proportion of CAT CAR$^+$ cells in the bone marrow was CD127 positive and showed greater levels of CD127 expression 15 days following infusion**

CD127 positive cells in bone marrow and expression levels were determined by flow cytometry after gating on CAR$^+$ T cells. (A) Proportion of CD127 positive cells (B) MFI of CD127 expression levels (C) Representative FACS plots. Data, mean $\pm$ SD, n=5 in FMC63 and n=9 in CAT; *, $P < 0.05$, ***, $P < 0.0001$, two-sided student t test.

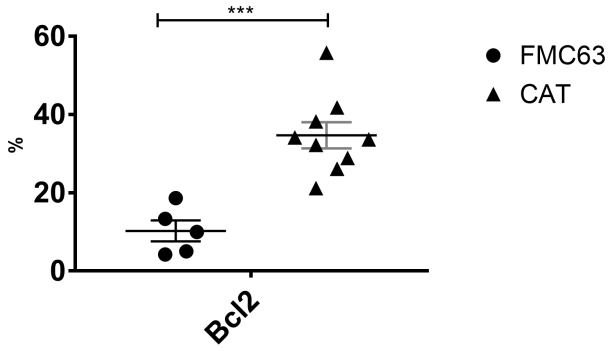

(a)

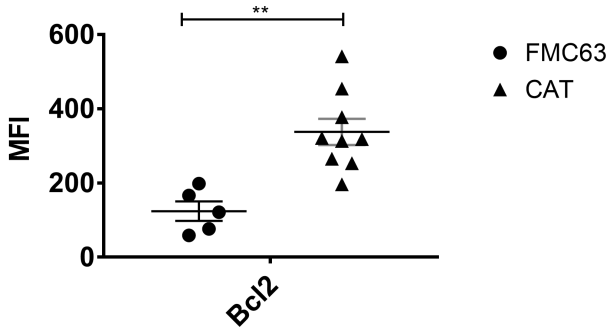

(b)

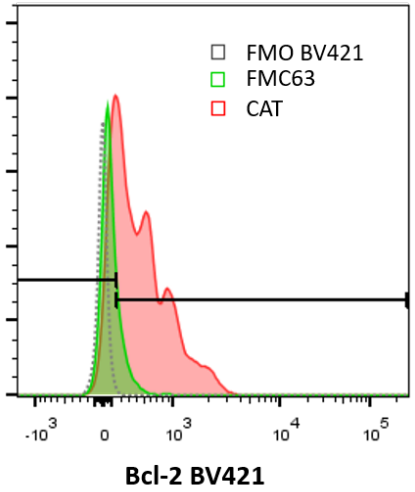

(c)

Figure 5.15: **A greater proportion of CAT CAR$^+$ cells in the bone marrow was Bcl2 positive and showed greater levels of expression 15 days following infusion**

Bcl2 positive cells in bone marrow and expression levels were determined by flow cytometry after gating on permeabilized CAR$^+$ T cells. (A) Proportion of Bcl-2 positive cells (B) MFI of Bcl-2 expression levels (C) Representative FACS plots. Data, mean $\pm$ SD, n=5 in FMC63 and n=9 in CAT;**P $<$ 0.01, ***,P $<$ 0.001, two-sided student t test.

5.3 Discussion

Whilst both CAT and FMC63 CAR transduced T cells were able to mediate effective dose-responsive anti-tumour responses in a xenogeneic model, when more stringent conditions were used to favour the tumour, CAT CAR transduced T cells showed enhanced disease clearance, TNF-α secretion and accumulation both in the bone marrow and the periphery. These data reflect our *in vitro* findings that CAT CAR T cells are able to proliferate more and show enhanced Th1 cytokine secretion in response to $CD19^+$ targets.

It has been previously reported that increased TCR-pMHC interactions *in vivo* result in decreased proliferation, cytokine production and memory formation [185] and intermediate affinity T cells are suggested to better control tumour growth than their high affinity counterparts [178, 185]. In addition, it has been demonstrated that chronic viral infection in mice can convert an otherwise effective antiviral $CD8^+$ T cell response to an ineffective or inefficient response. This conversion is associated with a step-wise impairment, or exhaustion, in the effector functions and proliferative capacity of responding antigen-specific $CD8^+$ T cells[186]. We observed significantly higher levels of IL-7Rα and Bcl-2 expression in CAT CAR transduced T cells responding to persistent tumour burden compared to FMC63 CAR transduced T cells. Overexpression of these markers has shown significant impact on proliferation and protection from activation induced cell death (AICD) [187] and previous studies indicated that the generation of memory $CD8^+$ T cells critically depends on the function of Bcl-2 during the contraction phase of a T cell response [188]. The upregulation of IL-7Rα and Bcl-2 in CAT-CAR transduced T cells responding to persistent tumour burden compared to FMC63 CAR transduced T cells may reflect differences in downstream CAR signalling and changes in intracellular signalling, thus it is possible that the greater accumulation of CAT CAR T cells was related to a reduction in apoptosis and greater survival, though increased proliferation of CAT CAR T cell or trafficking of FMC63 out of the secondary lymphoid compartments can not be excluded.

Although the xenograft NSG model is commonly used as a model to study efficacy of CAR transduced T cells, due to their receptivity to human cells, this model is also limited by the development of xenogeneic (xeno-)GvHD. We observed symptoms related to xeno-GvHD (piloerection, hunched posture, weight loss) two weeks following T cell injection, limiting us in the duration that we could study our different cohorts. The increased proliferative response of CAT CAR transduced T cells and its apparent improved fitness justified further studies in the persistence of these CAR T cells and their ability to clear disease when being re-challenged with tumour cells.

In addition, because this is an immunocompromised model, we are unable to study the interaction of CAR T cells with other components of the immune system, such as macrophages, playing a pivotal role in toxicities caused by CAR T cells such as CRS [159, 189, 190]. The pathological mechanisms are not yet understood, but T cell-mediated therapies lead to proinflammatory cytokine production, which may trigger CRS. Whether a low affinity CAR T cell interaction might also influence the interaction with bystander immune cells is yet unidentified.

Chapter 6

General discussion and future work

6.1 CD19 binding kinetics

CAR T cell therapy holds great promise for the therapy of cancer, but the optimal design of CARs has yet to be established. The overarching aim of this project was to investigate the impact of scFv affinity, and in particular the off rate, on CAR-mediated T-cell function. We generated 2 CARs that are identical in backbone other than their CD19-targeting domain. The data presented here show that the affinity of the different anti CD19 scFvs, ranging from K_D 0.9nM to 116nM, is significantly higher than the wild type TCR affinity, ranging from K_D 1µM to 50µM[31]. However, the influences of differences in on- and off-rates underlying the binding kinetics of CD19 CARs on downstream CAR T cell responses have never been directly compared. We sought to explore this effect specifically and constructed a novel anti-CD19 CAR derived from the CAT hybridoma.

SPR analysis by Biacore revealed a distinct kinetic profile for this new scFv CAT demonstrating a greater off-rate (k_d FMC63 $5.5x10^{-4}$ and k_d CAT $7.07x10^{-2}$), whilst maintaining an on-rate nearly identical to FMC63 (k_a FMC63 $6.24x10^5$ and k_a CAT $6.09x10^5$), employed in published clinical studies [78, 85]. The differences in affinity were confirmed against naturally expressing Raji cells by Scatchard analysis. Clearly, neither of these assays fully recapitulate the binding of a membrane bound CAR on a T cell to CD19 on the target cell and both eliminate cell adhesion and binding of other ligand-receptor pairs which may affect functional avidity

but nonetheless these are currently the best assays available for addressing this issue and provide valuable insights into the binding of a soluble scFv-Fc to soluble or naturally expressed antigen respectively. The affinity as compared to functional avidity describes the thermodynamic parameter, the K_D value, defined by a simple equilibrium binding reaction. The functional avidity describes the ability of a CAR T cell to respond to the stimulation provided by tumour associated antigens and is influenced by CAR T cell affinity, CAR expression levels and the location of the recognized epitope on the antigen [191].

To investigate the epitope binding specificity of CAT scFv compared to FMC63 we constructed the full length peptide and three variants with increasing truncation of CD19 (Δex2, Δex2-3, Δex2-3-4). Although we did not perform formal epitope mapping studies, we were able to confirm binding of both FMC63 and CAT scFv to the first Ig loop in exon 2. This suggests that differences in synapse width were unlikely to contribute to differences in CAR T cell responses, however this cannot be completely excluded. We and others have observed that the the frameshift mutations clustered in the nonconstitutive exon 2 eliminate full-length CD19, but allow expression of the Δex2 isoform in the cytosol [95]. The cytosolic localisation of Δ ex2 CD19 precludes it being targeted by novel CD19 CARs that target the second Ig loop, as a way to prevent escape, because of their restriction to binding cell surface molecules.

6.2 Delineating the impact of binding-domain affinity on CAR T-cell function

TCR affinity influences the sensitivity and polyfunctionality of T cells. In targeting of antigens for therapeutic purposes, it was previously assumed that the higher affinity of the interaction, the greater the associated cellular immune response. This was based on observations such as TCRs specific for pathogens (non-self) having a higher affinity and K_D values that are generally about 10-fold lower when compared to TCRs specific for TAAs (as self-antigens) [21]. Taking this to its natural conclusion, TCRs were then affinity matured with the aim of enhancing downstream T cell responses. This was beneficial in some cases, supported by observations that a high-affinity MART-1/HLA-A2 TCR mediated improved objective response rates compared to a lower affinity TCR, and the observation that an affinity-enhanced NY-ESO1 TCR mediated significant clinical responses [21]. However, it was also shown that T cell function could not be further improved raising TCR affinity above the natural range ($K_D < 1\mu M$) [150] and by doing so the increased affinity led to loss of antigen sensitivity, specificity and cross-reactivity [20, 22, 192], resulting in treatment-related toxicity including severe but treatable inflammation of skin, eyes, ears (MART-1/HLA-A2; gp100/HLA-A2), and colon (CEA/HLA-A2) [21].

There are different theories as to what kinetic properties underlie the best T cell activation and signalling. The kinetic proofreading model suggests that off rates should be sufficiently slow to allow a threshold for immunoreceptor-based signalling to be surpassed and full T cell activation to occur. A study with the human NY-ESO-TCR showed that an increase in $t_{1/2}$ from 2.2 seconds for the wild-type TCR to 19 seconds for an affinity-matured TCR improved the ability of TCR transduced $CD8^+$ T cells to recognize NY-ESO-expressing tumour cells, and this improvement was not seen with an affinity-matured TCR with a $t_{1/2}$ of 41 seconds [193]. This was supported by findings that optimal TCR peptide sensitivity is achieved with dissociation half time ($t_{1/2}$) of 9.3 seconds, and that when $t_{1/2}$ was increased to 348, 1320, and 3120 seconds this resulted in a progressive loss of peptide sensitivity and even impaired T cell function. [31, 33]. The half-lives of the

interactions between a TCR and foreign-pMHC agonists are characteristically 2-10 seconds [14]. At low antigen density, which is most physiologically relevant, sufficient T cell activation requires serial triggering. Tumour-associated peptide antigens are generally present at fewer than 50 copies per cell [22]. It is possible that TCR-pMHC interactions that have excessively long half-lives could impair the serial engagement of TCRs by low-density cognate pMHC on the target-cell surface, which would prevent T cell activation. However, when one considers the setting of increased antigen density, the abundance of antigen leads to simultaneous binding of sufficient pMHC complexes to TCRs, diminishing the need for serial triggering and the inhibition caused by the longer $t_{1/2}$ is lessened. The potential inhibition of T cell functions as a result of a long $t_{1/2}$ may well underlie the absence of a mechanism for affinity maturation of TCRs during T cell responses to pathogens, which in contrast to adaptive antibody-mediated immune responses is associated with lower affinities.

Irving *et al.* observed that there were maximal T cell responses at lower affinities, with a plateau of functional output between K_D 1 μM and 5 μM [23]. Reducing the TCR affinity further however, has demonstrated to affect different parameters of T cell activation such as the phosphorylation of CD3ζ, the activation of the MAP kinase pathways and the ability to recruit cytotoxic granules [16, 24, 25]. Thus, there appears to be a defined window of half-life of TCR-ligand interactions and number of TCRs engaged. While very short half-lives avert productive TCR triggering, half-lives exceeding the optimum interaction time decrease the efficiency of TCR serial engagement.

Studying CAR T cell functional efficacy, Turatti *et al.* show that when CAR and antigen levels are both high, the threshold for complete T cell activation is readily met, regardless of CAR affinity, due to high numbers of simultaneous CAR-antigen binding events. However, when both the expression levels of CAR and antigen are low, the function of the CAR appears to be determined by the affinity of the CAR: low affinity CARs with high off-rates remain functional, whereas high affinity CARs appear impaired [146]. Lehner *et al.* report that CAR T cells require

at least a 100-fold higher target antigen densities than natural TCRs because of the higher affinity of the CAR for antigen, resulting in a longer half life of interaction, and an inability to support efficient serial triggering as a result, although this study did not test CARs with quick dissociation rates [194]. In T cells transduced with affinity matured TCR (engineered to enhance affinity for pMHC), this was also described. To trigger T cell responses in these transduced T cells, again a 100-fold higher pMHC densities was required compared to wild-type TCR [31]. Thus CAR affinity may be a relevant determinant of CAR T cell activation in response to CD19, were primary cell targets typically express 3000 CD19 molecules per cell.

A study by Oren *et al.* in which they compared TCR-like Abs, targeting HLA-A2-WT1Db126 complexes, as a binding moiety in CAR T cell therapy to a native low affinity αβ-TCR chain, again revealed that above a threshold of TCR-pMHC affinity ($K_D < 5\mu M$) T cell function could not be further enhanced. In addition work performed on NYESO-1 αβ-TCR CARs defined the upper affinity limit of TCR for specific Ag recognition as 280-450 nM [150].

Chmielewski *et al.* investigated the effect of receptor binding affinity on CAR effectiveness, by the use of a library of affinity matured anti-ERB2 scFvs, with affinities ranging broadly from K_D $3x10^{-7}$ to $1.5x10^{-11}$ M. Importantly these scFvs had identical epitope specifity and the CAR backbone was otherwise identical. They showed that there is a threshold affinity beyond which no improvement in T cell function is achieved, defined as "the affinity ceiling" [147]. The likely explanation for the plateau effect is that the avidity of the CAR needed for maximal T-cell activation is a function of the number and density of the expressed receptors as well as their affinity. In their model the CAR-mediated cytotoxic effect on target cells and the release of IFN-γ and IL-2 did not increase above an affinity of $K_D < 1x10^{-8}$ M. This was supported by a study conducted by Haso *et al.* in which CARs containing three distinct binding domains targeting CD22 were compared. They showed that CAR lytic activity did not vary based on scFv affinity (comparing 2 murine CD22 scFvs with respective K_D values of 5.8 nM and 2.3 nM, and a humanized scFv with a K_D value of 20nM), but rather on the epitope specificity, with CARs targeting a

proximal CD22 epitope demonstrating superior antileukaemic activity [148]. However, CARs specific for ROR1 with varying affinity of scFv were also investigated to determine the impact of affinity on CAR-mediated T-cell function and higher affinity was associated with increased T cell function in this study as measured by cytokine production, proliferation and *in vivo* efficacy. Biacore assessment of the scFv with the highest affinity revealed a balanced distribution of both a high k_{on} and a low k_{off} contributing to the low K_D value [128]. Discrepancies between the previous studies can be accounted for by methodological differences. In the ROR1 study CARs with different backbones were compared with respect to their efficacy in redirecting T cells. Also, the two binding domains compared in this study had different epitope specificity.

Caruso *et al.* compared two scFvs (derived from mAbs Nimotuzumab and Cetuximab) of different affinity targeting EGFR. Nimotuzumab had a nearly 60- fold reduced on-rate of binding compared to Cetuximab and a resulting reduced affinity of binding to EGFR (SPR Biacore Nimotuzumab: $K_D = 2.1x10^8$ mol/L, $k_{on} = 5.2x10^4$, $k_{off} = 1.1x10^3$; Cetuximab: $K_D = 1.8x10^9$, $k_{on} = 3.1x10^6$, $k_{off} = 5.8x10^3$) [195]. In Caruso's study the Nimotuzumab CAR with reduced affinity was unable to recognize EGFR expressed at reduced levels, exhibiting a gradient of T-cell activation that directly correlated with density of expression of EGFR [151]. These results were in contrast to our findings where it appeared that CAT CAR transduced cells showed improved functional avidity against the SUPT1CD19LO cell line in a 24hour cytotoxicity assay compared to FMC63 transduced T cells. It is possible that the reduced affinity of Nimotuzumab CAR transduced T cell as a result of a much slower on-rate may explain these differences in outcome. In fact, the higher affinity Cetuximab has a quicker off-rate and when one calculates the interaction half-time Cetuximab has a $t_{1/2}$ of 119 minutes, compared to a $t_{1/2}$ of Nimotuzumab of 149 minutes. This in combination with antigen expression levels of approximately 30,000 copies of EGFR/cell on their lowest expressing cell line, which is significantly higher than the 140 copies/cell on SupT1CD19LO, suggest that these results do not reflect differences in serial triggering but instead show reduced acti-

vation of Nimotuzumab CAR T cells as a result of a reduced on-rate. Site-directed mutagenesis excluded differences in epitope specificity as a potential contributor, showing that the Nimotuzumab epitope strongly overlaps with the Cetuximab binding site [195].

6.2.1 Lower CAR affinity in the context of a faster off-rate results in increased antigen-specific responses and is associated with enhanced proliferation

Our comparison shows that higher affinity scFvs do not translate into greater proliferation or cytotoxicity. In fact the opposite appears to be the case. The scFvs of which the CD19 CARs were derived differed mostly in off-rate as opposed to on-rate and so greater affinity was caused by prolonged association with the antigen. Evidence supports both K_d and k_{off} as determinants of T-cell function [196]. By the use of *in vitro* pre-clinical models we were able to demonstrate that CAT-CAR$^+$ T cells show increased proliferation following antigenic stimulation in cytokine-free conditions, and increased capacity to produce TNFα and perhaps IL-2 in response to encounter with antigen in comparison to T cells from the same donors expressing FMC63 CAR. These findings were replicated in our *in vivo* model system. CAT CAR transduced T cells showed enhanced cytotoxicity than FMC63 in cell lines with high antigen density. Against targets with low antigen density our data suggest that CAT CAR T cells show a trend towards an improved ability to kill compared with FMC63 at low E:T ratios. The reduced affinity of CAT might therefore be mitigated by its short dissociation rate, favouring serial triggering as well as serial killing. Using live cell imaging, we observed a significantly greater number of effector:target interactions with CAT CAR over 20 hours. In addition, it appeared that CAT CAR T cells accumulated several contemporaneous interactions with targets cells. Interestingly, the duration of these interactions were not significantly reduced compared to FMC63 transduced T cell, though marked differences were found in the motility of CAT transduced T cells, showing greater displacement over time.

Thus, the lower affinity of CAT CAR-CD19 interaction may facilitate more rapid interaction with multiple $CD19^+$ targets.

It has been hypothesized that there is a potential upper limit to increased responsiveness to high affinity interactions, otherwise leading to attenuation of intracellular signalling and expansion [197]. An interesting systematic analysis of T cell responses by Omer Dushek's lab of the high-affinity engineered c58c61 TCR that binds the NY-ESO-1 cancer antigen, to measure primary human T-cell activation in response to a 1 million-fold variation in pMHC affinity and dose, concluded that there is a bell-shaped response with reduced cytokine production at high peptide-MHC concentrations, and the peak amplitude of the dose-response response curve is independent of the affinity of the interaction. However, an intermediate affinity interaction produces the largest response at low doses of pMHC [36]. The intermediate affinity ligand employed had very similar kinetic characteristics to the CAT scFv. Although a bell-shaped dose-response can be a result of AICD, they show that this was unlikely to be the case in their experiment. They found that the dose-response for cytokine production appeared bell-shaped at all times with continued cytokine production to the right of the peak. Moreover, direct detection of apoptosis by annexin V binding revealed a maximum of only 10%, which is insufficient to explain the observed reduction in cytokine production. These observations suggested a reduced rate of cytokine production per cell at high pMHC doses, which they confirmed using single-cell cytokine production.

Using model identification algorithms they propose a model in which the TCR-pMHC complex directly inhibits a node P and indirectly activates P (by activating Y, which itself is able to activate P). The model can produce inhibition at high pMHC concentrations if the activatory pathway (through Y) saturates, allowing inhibition to dominate at the highest pMHC concentrations. This model however, would result in a bell-shaped dose-response for all pMHC ligands independent of their affinity. They then introduce kinetic proofreading, by means that the pMHC ligand does not trigger signalling immediately upon binding TCR but instead must remain bound until it becomes signalling-competent (denoted as C_1). This delay

means that low-affinity pMHCs (with faster k_{off}) induce a lower maximal concentration of C_1. If this is below the level at which Y saturates then inhibition at high pMHC concentrations will not be observed with low-affinity pMHC. This model, however, is also rejected because it predicts that the highest-affinity ligand will produce the largest response left of the peak in contrast to experimental observations. They then introduce limited signalling into kinetic proofreading. In this model, activated TCR-pMHC complexes (C_1) signal for a limited period before converting to a nonsignalling state (C_2), thereby introducing a penalty for pMHCs that remain bound for long periods of time. This model is now able to explain all key features and is accepted as a plausible signalling model for T-cell activation [36] and may be an explanation for the different functional output of CAT CAR transduced T cells compared to FMC63. An experiment in which we would compare CAR T cell functionality targeting a full range of SupT1 cells expressing CD19 antigen at varying levels, would give further insight. We would expect to see a bell-shape dose response curve in FMC63 CAR T cells and potentially CAT CAR T cells, although we hypothesize that the curve of CAT CAR transduced T cells may look significantly different, as the activation pathway might never be saturated, compared to the inhibitory pathway by means of its quick dissociation.

In resting T cells the TCR/CD3 complex is stable and gets rapidly recycled after internalization [168, 198]. Internalization is a parameter for TCR serial triggering and is characteristic of productive TCR engagement by agonist ligands [34]. Following ligation of the TCR the downregulation is mediated by intracellular retention, preventing recycling, and degradation by lysosomes and proteasomes[145, 198]. CAR downregulation has been described previously[194]. In our study, antigen-induced CAR downregulation was only observed for CAT-CAR transduced cells. T cells expressing FMC63 did not significantly downregulate their CAR expression. These results are in agreement with our *in vitro* findings, suggesting increased activation in CAT possibly resulting by serial triggering. Sustained CAR signalling has been associated with AICD, suggesting that CAR down-

regulation might be beneficial to reduce the ongoing signalling in the presence of large antigen burdens.

The TCR signalling machinery is pivotal in regulating the response of a T cell following antigen exposure [14]. Interactions of the TCR with pMHC complexes induce full calcium signalling, crucial for T cell activation, requiring multiple intracellular reactions that are completed within 6-7 seconds following TCR ligation [14], as discussed in section 1.2.2. Signal initiation and propagation are driven by rapid biochemical reactions that induce or amplify the physical connectivity and catalytic activity of signalling components. Regulatory mechanisms that oppose these events allow the signals to be controlled or stopped and secure appropriate responses. Following TCR engagement, phosphorylation and dephosphorylation reactions allow signalling circuits to rapidly establish a new steady-state [14]. As shown in figure 6.1 $t_{1/2}$ of TCR-MHC interaction impacts the T cell functional outcome. A long $t_{1/2}$ might induce a state of tonic signalling, negatively affecting functional avidity by means of preventing cells from recovering to a more quiescent state, which in turn would prevent further productive T cell activation and induce AICD. We hypothesize that FMC63 CAR T cells were potentially unable to re-engage with new target cells because of tonic signalling in the presence of antigen-bearing cells. CAT CAR T cells showed a greater ability to repeatedly productively engage targets, however whether longer $t_{1/2}$ of CAR binding results in impaired ability of CAR T cells to serially engage multiple targets, by means of preventing T cell recovery and/or inducing AICD has not yet been studied. The relation between $t_{1/2}$, CAR T cell recovery and CAR T cell motility warrants further studies, as will further be discussed in more detail.

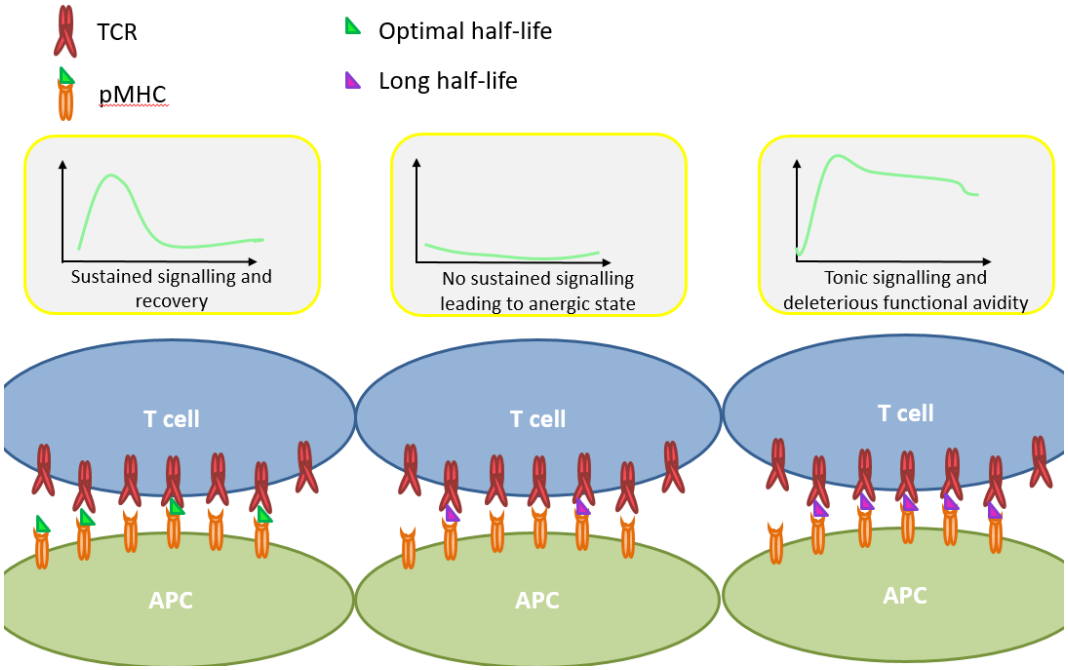

Figure 6.1: **Optimal window of TCR-pMHC interaction time**

Adapted from [28]

6.2.2 Low affinity CD19-CAR$^+$ T cells show improved *in vivo* anti-leukaemic efficacy

Although functional effector T cells can transiently express inhibitory receptors during activation, prolonged and/or high expression of multiple inhibitory/activation receptors is a key feature of the exhaustion of CD8$^+$ and CD4$^+$ T cells [170]. Loss of effector function during T cell exhaustion has first been identified during chronic LCMV infection. CD8$^+$ loss of function occurs in a hierarchical manner [170]. The expression of PD-1 and TIM3 on FMC63 and CAT CAR transduced T cells was analysed 7 days after the start of a 1:1 co-culture with irradiated Raji cells, and showed no significant difference between CAT and FMC63 CAR transduced T cells. Because of induced apoptosis of the target cells, following irradiation, CAR$^+$ T cells were not chronically stimulated and we were therefore unable to investigate the effect of persistent antigen encounter. However, it has been shown that early interactions with target cells dictate the eventual fate of CD8$^+$ cells and their memory recall capacity [199]. Long *et al.* showed that early T cell exhaustion is a primary factor limiting the antitumour efficacy of CAR-expressing T cells and that CAR structure has a central role in predisposing CAR T cells to chronic activation and exhaustion, affecting 3 pathways: i) response to hypoxia, ii) cellular metabolism and iii) negative regulation of apoptosis, however they did not investigate the impact of CAR T cell affinity in this study.

The *in vivo* studies discussed in chapter 5 investigated the effect of chronic antigen stimulation on CAR T cell exhaustion. We hypothesized that by subjecting CAR transduced T cells to a "stress test", letting the tumour cells fully engraft prior to infusion of suboptimal T cell doses, we would identify differences that may not have become clear in our *in vitro* studies, such as T cell exhaustion resulting in reduced anti-leukaemic efficacy. It has been shown that increased TCR-pMHC interactions *in vivo* result in decreased proliferation, cytokine production and memory formation. Corse *et al.* showed that optimal *in vivo* responses occur to ligands with intermediate TCR/pMHC half-lives[185]. In fact they observed a diminished response to the ligand exhibiting the longest half-life, associated with attenuation of

intracellular signalling, expansion and T cell function. Various groups have shown that when $CD8^+$ expressing high-affinity TCRs, are given as adoptive T cell therapy, they lose their cytotoxic effector properties, fail to infiltrate tumours and are rapidly deleted both in the tumour as well as the periphery [176–178]. When antigen is not cleared functional antigen-specific T cells are eventually lost. Both early fate decisions, such as survival and memory precursor formation, and late fitness of antigen-specific $CD8^+$ populations can be compromised [199]. The level of individual peptides presented *in vivo* is an important determinant of both functional exhaustion and physical deletion and a high level of persistent epitope presentation may lead to deletion, while persistence of lower-level TAAs stimulation may result in functional impairment, as a result of strong coinhibitory signals and progressive loss of effector function[200].

Our results from two independent experiments indicate that greater disease control was achieved by lower affinity CAR T cells *in vivo*. Both the FMC63 and CAT cohort were able to delay tumour growth but CAT transduced T cells were more effective at inhibiting tumour growth compared to FMC63 expressing T cells from the same donors and on day 12 post T cell injection substantial differences were seen in tumour burden (Fig. 5.8, BLI CAT CAR: $1.1x10^8 \pm 9.3x10^7$, FMC63 CAR $3.2x10^9 \pm 7.7x10^8$ Mean ph/sec/cm^2). CAT CAR T cells accumulated greater at the disease site, as well as in periphery (blood and spleen). This may result from their greater proliferative capacity or protection from activation induced cell death (AICD) or both. However we cannot exclude distribution of CAR T cells into organs other than secondary lymphoid compartments, as we did not investigate any further organs, which could potentially explain the difference in absolute number between FMC63 and CAT CAR transduced T cells.

Early, functional T cells in acute infections temporarily express high levels of inhibitory receptors such as PD-1, LAG-3 and TIM3 [182]. The expression of these inhibitory receptors was not significantly different in the CAR transduced T cells. These phenotypic characterisations were first described in persisting LCMV infections. Subsequently, they were also found in HIV and hepatitis C virus infections

and the presence of this chronic phenotype is generally considered a sign of a deteriorating T cell response [201]. A potential explanation for the lack of up-regulation of these parameters in FMC63 transduced T cells might be that the earliest timepoint chosen to study these phenotypic characterisations was two weeks following injection, and therefore exhausted T cells might already have undergone AICD. Unpublished results from our group revealed significantly lower levels of PD-1 expression in CAT CAR transduced T cells compared to FMC63 CAR transduced T cells 10 days following CAR infusion in a different *in vivo* tumour rescue model, where CAR T cells were infused 24 hours following Raji tumour cell infusion and disease had been eliminated for several days before the timepoint at which PD-1 expression was analysed.

The hierarchical loss of effector function describes the loss of the ability of virus-specific $CD8^+$ T cells to produce TNF-α and IL-2. Interestingly, the ability to produce IFN-γ is maintained and more resistant to inactivation [200]. *In vitro* we had already shown a significantly greater production of TNF-α (Mean concentration $\pm$ SEM: CAT CAR T cells: 750.7 $\pm$ 103.3 pg/ml, FMC CAR T cells: 292.1 $\pm$ 36.51 pg/ml) and a trend towards greater production of IL-2 by CAT CAR transduced T cells (Mean concentration $\pm$ SD CAT CAR T cells: 11156 $\pm$ 2777 pg/ml, FMC63 CAR T cells: 5501 $\pm$ 1285 pg/ml) (Fig. 4.8), as discussed in section 4.2.4.1. These results were obtained after a relative short exposure of 48 hours to irradiated antigens and can therefore not be explained as a result of reduced exhaustion of CAT CAR transduced T cells compared to FMC63 transduced T cells. Interestingly however, our findings *in vivo* seemingly reflect these differences indicating that CAT CAR T cells at the tumour site show a greater ability to express TNF-α and again a trend towards greater expression of IL-2 as well, 12 days following transfer to tumour bearing hosts.

Several studies have suggested that the expansion and differentiation program is imprinted shortly after antigenic stimulation [181]. A typical CD8 T cell response consists of three main developmental stages: effector cell expansion and differentiation; effector cell contraction; and stabilization and maintenance of the memory

cell population [183]. IL-7 is involved in maintaining memory populations after the clearance of antigen, and IL-7Rα signalling has an important function in T cell survival by increasing the expression of anti-apoptotic molecules (Bcl-2 and Bcl-XL) and by maintaining glycolysis and respiration levels in T cells through activation of multiple signal transduction pathways [183]. Van Leeuwen *et al.* describe that in chronic infections IL-7Rα$^+$ T cells express higher levels of Bcl-2 show a superior recall response and enhanced proliferation in response to homeostatic signals [181]. Interestingly when we investigated IL-7Rα expression (CD127) on CAR transduced T cells 15 days following infusion *in vivo*, we showed a significantly greater proportion of IL-7Rα$^+$ CAT CAR transduced T cells, as well as significantly higher expression levels. This directly correlated with an upregulation of the anti-apoptotic molecule Bcl-2, akin to results previously reported in chronic infections [183]. We speculate that the higher levels of Bcl-2 in CAT CAR T cells may contribute to their expansion and persistence by preventing apoptosis and AICD. The downstream mechanisms by which signalling through the CAT CAR results in greater upregulation of Bcl-2 compared to signalling through FMC63 are clearly of great interest and merit further investigation.

6.2.3 Directions for further investigation

Activation of mTOR-dependent pathways regulates the differentiation of CD8$^+$ and CD4$^+$ T cell subsets [202]. T cell stimulation and expansion induces a shift from oxidative respiration to aerobic glyocolysis [203]. This shift in the metabolic balance is regulated by the mTOR kinase pathway, through the MTORC1 and MTORC2 complexes. Upon T cell activation mTORC1 kinase activity is triggered leading to cell growth, expansion and differentiation of effector cells, resulting in reduced expression of CD62L (a lymph node homing molecule) and a switch to aerobic glycolysis [203]. Corse *et al.* observed attenuation at the level of intracellular signalling intermediates associated with Akt kinase activation and cytokine signalling, depending on TCR affinity. Upon stimulation high affinity TCR T cells were positive for pAKT, indicating greater activity of mTORC2 [185]. It has been shown that increased mTORC1 activity promotes earlier tumour infiltration and enhanced

disease clearance in a murine EL4-NP thymoma model [203]. However these activated T cells show reduced persistence, which has been reported to be essential for effective clinical activity of CAR T cells [73, 74]. When mTORC1 activity was completely inhibited, the $F5^+$ TCR T cells showed a reduced effector response and reduced tumour infiltration as a result of a quiescent state, as well as high expression levels of CD62L and CD127, markers associated with central memory differentiation. Complete inhibition of mTORC1 activity, can lead to anergic T cells incapable of generating effector cells either during the primary response or recall [203]. When investigating the specific effect of mTORC2 on $CD8^+$ T cell memory, Pollizzi *et al.* showed that T cell deficient for mTORC2 showed equivalent or enhanced cytotoxicity and accumulation of antigen specific T cells, where mTORC1 deficient mice were unable to get activated or proliferate, like indicated earlier [202, 203]. Interestingly however, was the upregulation of CD127 and Bcl2 in mTORC2 deficient cells, through FOXO-induced expression, which directly correlated to improved persistence and a better recall response compared to wild type. Thus, mTORC2 deficient mice generated a robust effector response, whilst simultaneously upregulating markers associated with increased T cell fitness and reduced apoptosis. We hypothesize that given the increased expression levels of CD127 and Bcl2 on CAT CAR transduced T cells as well as their increased functionality and accumulation *in vivo*, that mTORC1 and mTORC2 are differentially activated in CAT compared to FMC63 transduced T cells, potentially showing a greater activity of mTORC2 in FMC63 transduced T cells. Important for an effective CAR T cell response is the differentiation of effector cells while at the same time enabling self-renewal needed for long-term memory. Rapamycin inhibits mTOR activity and has been shown to enhance antitumour $CD8^+$ activity as well as increased persistence of tumour-infiltrating lymphocytes [204]. When given at low dose, the initial expansion of effector cells is maintained, but persistence is improved both by increasing the number of effector memory precursors in the expansion phase, as well as promoting central memory T cells during the contraction phase [204] and both Velica *et al.* and Pollizzi *et al.* showed that temporarily blocking mTOR activity

promotes the generation of functional memory T cells. We suggest that future experiments inhibiting the mTOR activity in FMC63 CAR transduced T cells, and selective inhibition of mTORC2 activity specifically may improve FMC63 CAR T cell functionality, accumulation and persistence *in vivo* further unravelling the effect of CAR T cell affinity on intracellular signalling pathways.

In early correlative studies of patients treated with TCR-engineered cells, the ability of the engineered cells to function upon tumour encounter immediately *ex vivo* was the single difference found between responders and non-responders. Both groups had high levels of engineered T cell in circulation one month after treatment, however only T cells from patients who showed a clinical response were responsive to *ex vivo* tumour exposure, as identified by IFN-γ and IL-2 production [205]. To further investigate the fitness of FMC63 and CAT CAR transduced T cells we propose *ex vivo* proliferation experiments and cytokine response experiments of CAR T cells following tumour clearance *in vivo*. Furthermore, secondary transfer of CAR T cell effectors should provide essential further insight. We hypothesize, given the reduced number of FMC63 CAR T cells and a reduced capacity to produce cytokines following antigen specific stimulation *in vivo*, which may be a reflection of AICD and exhaustion, that FMC63 CAR transduced T cells would show an impaired proliferative response following secondary stimulation *ex vivo* as well as a reduced cytokine response. It has been shown in the case of chronic antigen exposure that virus-specific $CD8^+$ T cells generated during chronic LCMV infection fail to persist when adoptively transferred to naive uninfected mice, indicating possible defects in memory T cell homeostasis [206]. Unfortunately we were unable to study persistence of CAR T cells *in vivo*, due to development of xeno-GvHD so that prolonged experiments were not feasible. Our aim to re-challenge after successful tumour elimination, examining the memory recall responses would require higher doses of CAR T cells, as we did not establish disease clearance. Consequently, to reduce the total number of total T cells infused we propose to use sorted populations of CAR T cells in future experiments, thereby reducing the risk for xeno-GvHD. We would expect this memory recall response to be impaired in FMC63 CAR T cells

again as a result of exhaustion as well as potential differences in mTOR activity [199, 202, 203].

To identify the molecular mechanisms underlying these functional effects thorough investigation of signalling pathways downstream as well as global gene expression and activatory/inhibitory membrane receptors on human $CD8^+$ T cells engineered with CARs of incremental affinity will likely lend further understanding into these mechanisms, as well as the biochemistry of CAR T cell activation in general. The functional impairment of high avidity T cells in the presence of high levels of antigen has been described to be related to enhanced activity of downstream sarcoma homology domain 2 phosphatase (SHP)1 [21]. SHP-1 phosphatase may represent an important regulatory molecule in $CD8^+$ T cells with incremental affinity TCR variants. Strikingly, is has been shown that SHP-1 mediates a gradual functional inhibition of $CD8^+$ T cells, along with TCR-binding affinity, independently of PD-1 involvement [192]. In addition, in T cells expressing expressing TCRs with supraphysiological affinities ZAP-70 phosphorylation declined rapidly and substantially following specific stimulation and a transient and rapid loss of ERK1/2 phosphorylation following TCR stimulation was observed [192]. The assessment of SHP1 , the activation levels of ZAP-70, a proximal activatory molecule of TCR signalling and of the distal MAPK family members ERK1/2 is therefore warranted. Gene expression profiles specific for exhausted T cells [119] and specific for the metabolic profile of T cells [122] have been described and could be further exploited in the comparison of FMC63 and CAT CAR transduced cells as well.

Lastly, the difference in motility and number of (contemporaneous) interactions of CAT CAR transduced T cells provides a new direction of research in CAR T cell biology, particularly relevant when targeting solid cancers. Actin remodelling is an important component of immunological synapse formation and cytoskeleton organization is tightly integrated with T cell activation and signalling [17]. The adhesion and signal transduction depend on physical forces exerted by actin cytoskeletal dynamics. Immunological synapse (IS)-associated signalling molecules

are physically linked to actin filaments; conformational changes exerted by these forces are needed for full T cell activation [18]. Research by Bousso's lab, investigating T cell motility in relation to TCR affinity, has shown that extracellular calcium influx is involved in T-cell motility arrest during antigen recognition. They observed robust calcium elevation in T cells stimulated with high affinity protein complexes, but low affinity protein complexes resulted in little or no signal[207]. They show that low-affinity antigen induces a calcium-independent partial deceleration, whereas high-affinity antigen provides an additional calcium-dependent signal that facilitates complete T-cell arrest. Furthermore, LAT protein that has been shown to be enriched in the uropod of migrating T cells was differentially organised in high affinity TCR reactions compared to low affinity, being more at the front of the low affinity T cells, in contrast to restriction in the uropod region of high affinity T cells. Altogether, these experiments establish the existence of distinct cellular organization patterns that differ in the presence of low-affinity peptide compared with steady-state conditions, strongly suggesting that a switch in the mode of migration underlies T cell motility. Their results suggest that TCR engagement acts by two mechanisms to promote T cell deceleration: binding to pMHC may promote adhesion and switching of migration mode, whereas strong intracellular TCR signals are required for full arrest. Deceleration induced by low-affinity antigenic complexes was dependent on TCR engagement, but appeared largely independent of downstream TCR signals[207]. It is therefore possible that TCR signalling interferes with molecular motors that impact T cell motility. Little is known about CAR T cell synapse formation. Neeson *et al.* have shown reduced accumulation of LFA-1 integrin, mediating adhesion between T cells and APCs, in the synapse of CAR T cell [125]. There have been no further studies however. Having observed such distinct kinetic profiles between FMC63 and CAT CAR transduced cells, we hypothesize that there could be differences in synapse formation depending on CAR T cell affinity, which may affect actin remodelling and adhesion. However, using live cell imaging we saw no difference in effector:target interaction dwell time between FMC63 and CAT CAR transduced T cells. We therefore propose that a longer

$t_{1/2}$ of CAR transduced cells may result in differences in downstream signalling and impair T cell recovery, affecting switching of the migration mode and resulting in a full T cell arrest, which necessitates further studies.

6.3 Final conclusion

We have developed a novel CD19-CAR which confers enhanced cytotoxicity and proliferative responses compared to existing CD19-CARs. Our work indicates that the kinetics of scFv binding significantly impact the functional avidity of CAR-transduced T cells, providing important implications for the development of future CARs. It is possible that the improved functional avidity associated with the off-rate of the CAR binding domain is a feature specific for CD19 as the antigen, as it has previously been asserted that a lower affinity CAR results in diminished functional avidity when a different antigen was targeted[151, 152]. However, we rationalize that, analogous to the natural TCR and as indicated by previous work on bi-specific T-cell engagers, a lower overall binding affinity for a target might be mitigated by a relatively faster off-rate in the setting of a constant on-rate, allowing for serial triggering and rapid regaining of quiescence because of more rapid termination of immunoreceptor signalling. Collectively, these data emphasize the potential impact of CAR-binding affinity in relation to T cell activation and highlight the need to carefully assess CAR affinity/avidity in relation to its functional efficacy. In other words, one should separately scrutinize the two determinants of affinity, the on- and off-rate in determining optimal CAR binding characteristics. We believe this to be of particular relevance when target antigen expression levels are low and further work is needed to investigate this effect on low-expressed antigens. Most importantly, clinical evaluation of CAT-CAR is being undertaken in the CARPALL trial (clinicaltrials.gov, NCT02443831), in which we aim to specifically study the impact of using this low affinity CD19 CAR on disease response, T cell expansion and persistence.

Bibliography

[1] N Howlader, AM Noone, M Krapcho, J Garshell, D Miller, SF Altekruse, CL Kosary, M Yu, J Ruhl, Z Tatalovich, A Mariotto, DR Lewis, HS Chen, EJ Feuer, and KA Cronin. SEER Cancer Statistics Review, 1975-2012, National Cancer Institute. apr 2015.

[2] Hiroto Inaba, Mel Greaves, and Charles G. Mullighan. Acute lymphoblastic leukaemia. *Lancet*, 381(9881), jun 2013.

[3] Stephen P. Hunger and Charles G. Mullighan. Redefining ALL classification: toward detecting high-risk ALL and implementing precision medicine. *Blood*, 125(26):3977–3987, jun 2015.

[4] Ching-Hon Pui and William E. Evans. A 50-Year Journey to Cure Childhood Acute Lymphoblastic Leukemia. *Semin. Hematol.*, 50(3):185–196, jul 2013.

[5] Dianne Pulte, Adam Gondos, and Hermann Brenner. Improvement in survival in younger patients with acute lymphoblastic leukemia from the 1980s to the early 21st century. *Blood*, 113(7):1408–1411, feb 2009.

[6] Kathryn G. Roberts and Charles G. Mullighan. Genomics in acute lymphoblastic leukaemia: insights and treatment implications. *Nat. Rev. Clin. Oncol.*, advance on, mar 2015.

[7] Mark B. Geyer and Renier J. Brentjens. Review: Current clinical applications of chimeric antigen receptor (CAR) modified T cells. *Cytotherapy*, aug 2016.

[8] C-H Pui, D Pei, JT Sandlund, RC Ribeiro, JE Rubnitz, SC Raimondi, M Onciu, D Campana, LE Kun, S Jeha, C Cheng, SC Howard, ML Metzger,

D Bhojwani, JR Downing, WE Evans, and MV Relling. Long-term results of St. Jude Total Therapy studies 11, 12, 13A, 13B and 14 for childhood acute lymphoblastic leukemia. *Leukemia*, 24(2):371–382, feb 2010.

[9] Stephen P. Hunger, Xiaomin Lu, Meenakshi Devidas, Bruce M. Camitta, Paul S. Gaynon, Naomi J. Winick, Gregory H. Reaman, and William L. Carroll. Improved Survival for Children and Adolescents With Acute Lymphoblastic Leukemia Between 1990 and 2005: A Report From the Children's Oncology Group. *J. Clin. Oncol.*, 30(14):1663–1669, may 2012.

[10] Ruslan Medzhitov and Charles A. Janeway. Decoding the patterns of self and nonself by the innate immune system. *Science*, 296(5566):298–300, apr 2002.

[11] Vanessa Venturi, Katherine Kedzierska, Mark M. Tanaka, Stephen J. Turner, Peter C. Doherty, and Miles P. Davenport. Method for assessing the similarity between subsets of the T cell receptor repertoire. *J. Immunol. Methods*, 329(12):67–80, jan 2008.

[12] Kemeng Wang, Guoqing Wei, and Delong Liu. CD19: a biomarker for B cell development, lymphoma diagnosis and therapy. *Exp. Hematol. Oncol.*, 1(1):36, 2012.

[13] Charles A. Janeway, Paul Travers, Mark Walport, Mark J. Shlomchik, Charles A. Janeway Jr, Paul Travers, Mark Walport, and Mark J. Shlomchik. *Immunobiology*. Garland Science, 5th edition, 2001.

[14] Oreste Acuto, Vincenzo Di Bartolo, and Frédérique Michel. Tailoring T-cell receptor signals by proximal negative feedback mechanisms. *Nat. Rev. Immunol.*, 8(9):699–712, sep 2008.

[15] Jia-huai Wang and Ellis L. Reinherz. The structural basis of $\alpha\beta$ T-lineage immune recognition: TCR docking topologies, mechanotransduction, and co-receptor function. *Immunol. Rev.*, 250(1):102–119, nov 2012.

[16] Gilbert J Kersh, Ellen N Kersh, Daved H Fremont, and Paul M Allen. High- and Low-Potency Ligands with Similar Affinities for the TCR: The Importance of Kinetics in TCR Signaling. *Immunity*, 9(6):817–826, dec 1998.

[17] Ken Nguyen, Nicholas R. Sylvain, and Stephen C. Bunnell. T Cell Costimulation via the Integrin VLA-4 Inhibits the Actin-Dependent Centralization of Signaling Microclusters Containing the Adaptor SLP-76. *Immunity*, 28(6):810–821, jun 2008.

[18] William A. Comrie and Janis K. Burkhardt. Action and Traction: Cytoskeletal Control of Receptor Triggering at the Immunological Synapse. *Front. Immunol.*, 7, 2016.

[19] Salvatore Valitutti, Daniel Coombs, and Loïc Dupré. The space and time frames of T cell activation at the immunological synapse. *FEBS Lett.*, 584(24):4851–4857, dec 2010.

[20] Jennifer D Stone, Adam S Chervin, and David M Kranz. T-cell receptor binding affinities and kinetics: impact on T-cell activity and specificity. *Immunology*, 126(2):165–176, feb 2009.

[21] Andre Kunert, Trudy Straetemans, Coen Govers, Cor Lamers, Ron Mathijssen, Stefan Sleijfer, and Reno Debets. TCR-Engineered T Cells Meet New Challenges to Treat Solid Tumors: Choice of Antigen, T Cell Fitness, and Sensitization of Tumor Milieu. *Front. Immunol.*, 4, nov 2013.

[22] M. P. Tan, A. B. Gerry, J. E. Brewer, L. Melchiori, J. S. Bridgeman, A. D. Bennett, N. J. Pumphrey, B. K. Jakobsen, D. A. Price, K. Ladell, and A. K. Sewell. T cell receptor binding affinity governs the functional profile of cancer-specific CD8+ T cells. *Clin. Exp. Immunol.*, 180(2):255–270, may 2015.

[23] Melita Irving, Vincent Zoete, Michael Hebeisen, Daphné Schmid, Petra Baumgartner, Philippe Guillaume, Pedro Romero, Daniel Speiser, Immanuel

Luescher, Nathalie Rufer, and Olivier Michielin. Interplay between T Cell Receptor Binding Kinetics and the Level of Cognate Peptide Presented by Major Histocompatibility Complexes Governs CD8+ T Cell Responsiveness. *J. Biol. Chem.*, 287(27):23068–23078, jun 2012.

[24] Caridad Rosette, Guy Werlen, Mark A Daniels, Philmore O Holman, S. Munir Alam, Paul J Travers, Nicholas R. J Gascoigne, Ed Palmer, and Stephen C Jameson. The Impact of Duration versus Extent of TCR Occupancy on T Cell Activation: A Revision of the Kinetic Proofreading Model. *Immunity*, 15(1):59–70, jul 2001.

[25] Misty R. Jenkins, Andy Tsun, Jane C. Stinchcombe, and Gillian M. Griffiths. The Strength of T Cell Receptor Signal Controls the Polarization of Cytotoxic Machinery to the Immunological Synapse. *Immunity*, 31(4):621–631, oct 2009.

[26] Anthony F. O. Daniyan and Renier J. Brentjens. At the bench: chimeric antigen receptor (CAR) T cell therapy for the treatment of B cell malignancies. *J. Leukoc. Biol.*, pages jlb.5BT1215–556RR, oct 2016.

[27] Robert J. Salmond, Andrew Filby, Ihjaaz Qureshi, Stefano Caserta, and Rose Zamoyska. T-cell receptor proximal signaling via the Src-family kinases, Lck and Fyn, influences T-cell activation, differentiation, and tolerance. *Immunol. Rev.*, 228(1):9–22, mar 2009.

[28] Salvatore Valitutti. The Serial Engagement Model 17Years After: From TCR Triggering to Immunotherapy. *Front. Immunol.*, 3, aug 2012.

[29] J. D. Rabinowitz, C. Beeson, D. S. Lyons, M. M. Davis, and H. M. McConnell. Kinetic discrimination in T-cell activation. *Proc. Natl. Acad. Sci.*, 93(4):1401–1405, feb 1996.

[30] T. W. McKeithan. Kinetic proofreading in T-cell receptor signal transduction. *Proc. Natl. Acad. Sci.*, 92(11):5042–5046, may 1995.

[31] Sharyn Thomas, Shao-An Xue, Charles R. M. Bangham, Bent K. Jakobsen, Emma C. Morris, and Hans J. Stauss. Human T cells expressing affinity-matured TCR display accelerated responses but fail to recognize low density of MHC-peptide antigen. *Blood*, 118(2):319–329, jul 2011.

[32] Hans J Stauss, Emma C Morris, and Hinrich Abken. Cancer gene therapy with T cell receptors and chimeric antigen receptors. *Curr. Opin. Pharmacol.*, 24:113–118, oct 2015.

[33] Alexis M. Kalergis, Nicole Boucheron, Marie-Agnés Doucey, Edith Palmieri, Earl C. Goyarts, Zsuzsanna Vegh, Immanuel F. Luescher, and Stanley G. Nathenson. Efficient T cell activation requires an optimal dwell-time of interaction between the TCR and the pMHC complex. *Nat. Immunol.*, 2(3):229–234, mar 2001.

[34] Salvatore Valitutti, Sabina Muller, Marina Cella, Elisabetta Padovan, and Antonio Lanzavecchia. Serial triggering of many T-cell receptors by a few peptide-MHC complexes. *Nature*, 375(6527):148–51, may 1995.

[35] Jun Huang, Mario Brameshuber, Xun Zeng, Jianming Xie, Qi-jing Li, Yueh-hsiu Chien, Salvatore Valitutti, and Mark M. Davis. A Single Peptide-Major Histocompatibility Complex Ligand Triggers Digital Cytokine Secretion in CD4+ T Cells. *Immunity*, 39(5):846–857, nov 2013.

[36] Melissa Lever, Hong-Sheng Lim, Philipp Kruger, John Nguyen, Nicola Trendel, Enas Abu-Shah, Philip Kumar Maini, Philip Anton van der Merwe, and Omer Dushek. Architecture of a minimal signaling pathway explains the T-cell response to a 1 million-fold variation in antigen affinity and dose. *Proc. Natl. Acad. Sci.*, 113(43):E6630–E6638, oct 2016.

[37] Antonio Lanzavecchia, Giandomenica Iezzi, and Antonella Viola. From TCR Engagement to T Cell Activation: A Kinetic View of T Cell Behavior. *Cell*, 96(1):1–4, jan 1999.

[38] Macfarlane Burnet. CancerA Biological Approach. *Br. Med. J.*, 1(5022):779–786, apr 1957.

[39] Gavin P. Dunn, Allen T. Bruce, Hiroaki Ikeda, Lloyd J. Old, and Robert D. Schreiber. Cancer immunoediting: from immunosurveillance to tumor escape. *Nat. Immunol.*, 3(11):991–998, nov 2002.

[40] Roy M. Bremnes, Lill-Tove Busund, Thomas L. Kilvær, Sigve Andersen, Elin Richardsen, Erna Elise Paulsen, Sigurd Hald, Mehrdad Rakaee Khanehkenari, Wendy A. Cooper, Steven C. Kao, and Tom Dønnem. The Role of Tumor-Infiltrating Lymphocytes in Development, Progression, and Prognosis of Non-Small Cell Lung Cancer. *J. Thorac. Oncol. Off. Publ. Int. Assoc. Study Lung Cancer*, 11(6):789–800, jun 2016.

[41] Yan Mao, Qing Qu, Xiaosong Chen, Ou Huang, Jiayi Wu, and Kunwei Shen. The Prognostic Value of Tumor-Infiltrating Lymphocytes in Breast Cancer: A Systematic Review and Meta-Analysis. *PLoS One*, 11(4):e0152500, 2016.

[42] Sanne Evelien Matlung, Pauline Maria Wilhelmina van Kempen, Niels Bovenschen, Debbie van Baarle, and Stefan Martin Willems. Differences in T-cell infiltrates and survival between HPV+ and HPV- oropharyngeal squamous cell carcinoma. *Futur. Sci. OA*, 2(1):FSO88, mar 2016.

[43] Sarah A. Weiss, Douglas Hanniford, Eva Hernando, and Iman Osman. Revisiting determinants of prognosis in cutaneous melanoma. *Cancer*, 121(23):4108–4123, dec 2015.

[44] Michał Bieńkowski and Matthias Preusser. Prognostic role of tumour-infiltrating inflammatory cells in brain tumours: literature review. *Curr. Opin. Neurol.*, 28(6):647–658, dec 2015.

[45] Ida Ricciardelli, Michael Patrick Blundell, Jennifer Brewin, Adrian Thrasher, Martin Pule, and Persis J. Amrolia. Towards gene therapy for EBV-associated posttransplant lymphoma with genetically modified EBV-specific cytotoxic T cells. *Blood*, 124(16):2514–2522, oct 2014.

[46] Hirokazu Matsushita, Matthew D. Vesely, Daniel C. Koboldt, Charles G. Rickert, Ravindra Uppaluri, Vincent J. Magrini, Cora D. Arthur, J. Michael White, Yee-Shiuan Chen, Lauren K. Shea, Jasreet Hundal, Michael C. Wendl, Ryan Demeter, Todd Wylie, James P. Allison, Mark J. Smyth, Lloyd J. Old, Elaine R. Mardis, and Robert D. Schreiber. Cancer exome analysis reveals a T-cell-dependent mechanism of cancer immunoediting. *Nature*, 482(7385):400–404, feb 2012.

[47] Lotta von Boehmer, Muriel Mattle, Peter Bode, Alexandro Landshammer, Carolin Schäfer, Natko Nuber, Gerd Ritter, Lloyd Old, Holger Moch, Niklaus Schäfer, Elke Jäger, Alexander Knuth, and Maries van den Broek. NY-ESO-1-specific immunological pressure and escape in a patient with metastatic melanoma. *Cancer Immun.*, 13:12, 2013.

[48] Theo Nicholaou, Weisan Chen, Ian D. Davis, Heather M. Jackson, Nektaria Dimopoulos, Catherine Barrow, Judy Browning, Duncan Macgregor, David Williams, Wendie Hopkins, Eugene Maraskovsky, Ralph Venhaus, Linda Pan, Eric W. Hoffman, Lloyd J. Old, and Jonathan Cebon. Immunoediting and persistence of antigen-specific immunity in patients who have previously been vaccinated with NY-ESO-1 protein formulated in ISCOMATRIX. *Cancer Immunol. Immunother. CII*, 60(11):1625–1637, nov 2011.

[49] Deepak Mittal, Matthew M Gubin, Robert D Schreiber, and Mark J Smyth. New insights into cancer immunoediting and its three component phases elimination, equilibrium and escape. *Curr. Opin. Immunol.*, 27:16–25, apr 2014.

[50] Anusha Kalbasi, Carl H. June, Naomi Haas, and Neha Vapiwala. Radiation and immunotherapy: a synergistic combination. *J. Clin. Invest.*, 123(7):2756–2763, jul 2013.

[51] S R Riddell, K S Watanabe, J M Goodrich, C R Li, M E Agha, and P D Greenberg. Restoration of viral immunity in immunodeficient humans by the adoptive transfer of T cell clones. *Science*, 257(5067):238–241, jul 1992.

[52] E B Papadopoulos, M Ladanyi, D Emanuel, S Mackinnon, F Boulad, M H Carabasi, H Castro-Malaspina, B H Childs, a P Gillio, and T N Small. Infusions of donor leukocytes to treat Epstein-Barr virus-associated lymphoproliferative disorders after allogeneic bone marrow transplantation. *N. Engl. J. Med.*, 330(17):1185–1191, apr 1994.

[53] S a Rosenberg, B S Packard, P M Aebersold, D Solomon, S L Topalian, S T Toy, P Simon, M T Lotze, J C Yang, and C a Seipp. Use of tumor-infiltrating lymphocytes and interleukin-2 in the immunotherapy of patients with metastatic melanoma. A preliminary report. *N. Engl. J. Med.*, 319(25):1676–1680, dec 1988.

[54] H J Kolb, J Mittermüller, C Clemm, E Holler, G Ledderose, G Brehm, M Heim, and W Wilmanns. Donor leukocyte transfusions for treatment of recurrent chronic myelogenous leukemia in marrow transplant patients. *Blood*, 76(12):2462–2465, dec 1990.

[55] Timothy M. Clay, Mary C. Custer, Jessica Sachs, Patrick Hwu, Steven A. Rosenberg, and Michael I. Nishimura. Efficient Transfer of a Tumor Antigen-Reactive TCR to Human Peripheral Blood Lymphocytes Confers Anti-Tumor Reactivity. *J. Immunol.*, 163(1):507–513, jul 1999.

[56] Gavin M. Bendle, Carsten Linnemann, Anna I. Hooijkaas, Laura Bies, Moniek A. de Witte, Annelies Jorritsma, Andrew D. M. Kaiser, Nadine Pouw, Reno Debets, Elisa Kieback, Wolfgang Uckert, Ji-Ying Song, John B. A. G. Haanen, and Ton N. M. Schumacher. Lethal graft-versus-host disease in mouse models of T cell receptor gene therapy. *Nat. Med.*, 16(5):565–570, may 2010.

[57] Michael H. Kershaw, Jennifer A. Westwood, and Phillip K. Darcy. Gene-engineered T cells for cancer therapy. *Nat. Rev. Cancer*, 13(8):525–541, aug 2013.

[58] Z Eshhar, T Waks, G Gross, and D G Schindler. Specific activation and targeting of cytotoxic lymphocytes through chimeric single chains consisting of antibody-binding domains and the gamma or zeta subunits of the immunoglobulin and T-cell receptors. *Proc. Natl. Acad. Sci. U. S. A.*, 90(2):720–724, jan 1993.

[59] M. Pule, H. Finney, and A. Lawson. Artificial T-cell receptors. *Cytotherapy*, 5(3):211–226, 2003.

[60] Michael C. Jensen and Stanley R. Riddell. Design and implementation of adoptive therapy with chimeric antigen receptor-modified T cells. *Immunol. Rev.*, 257(1):127–144, jan 2014.

[61] Juan F. Vera, Malcolm K. Brenner, and Gianpietro Dotti. Immunotherapy of Human Cancers Using Gene Modified T Lymphocytes. *Curr. Gene Ther.*, 9(5):396–408, oct 2009.

[62] Salima Hacein-Bey-Abina, Alexandrine Garrigue, Gary P. Wang, Jean Soulier, Annick Lim, Estelle Morillon, Emmanuelle Clappier, Laure Caccavelli, Eric Delabesse, Kheira Beldjord, Vahid Asnafi, Elizabeth MacIntyre, Liliane Dal Cortivo, Isabelle Radford, Nicole Brousse, François Sigaux, Despina Moshous, Julia Hauer, Arndt Borkhardt, Bernd H. Belohradsky, Uwe Wintergerst, Maria C. Velez, Lily Leiva, Ricardo Sorensen, Nicolas Wulffraat, Stéphane Blanche, Frederic D. Bushman, Alain Fischer, and Marina Cavazzana-Calvo. Insertional oncogenesis in 4 patients after retrovirus-mediated gene therapy of SCID-X1. *J. Clin. Invest.*, 118(9):3132–3142, sep 2008.

[63] Steven J. Howe, Marc R. Mansour, Kerstin Schwarzwaelder, Cynthia Bartholomae, Michael Hubank, Helena Kempski, Martijn H. Brugman,

Karin Pike-Overzet, Stephen J. Chatters, Dick de Ridder, Kimberly C. Gilmour, Stuart Adams, Susannah I. Thornhill, Kathryn L. Parsley, Frank J.T. Staal, Rosemary E. Gale, David C. Linch, Jinhua Bayford, Lucie Brown, Michelle Quaye, Christine Kinnon, Philip Ancliff, David K. Webb, Manfred Schmidt, Christof von Kalle, H. Bobby Gaspar, and Adrian J. Thrasher. Insertional mutagenesis combined with acquired somatic mutations causes leukemogenesis following gene therapy of SCID-X1 patients. *J. Clin. Invest.*, 118(9):3143–3150, sep 2008.

[64] Marion G. Ott, Manfred Schmidt, Kerstin Schwarzwaelder, Stefan Stein, Ulrich Siler, Ulrike Koehl, Hanno Glimm, Klaus Kühlcke, Andrea Schilz, Hana Kunkel, Sonja Naundorf, Andrea Brinkmann, Annette Deichmann, Marlene Fischer, Claudia Ball, Ingo Pilz, Cynthia Dunbar, Yang Du, Nancy A. Jenkins, Neal G. Copeland, Ursula Lüthi, Moustapha Hassan, Adrian J. Thrasher, Dieter Hoelzer, Christof von Kalle, Reinhard Seger, and Manuel Grez. Correction of X-linked chronic granulomatous disease by gene therapy, augmented by insertional activation of MDS1-EVI1, PRDM16 or SETBP1. *Nat. Med.*, 12(4):401–409, apr 2006.

[65] Therese Liechtenstein, Noemi Perez-Janices, and David Escors. Lentiviral Vectors for Cancer Immunotherapy and Clinical Applications. *Cancers (Basel).*, 5(3):815–837, jul 2013.

[66] Erin P O'Keefe. Nucleic Acid Delivery: Lentiviral and Retroviral Vectors. *Mater. Methods*, 3, mar 2013.

[67] John Scholler, Troy L. Brady, Gwendolyn Binder-Scholl, Wei-Ting Hwang, Gabriela Plesa, Kristen M. Hege, Ashley N. Vogel, Michael Kalos, James L. Riley, Steven G. Deeks, Ronald T. Mitsuyasu, Wendy B. Bernstein, Naomi E. Aronson, Bruce L. Levine, Frederic D. Bushman, and Carl H. June. Decade-Long Safety and Function of Retroviral-Modified Chimeric Antigen Receptor T-cells. *Sci. Transl. Med.*, 4(132):132ra53, may 2012.

[68] Martin Jinek, Krzysztof Chylinski, Ines Fonfara, Michael Hauer, Jennifer A. Doudna, and Emmanuelle Charpentier. A Programmable Dual-RNAGuided DNA Endonuclease in Adaptive Bacterial Immunity. *Science (80-.).*, 337(6096):816–821, aug 2012.

[69] Jennifer L. Gori, Patrick D. Hsu, Morgan L. Maeder, Shen Shen, G. Grant Welstead, and David Bumcrot. Delivery and Specificity of CRISPR/Cas9 Genome Editing Technologies for Human Gene Therapy. *Hum. Gene Ther.*, 26(7):443–451, jun 2015.

[70] Justin Eyquem, Jorge Mansilla-Soto, Theodoros Giavridis, Sjoukje J. C. van der Stegen, Mohamad Hamieh, Kristen M. Cunanan, Ashlesha Odak, Mithat Gönen, and Michel Sadelain. Targeting a CAR to the TRAC locus with CRISPR/Cas9 enhances tumour rejection. *Nature*, 543(7643):113–117, mar 2017.

[71] Levi J. Rupp, Kathrin Schumann, Kole T. Roybal, Rachel E. Gate, Chun J. Ye, Wendell A. Lim, and Alexander Marson. CRISPR/Cas9-mediated PD-1 disruption enhances anti-tumor efficacy of human chimeric antigen receptor T cells. *Sci. Rep.*, 7(1):737, apr 2017.

[72] Cor H. J. Lamers, Stefan Sleijfer, Arnold G. Vulto, Wim H. J. Kruit, Mike Kliffen, Reno Debets, Jan W. Gratama, Gerrit Stoter, and Egbert Oosterwijk. Treatment of Metastatic Renal Cell Carcinoma With Autologous T-Lymphocytes Genetically Retargeted Against Carbonic Anhydrase IX: First Clinical Experience. *J. Clin. Oncol.*, 24(13):e20–e22, may 2006.

[73] Michael H. Kershaw, Jennifer A. Westwood, Linda L. Parker, Gang Wang, Zelig Eshhar, Sharon A. Mavroukakis, Donald E. White, John R. Wunderlich, Silvana Canevari, Linda Rogers-Freezer, Clara C. Chen, James C. Yang, Steven A. Rosenberg, and Patrick Hwu. A Phase I Study on Adoptive Immunotherapy Using Gene-Modified T Cells for Ovarian Cancer. *Clin. Cancer Res.*, 12(20):6106–6115, oct 2006.

[74] Brian G. Till, Michael C. Jensen, Jinjuan Wang, Eric Y. Chen, Brent L. Wood, Harvey A. Greisman, Xiaojun Qian, Scott E. James, Andrew Raubitschek, Stephen J. Forman, Ajay K. Gopal, John M. Pagel, Catherine G. Lindgren, Philip D. Greenberg, Stanley R. Riddell, and Oliver W. Press. Adoptive immunotherapy for indolent non-Hodgkin lymphoma and mantle cell lymphoma using genetically modified autologous CD20-specific T cells. *Blood*, 112(6):2261–2271, sep 2008.

[75] Michael C. Jensen, Leslie Popplewell, Laurence J. Cooper, David DiGiusto, Michael Kalos, Julie R. Ostberg, and Stephen J. Forman. Antitransgene rejection responses contribute to attenuated persistence of adoptively transferred CD20/CD19-specific chimeric antigen receptor redirected T cells in humans. *Biol. Blood Marrow Transplant. J. Am. Soc. Blood Marrow Transplant.*, 16(9):1245–1256, sep 2010.

[76] David L. Porter, Bruce L. Levine, Michael Kalos, Adam Bagg, and Carl H. June. Chimeric Antigen ReceptorModified T Cells in Chronic Lymphoid Leukemia. *N. Engl. J. Med.*, 365(8):725–733, aug 2011.

[77] Michael Kalos, Bruce L. Levine, David L. Porter, Sharyn Katz, Stephan A. Grupp, Adam Bagg, and Carl H. June. T Cells with Chimeric Antigen Receptors Have Potent Antitumor Effects and Can Establish Memory in Patients with Advanced Leukemia. *Sci. Transl. Med.*, 3(95):95ra73–95ra73, aug 2011.

[78] James N. Kochenderfer, Mark E. Dudley, Steven A. Feldman, Wyndham H. Wilson, David E. Spaner, Irina Maric, Maryalice Stetler-Stevenson, Giao Q. Phan, Marybeth S. Hughes, Richard M. Sherry, James C. Yang, Udai S. Kammula, Laura Devillier, Robert Carpenter, Debbie-Ann N. Nathan, Richard A. Morgan, Carolyn Laurencot, and Steven A. Rosenberg. B-cell depletion and remissions of malignancy along with cytokine-associated toxicity in a clinical trial of anti-CD19 chimeric-antigen-receptor-transduced T cells. *Blood*, 119(12):2709–2720, mar 2012.

[79] Renier J. Brentjens, Isabelle Rivière, Jae H. Park, Marco L. Davila, Xiuyan Wang, Jolanta Stefanski, Clare Taylor, Raymond Yeh, Shirley Bartido, Oriana Borquez-Ojeda, Malgorzata Olszewska, Yvette Bernal, Hollie Pegram, Mark Przybylowski, Daniel Hollyman, Yelena Usachenko, Domenick Pirraglia, James Hosey, Elmer Santos, Elizabeth Halton, Peter Maslak, David Scheinberg, Joseph Jurcic, Mark Heaney, Glenn Heller, Mark Frattini, and Michel Sadelain. Safety and persistence of adoptively transferred autologous CD19-targeted T cells in patients with relapsed or chemotherapy refractory B-cell leukemias. *Blood*, 118(18):4817–4828, nov 2011.

[80] Renier J. Brentjens, Elmer Santos, Yan Nikhamin, Raymond Yeh, Maiko Matsushita, Krista La Perle, Alfonso Quintás-Cardama, Steven M. Larson, and Michel Sadelain. Genetically Targeted T Cells Eradicate Systemic Acute Lymphoblastic Leukemia Xenografts. *Clin. Cancer Res.*, 13(18):5426–5435, sep 2007.

[81] Michael C. Milone, Jonathan D. Fish, Carmine Carpenito, Richard G. Carroll, Gwendolyn K. Binder, David Teachey, Minu Samanta, Mehdi Lakhal, Brian Gloss, Gwenn Danet-Desnoyers, Dario Campana, James L. Riley, Stephan A. Grupp, and Carl H. June. Chimeric Receptors Containing CD137 Signal Transduction Domains Mediate Enhanced Survival of T Cells and Increased Antileukemic Efficacy In Vivo. *Mol. Ther.*, 17(8):1453–1464, apr 2009.

[82] Claudia M. Kowolik, Max S. Topp, Sergio Gonzalez, Timothy Pfeiffer, Simon Olivares, Nancy Gonzalez, David D. Smith, Stephen J. Forman, Michael C. Jensen, and Laurence J. N. Cooper. CD28 Costimulation Provided through a CD19-Specific Chimeric Antigen Receptor Enhances In vivo Persistence and Antitumor Efficacy of Adoptively Transferred T Cells. *Cancer Res.*, 66(22):10995–11004, nov 2006.

[83] Marco L. Davila, Isabelle Riviere, Xiuyan Wang, Shirley Bartido, Jae Park, Kevin Curran, Stephen S. Chung, Jolanta Stefanski, Oriana Borquez-Ojeda,

Malgorzata Olszewska, Jinrong Qu, Teresa Wasielewska, Qing He, Mitsu Fink, Himaly Shinglot, Maher Youssif, Mark Satter, Yongzeng Wang, James Hosey, Hilda Quintanilla, Elizabeth Halton, Yvette Bernal, Diana C. G. Bouhassira, Maria E. Arcila, Mithat Gonen, Gail J. Roboz, Peter Maslak, Dan Douer, Mark G. Frattini, Sergio Giralt, Michel Sadelain, and Renier Brentjens. Efficacy and Toxicity Management of 19-28z CAR T Cell Therapy in B Cell Acute Lymphoblastic Leukemia. *Sci. Transl. Med.*, 6(224):224ra25–224ra25, feb 2014.

[84] Sara Ghorashian, Martin Pule, and Persis Amrolia. CD19 chimeric antigen receptor T cell therapy for haematological malignancies. *Br. J. Haematol.*, pages n/a–n/a, mar 2015.

[85] Daniel W Lee, James N Kochenderfer, Maryalice Stetler-Stevenson, Yongzhi K Cui, Cindy Delbrook, Steven A Feldman, Terry J Fry, Rimas Orentas, Marianna Sabatino, Nirali N Shah, Seth M Steinberg, Dave Stroncek, Nick Tschernia, Constance Yuan, Hua Zhang, Ling Zhang, Steven A Rosenberg, Alan S Wayne, and Crystal L Mackall. T cells expressing CD19 chimeric antigen receptors for acute lymphoblastic leukaemia in children and young adults: a phase 1 dose-escalation trial. *Lancet*, 385(9967):517–528, feb 2015.

[86] Shannon L. Maude, Noelle Frey, Pamela A. Shaw, Richard Aplenc, David M. Barrett, Nancy J. Bunin, Anne Chew, Vanessa E. Gonzalez, Zhaohui Zheng, Simon F. Lacey, Yolanda D. Mahnke, Jan J. Melenhorst, Susan R. Rheingold, Angela Shen, David T. Teachey, Bruce L. Levine, Carl H. June, David L. Porter, and Stephan A. Grupp. Chimeric Antigen Receptor T Cells for Sustained Remissions in Leukemia. *N. Engl. J. Med.*, 371(16):1507–1517, oct 2014.

[87] Renier Brentjens, Marco L Davila, Isabelle Riviere, Jae Park, Xiuyan Wang, Lindsay G Cowell, Shirley Bartido, Jolanta Stefanski, Clare Taylor, Malgorzata Olszewska, Oriana Borquez-Ojeda, Jinrong Qu, Teresa Wasielewska,

Qing He, Yvette Bernal, Ivelise V Rijo, Cyrus Hedvat, Rachel Kobos, Kevin Curran, Peter Steinherz, Joseph Jurcic, Todd Rosenblat, Peter Maslak, Mark Frattini, and Michel Sadelain. CD19-targeted T cells rapidly induce molecular remissions in adults with chemotherapy-refractory acute lymphoblastic leukemia. *Sci. Transl. Med.*, 5(177):177ra38, mar 2013.

[88] Cameron J. Turtle, Stanley R. Riddell, and David G. Maloney. CD19-targeted chimeric antigen receptor-modified T cell immunotherapy for B cell malignancies. *Clin. Pharmacol. Ther.*, may 2016.

[89] Stephan A. Grupp, Michael Kalos, David Barrett, Richard Aplenc, David L. Porter, Susan R. Rheingold, David T. Teachey, Anne Chew, Bernd Hauck, J. Fraser Wright, Michael C. Milone, Bruce L. Levine, and Carl H. June. Chimeric Antigen ReceptorModified T Cells for Acute Lymphoid Leukemia. *N. Engl. J. Med.*, 368(16):1509–1518, apr 2013.

[90] C. Rossig, M. Pule, B. Altvater, S. Saiagh, G. Wright, S. Ghorashian, L. Clifton-Hadley, K. Champion, Z. Sattar, B. Popova, A. Hackshaw, P. Smith, T. Roberts, E. Biagi, B. Dreno, R. Rousseau, S. Kailayangiri, M. Ahlmann, R. Hough, B. Kremens, M. G. Sauer, P. Veys, N. Goulden, M. Cummins, and P. J. Amrolia. Vaccination to improve the persistence of CD19CAR gene-modified T cells in relapsed pediatric acute lymphoblastic leukemia. *Leukemia*, jan 2017.

[91] Martin A. Cheever, James P. Allison, Andrea S. Ferris, Olivera J. Finn, Benjamin M. Hastings, Toby T. Hecht, Ira Mellman, Sheila A. Prindiville, Jaye L. Viner, Louis M. Weiner, and Lynn M. Matrisian. The Prioritization of Cancer Antigens: A National Cancer Institute Pilot Project for the Acceleration of Translational Research. *Clin. Cancer Res.*, 15(17):5323–5337, sep 2009.

[92] Nabil Ahmed, Vita S. Brawley, Meenakshi Hegde, Catherine Robertson, Alexia Ghazi, Claudia Gerken, Enli Liu, Olga Dakhova, Aidin Ashoori, Amanda Corder, Tara Gray, Meng-Fen Wu, Hao Liu, John Hicks, Nino

Rainusso, Gianpietro Dotti, Zhuyong Mei, Bambi Grilley, Adrian Gee, Cliona M. Rooney, Malcolm K. Brenner, Helen E. Heslop, Winfried S. Wels, Lisa L. Wang, Peter Anderson, and Stephen Gottschalk. Human Epidermal Growth Factor Receptor 2 (HER2) Specific Chimeric Antigen ReceptorModified T Cells for the Immunotherapy of HER2-Positive Sarcoma. *J. Clin. Oncol.*, 33(15):1688–1696, may 2015.

[93] Richard A Morgan, James C Yang, Mio Kitano, Mark E Dudley, Carolyn M Laurencot, and Steven A Rosenberg. Case Report of a Serious Adverse Event Following the Administration of T Cells Transduced With a Chimeric Antigen Receptor Recognizing ERBB2. *Mol. Ther.*, 18(4):843–851, apr 2010.

[94] Holly M. Horton, Matthew J. Bernett, Erik Pong, Matthias Peipp, Sher Karki, Seung Y. Chu, John O. Richards, Igor Vostiar, Patrick F. Joyce, Roland Repp, John R. Desjarlais, and Eugene A. Zhukovsky. Potent In vitro and In vivo Activity of an Fc-Engineered Anti-CD19 Monoclonal Antibody against Lymphoma and Leukemia. *Cancer Res.*, 68(19):8049–8057, oct 2008.

[95] Elena Sotillo, David M. Barrett, Kathryn L. Black, Asen Bagashev, Derek Oldridge, Glendon Wu, Robyn Sussman, Claudia Lanauze, Marco Ruella, Matthew R. Gazzara, Nicole M. Martinez, Colleen T. Harrington, Elaine Y. Chung, Jessica Perazzelli, Ted J. Hofmann, Shannon L. Maude, Pichai Raman, Alejandro Barrera, Saar Gill, Simon F. Lacey, Jan J. Melenhorst, David Allman, Elad Jacoby, Terry Fry, Crystal Mackall, Yoseph Barash, Kristen W. Lynch, John M. Maris, Stephan A. Grupp, and Andrei Thomas-Tikhonenko. Convergence of Acquired Mutations and Alternative Splicing of CD19 Enables Resistance to CART-19 Immunotherapy. *Cancer Discov.*, 5(12):1282–1295, dec 2015.

[96] H Zola, P.J. Macardle, T Bradford, H Weedon, H Yasui, and Y Kurosawa. Preparation and characterization of a chimeric CD19 monoclonal antibody. *Immunol Cell Biol*, 69(6):411–422, dec 1991.

[97] Shannon L. Maude, Michael A. Pulsipher, Michael W. Boyer, Stephan A. Grupp, Stella M. Davies, Christine L. Phillips, Michael R. Verneris, Keith J. August, Krysta Schlis, Timothy A. Driscoll, Rajen Mody, Christian M. Capitini, Carl H. June, Bruce L. Levine, Patricia A. Wood, Lan Yi, and John E. Levine. Efficacy and Safety of CTL019 in the First US Phase II Multicenter Trial in Pediatric Relapsed/Refractory Acute Lymphoblastic Leukemia: Results of an Interim Analysis. *Blood*, 128(22):2801–2801, dec 2016.

[98] Marco Ruella, David M. Barrett, Saad S. Kenderian, Olga Shestova, Ted J. Hofmann, Jessica Perazzelli, Michael Klichinsky, Vania Aikawa, Farzana Nazimuddin, Miroslaw Kozlowski, John Scholler, Simon F. Lacey, Jan J. Melenhorst, Jennifer J. D. Morrissette, David A. Christian, Christopher A. Hunter, Michael Kalos, David L. Porter, Carl H. June, Stephan A. Grupp, and Saar Gill. Dual CD19 and CD123 targeting prevents antigen-loss relapses after CD19-directed immunotherapies. *J. Clin. Invest.*, aug 2016.

[99] Elad Jacoby, Sang M. Nguyen, Thomas J. Fountaine, Kathryn Welp, Berkley Gryder, Haiying Qin, Yinmeng Yang, Christopher D. Chien, Alix E. Seif, Haiyan Lei, Young K. Song, Javed Khan, Daniel W. Lee, Crystal L. Mackall, Rebecca A. Gardner, Michael C. Jensen, Jack F. Shern, and Terry J. Fry. CD19 CAR immune pressure induces B-precursor acute lymphoblastic leukaemia lineage switch exposing inherent leukaemic plasticity. *Nat. Commun.*, 7, jul 2016.

[100] David T. Teachey, Simon F. Lacey, Pamela A. Shaw, J. Joseph Melenhorst, Shannon L. Maude, Noelle Frey, Edward Pequignot, Vanessa E. Gonzalez, Fang Chen, Jeffrey Finklestein, David M. Barrett, Scott L. Weiss, Julie C. Fitzgerald, Robert A. Berg, Richard Aplenc, Colleen Callahan, Susan R. Rheingold, Zhaohui Zheng, Stefan Rose-John, Jason C. White, Farzana Nazimuddin, Gerald Wertheim, Bruce L. Levine, Carl H. June, David L. Porter, and Stephan A. Grupp. Identification of Predictive Biomarkers for Cytokine

Release Syndrome after Chimeric Antigen Receptor T cell Therapy for Acute Lymphoblastic Leukemia. *Cancer Discov.*, pages CD–16–0040, apr 2016.

[101] Renier J. Brentjens, Jean-Baptiste Latouche, Elmer Santos, Francesc Marti, Michael C. Gong, Clay Lyddane, Philip D. King, Steven Larson, Mark Weiss, Isabelle Rivière, and Michel Sadelain. Eradication of systemic B-cell tumors by genetically targeted human T lymphocytes co-stimulated by CD80 and interleukin-15. *Nat. Med.*, 9(3):279–286, mar 2003.

[102] Helene M. Finney, Alastair D. G. Lawson, Christopher R. Bebbington, and A. Neil C. Weir. Chimeric Receptors Providing Both Primary and Costimulatory Signaling in T Cells from a Single Gene Product. *J. Immunol.*, 161(6):2791–2797, sep 1998.

[103] Andreas a Hombach, Gunter Rappl, and Hinrich Abken. Arming cytokine-induced killer cells with chimeric antigen receptors: CD28 outperforms combined CD28-OX40 "super-stimulation". *Mol. Ther.*, 21(12):2268–77, dec 2013.

[104] Syam Tammana, Xin Huang, Marianna Wong, Michael C Milone, Linan Ma, Bruce L Levine, Carl H June, John E Wagner, Bruce R Blazar, and Xianzheng Zhou. 4-1BB and CD28 signaling plays a synergistic role in redirecting umbilical cord blood T cells against B-cell malignancies. *Hum. Gene Ther.*, 21(1):75–86, jan 2010.

[105] Bryan A. Irving and Arthur Weiss. The cytoplasmic domain of the T cell receptor ζ chain is sufficient to couple to receptor-associated signal transduction pathways. *Cell*, 64(5):891–901, mar 1991.

[106] Patrick Tan, Claudio Anasetti, John Hansen, Jennifer Melrose, Mark Brunvand, Jeff Bradshaw, Jeffrey Ledbetter, and Peter Linsley. Induction of alloantigen-specific hyporesponsiveness in human T lymphocytes by blocking interaction of CD28 with its natural ligand B7/BB1. *J. Exp. Med.*, 177(1):165–173, jan 1993.

[107] T. Brocker and K. Karjalainen. Signals through T cell receptor-zeta chain alone are insufficient to prime resting T lymphocytes. *J. Exp. Med.*, 181(5):1653–1659, may 1995.

[108] Zelig Eshhar, Tova Waks, Alain Bendavid, and Daniel G. Schindler. Functional expression of chimeric receptor genes in human T cells. *J. Immunol. Methods*, 248(1-2):67–76, feb 2001.

[109] Andreas Hombach, Anja Wieczarkowiecz, Thomas Marquardt, Claudia Heuser, Loretta Usai, Christoph Pohl, Barbara Seliger, and Hinrich Abken. Tumor-Specific T Cell Activation by Recombinant Immunoreceptors: CD3ζ Signaling and CD28 Costimulation Are Simultaneously Required for Efficient IL-2 Secretion and Can Be Integrated Into One Combined CD28/CD3ζ Signaling Receptor Molecule. *J. Immunol.*, 167(11):6123–6131, dec 2001.

[110] John Maher, Renier J. Brentjens, Gertrude Gunset, Isabelle Rivière, and Michel Sadelain. Human T-lymphocyte cytotoxicity and proliferation directed by a single chimeric TCRζ /CD28 receptor. *Nat. Biotechnol.*, 20(1):70–75, jan 2002.

[111] Nicole M. Haynes, Marie B. Snook, Joseph A. Trapani, Loretta Cerruti, Stephen M. Jane, Mark J. Smyth, and Phillip K. Darcy. Redirecting Mouse CTL Against Colon Carcinoma: Superior Signaling Efficacy of Single-Chain Variable Domain Chimeras Containing TCR-ζ vs FcεRI-γ. *J. Immunol.*, 166(1):182–187, jan 2001.

[112] Dinorah Friedmann-Morvinski, Alain Bendavid, Tova Waks, Daniel Schindler, and Zelig Eshhar. Redirected primary T cells harboring a chimeric receptor require costimulation for their antigen-specific activation. *Blood*, 105(8):3087–3093, apr 2005.

[113] Barbara Savoldo, Carlos Almeida Ramos, Enli Liu, Martha P. Mims, Michael J. Keating, George Carrum, Rammurti T. Kamble, Catherine M. Bollard, Adrian P. Gee, Zhuyong Mei, Hao Liu, Bambi Grilley, Cliona M.

Rooney, Helen E. Heslop, Malcolm K. Brenner, and Gianpietro Dotti. CD28 costimulation improves expansion and persistence of chimeric antigen receptormodified T cells in lymphoma patients. *J. Clin. Invest.*, 121(5):1822–1826, may 2011.

[114] Helene M. Finney, Arne N. Akbar, and Alastair D. G. Lawson. Activation of Resting Human Primary T Cells with Chimeric Receptors: Costimulation from CD28, Inducible Costimulator, CD134, and CD137 in Series with Signals from the TCRζ Chain. *J. Immunol.*, 172(1):104–113, jan 2004.

[115] C. Imai, K. Mihara, M. Andreansky, I. C. Nicholson, C.-H. Pui, T. L. Geiger, and D. Campana. Chimeric receptors with 4-1BB signaling capacity provoke potent cytotoxicity against acute lymphoblastic. *Leukemia*, 18(4):676–684, feb 2004.

[116] Laurent Sabbagh, Gayle Pulle, Yuanqing Liu, Erdyni N. Tsitsikov, and Tania H. Watts. ERK-Dependent Bim Modulation Downstream of the 4-1BB-TRAF1 Signaling Axis Is a Critical Mediator of CD8 T Cell Survival In Vivo. *J. Immunol.*, 180(12):8093–8101, jun 2008.

[117] Yangbing Zhao, Qiong J. Wang, Shicheng Yang, James N. Kochenderfer, Zhili Zheng, Xiaosong Zhong, Michel Sadelain, Zelig Eshhar, Steven A. Rosenberg, and Richard A. Morgan. A Herceptin-Based Chimeric Antigen Receptor with Modified Signaling Domains Leads to Enhanced Survival of Transduced T Lymphocytes and Antitumor Activity. *J. Immunol.*, 183(9):5563–5574, nov 2009.

[118] Carmine Carpenito, Michael C. Milone, Raffit Hassan, Jacqueline C. Simonet, Mehdi Lakhal, Megan M. Suhoski, Angel Varela-Rohena, Kathleen M. Haines, Daniel F. Heitjan, Steven M. Albelda, Richard G. Carroll, James L. Riley, Ira Pastan, and Carl H. June. Control of large, established tumor xenografts with genetically retargeted human T cells containing CD28 and CD137 domains. *Proc. Natl. Acad. Sci.*, 106(9):3360–3365, mar 2009.

[119] Adrienne H. Long, Waleed M. Haso, Jack F. Shern, Kelsey M. Wanhainen, Meera Murgai, Maria Ingaramo, Jillian P. Smith, Alec J. Walker, M. Eric Kohler, Vikas R. Venkateshwara, Rosandra N. Kaplan, George H. Patterson, Terry J. Fry, Rimas J. Orentas, and Crystal L. Mackall. 4-1BB costimulation ameliorates T cell exhaustion induced by tonic signaling of chimeric antigen receptors. *Nat. Med.*, advance on, may 2015.

[120] Brian G. Till, Michael C. Jensen, Jinjuan Wang, Xiaojun Qian, Ajay K. Gopal, David G. Maloney, Catherine G. Lindgren, Yukang Lin, John M. Pagel, Lihua E. Budde, Andrew Raubitschek, Stephen J. Forman, Philip D. Greenberg, Stanley R. Riddell, and Oliver W. Press. CD20-specific adoptive immunotherapy for lymphoma using a chimeric antigen receptor with both CD28 and 4-1BB domains: pilot clinical trial results. *Blood*, 119(17):3940–3950, apr 2012.

[121] Jinjuan Wang, Michael Jensen, Yukang Lin, Xingwei Sui, Eric Chen, Catherine G. Lindgren, Brian Till, Andrew Raubitschek, Stephen J. Forman, Xiaojun Qian, Scott James, Philip Greenberg, Stanley Riddell, and Oliver W. Press. Optimizing Adoptive Polyclonal T Cell Immunotherapy of Lymphomas, Using a Chimeric T Cell Receptor Possessing CD28 and CD137 Costimulatory Domains. *Hum. Gene Ther.*, 18(8):712–725, aug 2007.

[122] Omkar U. Kawalekar, Roddy S. O'Connor, Joseph A. Fraietta, Lili Guo, Shannon E. McGettigan, Avery D. Posey, Prachi R. Patel, Sonia Guedan, John Scholler, Brian Keith, Nathaniel Snyder, Ian Blair, Michael C. Milone, and Carl H. June. Distinct Signaling of Coreceptors Regulates Specific Metabolism Pathways and Impacts Memory Development in CAR T Cells. *Immunity*, 44(2), 2016.

[123] Hinrich Abken. Costimulation Engages the Gear in Driving CARs. *Immunity*, 44(2):214–216, feb 2016.

[124] Shivani Srivastava and Stanley R. Riddell. Engineering CAR-T Cells: Design Concepts. *Trends Immunol.*

[125] Paul J. Neeson, Alexander James Davenport, Joseph A. Trapani, Michael Kershaw, Ryan Cross, H. Miles Prince, Ricky W. Johnstone, David Ritchie, Phil Darcy, and Misty R. Jenkins. Bigger, Stronger, Faster: Chimeric Antigen Receptor T Cells Are Olympic Killers. *Blood*, 128(22):814–814, dec 2016.

[126] D Moritz, W Wels, J Mattern, and B Groner. Cytotoxic T lymphocytes with a grafted recognition specificity for ERBB2-expressing tumor cells. *Proc. Natl. Acad. Sci. U. S. A.*, 91(10):4318–4322, may 1994.

[127] Ryan D. Guest, Robert E. Hawkins, Natalia Kirillova, Eleanor J. Cheadle, Jennifer Arnold, Allison O'Neill, Joely Irlam, Kerry A. Chester, John T. Kemshead, David M. Shaw, M. J. Embleton, Peter L. Stern, and David E. Gilham. The role of extracellular spacer regions in the optimal design of chimeric immune receptors: evaluation of four different scFvs and antigens. *J. Immunother. (Hagerstown, Md. 1997)*, 28(3):203–211, jun 2005.

[128] Michael Hudecek, Maria-Teresa Lupo-Stanghellini, Paula L. Kosasih, Daniel Sommermeyer, Michael C. Jensen, Christoph Rader, and Stanley R. Riddell. Receptor Affinity and Extracellular Domain Modifications Affect Tumor Recognition by ROR1-Specific Chimeric Antigen Receptor T Cells. *Clin. Cancer Res.*, 19(12):3153–3164, jun 2013.

[129] A Hombach, C Heuser, M Gerken, B Fischer, K Lewalter, V Diehl, C Pohl, and H Abken. T cell activation by recombinant FcRI γ-chain immune receptors: an extracellular spacer domain impairs antigen-dependent T cell activation but not antigen recognition. *Gene Ther.*, 7(12), jun 2000.

[130] D. Moritz and B. Groner. A spacer region between the single chain antibody- and the CD3 zeta-chain domain of chimeric T cell receptor components is required for efficient ligand binding and signaling activity. *Gene Ther.*, 2(8):539–546, oct 1995.

[131] Annette Künkele, Adam J. Johnson, Lisa S. Rolczynski, Cindy A. Chang, Virginia Hoglund, Karen S. Kelly-Spratt, and Michael C. Jensen. Functional Tuning of CARs Reveals Signaling Threshold Above Which CD8+ CTL Antitumor Potency is Attenuated Due to Cell Fas-FasL Dependent AICD. *Cancer Immunol. Res.*, page canimm.0200.2014, jan 2015.

[132] Michael Hudecek, Daniel Sommermeyer, Paula L. Kosasih, Anne Silva-Benedict, Lingfeng Liu, Christoph Rader, Michael C. Jensen, and Stanley R. Riddell. The Nonsignaling Extracellular Spacer Domain of Chimeric Antigen Receptors Is Decisive for In Vivo Antitumor Activity. *Cancer Immunol. Res.*, 3(2):125–135, feb 2015.

[133] H. Almåsbak, E. Walseng, A. Kristian, M. R. Myhre, E. M. Suso, L. A. Munthe, J. T. Andersen, M. Y. Wang, G. Kvalheim, G. Gaudernack, and J. A. Kyte. Inclusion of an IgG1-Fc spacer abrogates efficacy of CD19 CAR T cells in a xenograft mouse model. *Gene Ther.*, 22(5):391–403, may 2015.

[134] Bipulendu Jena, Gianpietro Dotti, and Laurence J. N. Cooper. Redirecting T-cell specificity by introducing a tumor-specific chimeric antigen receptor. *Blood*, 116(7):1035–1044, aug 2010.

[135] Bruce E. Bejcek, Duo Wang, Erica Berven, Christopher A. Pennell, Stephen C. Peiper, Sibrand Poppema, Fatih M. Uckun, and John H. Kersey. Development and Characterization of Three Recombinant Single Chain Antibody Fragments (scFvs) Directed against the CD19 Antigen. *Cancer Res.*, 55(11):2346–2351, jun 1995.

[136] F. M. Uckun, W. Jaszcz, J. L. Ambrus, A. S. Fauci, K. Gajl-Peczalska, C. W. Song, M. R. Wick, D. E. Myers, K. Waddick, and J. A. Ledbetter. Detailed studies on expression and function of CD19 surface determinant by using B43 monoclonal antibody and the clinical potential of anti- CD19 immunotoxins. *Blood*, 71(1):13–29, jan 1988.

[137] L. M. Nadler, K. C. Anderson, G. Marti, M. Bates, E. Park, J. F. Daley, and S. F. Schlossman. B4, a human B lymphocyte-associated antigen expressed on normal, mitogen-activated, and malignant B lymphocytes. *J. Immunol.*, 131(1):244–250, jul 1983.

[138] A. Pezzutto, B. Dörken, P. S. Rabinovitch, J. A. Ledbetter, G. Moldenhauer, and E. A. Clark. CD19 monoclonal antibody HD37 inhibits anti-immunoglobulin-induced B cell activation and proliferation. *J. Immunol.*, 138(9):2793–2799, may 1987.

[139] W. W. K. Cheng, D. Das, M. Suresh, and T. M. Allen. Expression and purification of two anti-CD19 single chain Fv fragments for targeting of liposomes to CD19-expressing cells. *Biochim. Biophys. Acta - Biomembr.*, 1768(1):21–29, jan 2007.

[140] James N. Kochenderfer, Wyndham H. Wilson, John E. Janik, Mark E. Dudley, Maryalice Stetler-Stevenson, Steven A. Feldman, Irina Maric, Mark Raffeld, Debbie-Ann N. Nathan, Brock J. Lanier, Richard A. Morgan, and Steven A. Rosenberg. Eradication of B-lineage cells and regression of lymphoma in a patient treated with autologous T cells genetically engineered to recognize CD19. *Blood*, 116(20):4099–4102, nov 2010.

[141] Elvin A. Kabat, Tai Te Wu, Harold M. Perry, Kay S. Gottesman, and Carl Foeller. *Sequences of Proteins of Immunological Interest*. DIANE Publishing, jun 1992.

[142] David K. Cole, Nicholas J. Pumphrey, Jonathan M. Boulter, Malkit Sami, John I. Bell, Emma Gostick, David A. Price, George F. Gao, Andrew K. Sewell, and Bent K. Jakobsen. Human TCR-Binding Affinity is Governed by MHC Class Restriction. *J. Immunol.*, 178(9):5727–5734, may 2007.

[143] Philip Anton van der Merwe and Simon Davis. Molecular Interactions Mediating T Cell Antigen Recognition. *Annu. Rev. Immunol.*, 21(1):659–684, 2003.

[144] M. E. Weijtens, E. H. Hart, and R. L. Bolhuis. Functional balance between T cell chimeric receptor density and tumor associated antigen density: CTL mediated cytolysis and lymphokine production. *Gene Ther.*, 7(1):35–42, jan 2000.

[145] Scott E. James, Philip D. Greenberg, Michael C. Jensen, Yukang Lin, Jinjuan Wang, Lihua E. Budde, Brian G. Till, Andrew A. Raubitschek, Stephen J. Forman, and Oliver W. Press. Correction: Mathematical Modeling of Chimeric TCR Triggering Predicts the Magnitude of Target Lysis and Its Impairment by TCR Downmodulation. *J. Immunol.*, 184(8):1340–1340, apr 2010.

[146] Fabio Turatti, Mariangela Figini, Emanuela Balladore, Paola Alberti, Patrizia Casalini, James D. Marks, Silvana Canevari, and Delia Mezzanzanica. Redirected activity of human antitumor chimeric immune receptors is governed by antigen and receptor expression levels and affinity of interaction. *J. Immunother. (Hagerstown, Md. 1997)*, 30(7):684–693, oct 2007.

[147] Markus Chmielewski, Andreas Hombach, Claudia Heuser, Gregory P. Adams, and Hinrich Abken. T Cell Activation by Antibody-Like Immunoreceptors: Increase in Affinity of the Single-Chain Fragment Domain above Threshold Does Not Increase T Cell Activation against Antigen-Positive Target Cells but Decreases Selectivity. *J. Immunol.*, 173(12):7647–7653, dec 2004.

[148] Waleed Haso, Daniel W. Lee, Nirali N. Shah, Maryalice Stetler-Stevenson, Constance M. Yuan, Ira H. Pastan, Dimiter S. Dimitrov, Richard A. Morgan, David J. FitzGerald, David M. Barrett, Alan S. Wayne, Crystal L. Mackall, and Rimas J. Orentas. Anti-CD22chimeric antigen receptors targeting B-cell precursor acute lymphoblastic leukemia. *Blood*, 121(7):1165–1174, feb 2013.

[149] Jennifer D. Stone and David M. Kranz. Role of T cell receptor affinity in the efficacy and specificity of adoptive T cell therapies. *Front. Immunol.*, 4:244, 2013.

[150] Ravit Oren, Moran Hod-Marco, Maya Haus-Cohen, Sharyn Thomas, Dan Blat, Nerri Duvshani, Galit Denkberg, Yael Elbaz, Fabrice Benchetrit, Zelig Eshhar, Hans Stauss, and Yoram Reiter. Functional Comparison of Engineered T Cells Carrying a Native TCR versus TCR-like AntibodyBased Chimeric Antigen Receptors Indicates Affinity/Avidity Thresholds. *J. Immunol.*, 193(11):5733–5743, dec 2014.

[151] Hillary G. Caruso, Lenka V. Hurton, Amer Najjar, David Rushworth, Sonny Ang, Simon Olivares, Tiejuan Mi, Kirsten Switzer, Harjeet Singh, Helen Huls, Dean A. Lee, Amy B. Heimberger, Richard E. Champlin, and Laurence J. N. Cooper. Tuning Sensitivity of CAR to EGFR Density Limits Recognition of Normal Tissue While Maintaining Potent Antitumor Activity. *Cancer Res.*, 75(17):3505–3518, sep 2015.

[152] Xiaojun Liu, Shuguang Jiang, Chongyun Fang, Shiyu Yang, Devvora Olalere, Edward C. Pequignot, Alexandria P. Cogdill, Na Li, Melissa Ramones, Brian Granda, Li Zhou, Andreas Loew, Regina M. Young, Carl H. June, and Yangbing Zhao. Affinity-Tuned ErbB2 or EGFR Chimeric Antigen Receptor T Cells Exhibit an Increased Therapeutic Index against Tumors in Mice. *Cancer Res.*, 75(17):3596–3607, sep 2015.

[153] Brian Philip, Evangelia Kokalaki, Leila Mekkaoui, Simon Thomas, Karin Straathof, Barry Flutter, Virna Marin, Teresa Marafioti, Ronjon Chakraverty, David Linch, Sergio A. Quezada, Karl S. Peggs, and Martin Pule. A highly compact epitope-based marker/suicide gene for easier and safer T-cell therapy. *Blood*, 124(8):1277–1287, aug 2014.

[154] Laura A. Johnson, John Scholler, Takayuki Ohkuri, Akemi Kosaka, Prachi R. Patel, Shannon E. McGettigan, Arben K. Nace, Tzvete Dentchev, Pramod

Thekkat, Andreas Loew, Alina C. Boesteanu, Alexandria P. Cogdill, Taylor Chen, Joseph A. Fraietta, Christopher C. Kloss, Avery D. Posey, Boris Engels, Reshma Singh, Tucker Ezell, Neeraja Idamakanti, Melissa H. Ramones, Na Li, Li Zhou, Gabriela Plesa, John T. Seykora, Hideho Okada, Carl H. June, Jennifer L. Brogdon, and Marcela V. Maus. Rational development and characterization of humanized antiEGFR variant III chimeric antigen receptor T cells for glioblastoma. *Sci. Transl. Med.*, 7(275):275ra22–275ra22, feb 2015.

[155] Dale J. Langford, Andrea L. Bailey, Mona Lisa Chanda, Sarah E. Clarke, Tanya E. Drummond, Stephanie Echols, Sarah Glick, Joelle Ingrao, Tammy Klassen-Ross, Michael L. Lacroix-Fralish, Lynn Matsumiya, Robert E. Sorge, Susana G. Sotocinal, John M. Tabaka, David Wong, Arn M. J. M. van den Maagdenberg, Michel D. Ferrari, Kenneth D. Craig, and Jeffrey S. Mogil. Coding of facial expressions of pain in the laboratory mouse. *Nat. Methods*, 7(6):447–449, jun 2010.

[156] Michael C Gong, Jean-Baptiste Latouche, Anja Krause, Warren DW Heston, Neil H Bander, and Michel Sadelain. Cancer Patient T Cells Genetically Targeted to Prostate-Specific Membrane Antigen Specifically Lyse Prostate Cancer Cells and Release Cytokines in Response to Prostate-Specific Membrane Antigen. *Neoplasia*, 1(2):123–127, jun 1999.

[157] A. Hombach, C. Heuser, R. Sircar, T. Tillmann, V. Diehl, C. Pohl, and H. Abken. An anti-CD30 chimeric receptor that mediates CD3-zeta-independent T-cell activation against Hodgkin's lymphoma cells in the presence of soluble CD30. *Cancer Res.*, 58(6):1116–1119, mar 1998.

[158] C. Rossig, C. M. Bollard, J. G. Nuchtern, D. A. Merchant, and M. K. Brenner. Targeting of G(D2)-positive tumor cells by human T lymphocytes engineered to express chimeric T-cell receptor genes. *Int. J. Cancer*, 94(2):228–236, oct 2001.

[159] Stephan A. Grupp, Shannon L. Maude, Pamela A. Shaw, Richard Aplenc, David M. Barrett, Colleen Callahan, Simon F. Lacey, Bruce L. Levine, J. Joseph Melenhorst, Laura Motley, Susan R. Rheingold, David T. Teachey, Patricia A. Wood, David Porter, and Carl H. June. Durable Remissions in Children with Relapsed/Refractory ALL Treated with T Cells Engineered with a CD19-Targeted Chimeric Antigen Receptor (CTL019). *Blood*, 126(23):681–681, dec 2015.

[160] Jae H. Park and Renier J. Brentjens. Are All Chimeric Antigen Receptors Created Equal? *J. Clin. Oncol.*, page JCO.2014.57.5472, jan 2015.

[161] Cellosaurus cell line CAT-13.1E10 (CVCL_1973).

[162] M. L. Donnelly, L. E. Hughes, G. Luke, H. Mendoza, E. ten Dam, D. Gani, and M. D. Ryan. The 'cleavage' activities of foot-and-mouth disease virus 2A site-directed mutants and naturally occurring '2A-like' sequences. *J. Gen. Virol.*, 82(Pt 5):1027–1041, may 2001.

[163] Jens Geginat, Antonio Lanzavecchia, and Federica Sallusto. Proliferation and differentiation potential of human CD8+ memory T-cell subsets in response to antigen or homeostatic cytokines. *Blood*, 101(11):4260–4266, jun 2003.

[164] Mark A. Daniels and Emma Teixeiro. TCR Signaling in T Cell Memory. *Front. Immunol.*, 6, dec 2015.

[165] Marion Pepper, Antonio J. Pagán, Botond Z. Igyártó, Justin J. Taylor, and Marc K. Jenkins. Opposing signals from the Bcl6 transcription factor and the interleukin-2 receptor generate T helper-1 central and effector memory cells. *Immunity*, 35(4):583–595, oct 2011.

[166] Christopher A. Klebanoff, Luca Gattinoni, and Nicholas P. Restifo. CD8+ T-cell memory in tumor immunology and immunotherapy. *Immunol. Rev.*, 211:214–224, jun 2006.

[167] Antonio Lanzavecchia. Understanding the Mechanisms of Sustained Signaling and T Cell Activation. *J. Exp. Med.*, 185(10):1717–1719, may 1997.

[168] Clemens Utzny, Daniel Coombs, Sabina Müller, and Salvatore Valitutti. Analysis of peptide/MHC-induced TCR downregulation. *Cell Biochem. Biophys.*, 46(2):101–111, oct 2006.

[169] P. Neeson, A. Shin, K. M. Tainton, P. Guru, H. M. Prince, S. J. Harrison, S. Peinert, M. J. Smyth, J. A. Trapani, M. H. Kershaw, P. K. Darcy, and D. S. Ritchie. Ex vivo culture of chimeric antigen receptor T cells generates functional CD8+ T cells with effector and central memory-like phenotype. *Gene Ther.*, 17(9):1105–1116, sep 2010.

[170] E. John Wherry. T cell exhaustion. *Nat. Immunol.*, 12(6):492–499, jun 2011.

[171] Alexander J. Davenport, Misty R. Jenkins, Ryan S. Cross, Carmen S. Yong, H. Miles Prince, David S. Ritchie, Joseph A. Trapani, Michael H. Kershaw, Phillip K. Darcy, and Paul J. Neeson. CAR-T Cells Inflict Sequential Killing of Multiple Tumor Target Cells. *Cancer Immunol. Res.*, 3(5):483–494, may 2015.

[172] HélèneD. Moreau, Fabrice Lemaître, Emmanuel Terriac, Georges Azar, Matthieu Piel, Ana-Maria Lennon-Dumenil, and Philippe Bousso. Dynamic In Situ Cytometry Uncovers T Cell Receptor Signaling during Immunological Synapses and Kinapses InVivo. *Immunity*, 37(2):351–363, aug 2012.

[173] Daphné A. Schmid, Melita B. Irving, Vilmos Posevitz, Michael Hebeisen, Anita Posevitz-Fejfar, J.-C. Floyd Sarria, Raquel Gomez-Eerland, Margot Thome, Ton N. M. Schumacher, Pedro Romero, Daniel E. Speiser, Vincent Zoete, Olivier Michielin, and Nathalie Rufer. Evidence for a TCR Affinity Threshold Delimiting Maximal CD8 T Cell Function. *J. Immunol.*, 184(9):4936–4946, may 2010.

[174] Nicola Bortoletto, Emmanuel Scotet, Yoichi Myamoto, Ugo D'Oro, and Antonio Lanzavecchia. Optimizing anti-CD3 affinity for effective T cell targeting against tumor cells. *Eur. J. Immunol.*, 32(11):3102–3107, nov 2002.

[175] Patrick Hoffmann, Robert Hofmeister, Klaus Brischwein, Christian Brandl, Sandrine Crommer, Ralf Bargou, Christian Itin, Nadja Prang, and Patrick A. Baeuerle. Serial killing of tumor cells by cytotoxic T cells redirected with a CD19-/CD3-bispecific single-chain antibody construct. *Int. J. Cancer*, 115(1):98–104, may 2005.

[176] A. S. Chervin, J. D. Stone, C. M. Soto, B. Engels, H. Schreiber, E. J. Roy, and D. M. Kranz. Design of T-cell receptor libraries with diverse binding properties to examine adoptive T-cell responses. *Gene Ther.*, 20(6):634–644, jun 2013.

[177] Boris Engels, Adam S Chervin, Andrea J Sant, David M Kranz, and Hans Schreiber. Long-term Persistence of CD4+ but Rapid Disappearance of CD8+ T Cells Expressing an MHC Class I-restricted TCR of Nanomolar Affinity. *Mol. Ther.*, 20(3):652–660, mar 2012.

[178] Claire N. Janicki, S. Rhiannon Jenkinson, Neil A. Williams, and David J. Morgan. Loss of CTL Function among High-Avidity Tumor-Specific CD8+ T Cells following Tumor Infiltration. *Cancer Res.*, 68(8):2993–3000, apr 2008.

[179] Zeguo Zhao, Maud Condomines, SjoukjeJ. C. vanderStegen, Fabiana Perna, ChristopherC. Kloss, Gertrude Gunset, Jason Plotkin, and Michel Sadelain. Structural Design of Engineered Costimulation Determines Tumor Rejection Kinetics and Persistence of CAR T Cells. *Cancer Cell*, 28(4):415–428, oct 2015.

[180] Rainer Loew, Niels Heinz, Mathias Hampf, Hermann Bujard, and Manfred Gossen. Improved Tet-responsive promoters with minimized background expression. *BMC Biotechnol.*, 10:81, nov 2010.

[181] Ester M. M. van Leeuwen, Godelieve J. de Bree, Ester B. M. Remmerswaal, Si-La Yong, Kiki Tesselaar, Ineke J. M. ten Berge, and René A. W. van Lier. IL-7 receptor α chain expression distinguishes functional subsets of virus-specific human CD8+ T cells. *Blood*, 106(6):2091–2098, sep 2005.

[182] E. John Wherry, Sang-Jun Ha, Susan M. Kaech, W. Nicholas Haining, Surojit Sarkar, Vandana Kalia, Shruti Subramaniam, Joseph N. Blattman, Daniel L. Barber, and Rafi Ahmed. Molecular Signature of CD8+ T Cell Exhaustion during Chronic Viral Infection. *Immunity*, 27(4):670–684, oct 2007.

[183] Susan M. Kaech, Joyce T. Tan, E. John Wherry, Bogumila T. Konieczny, Charles D. Surh, and Rafi Ahmed. Selective expression of the interleukin 7 receptor identifies effector CD8 T cells that give rise to long-lived memory cells. *Nat. Immunol.*, 4(12):1191–1198, dec 2003.

[184] Alexis Dunkle and You-Wen He. Apoptosis and Autophagy in the Regulation of T Lymphocyte Function. *Immunol. Res.*, 49(1-3):70–86, apr 2011.

[185] Emily Corse, Rachel A. Gottschalk, Michelle Krogsgaard, and James P. Allison. Attenuated T Cell Responses to a High-Potency Ligand In Vivo. *PLoS Biol*, 8(9):e1000481, sep 2010.

[186] Luca Gattinoni, Christopher A. Klebanoff, Douglas C. Palmer, Claudia Wrzesinski, Keith Kerstann, Zhiya Yu, Steven E. Finkelstein, Marc R. Theoret, Steven A. Rosenberg, and Nicholas P. Restifo. Acquisition of full effector function in vitro paradoxically impairs the in vivo antitumor efficacy of adoptively transferred CD8+ T cells. *J. Clin. Invest.*, 115(6):1616–1626, jun 2005.

[187] David A. Hildeman, Yanan Zhu, Thomas C. Mitchell, Philippe Bouillet, Andreas Strasser, John Kappler, and Philippa Marrack. Activated T Cell Death In Vivo Mediated by Proapoptotic Bcl-2 Family Member Bim. *Immunity*, 16(6):759–767, jun 2002.

[188] Sema Kurtulus, Pulak Tripathi, Maria E. Moreno-Fernandez, Allyson Sholl, Jonathan D. Katz, H. Leighton Grimes, and David A. Hildeman. Bcl-2 Allows Effector and Memory CD8+ T Cells To Tolerate Higher Expression of Bim. *J. Immunol.*, 186(10):5729–5737, may 2011.

[189] David T. Teachey, Susan R. Rheingold, Shannon L. Maude, Gerhard Zugmaier, David M. Barrett, Alix E. Seif, Kim E. Nichols, Erica K. Suppa, Michael Kalos, Robert A. Berg, Julie C. Fitzgerald, Richard Aplenc, Lia Gore, and Stephan A. Grupp. Cytokine release syndrome after blinatumomab treatment related to abnormal macrophage activation and ameliorated with cytokine-directed therapy. *Blood*, 121(26):5154–5157, jun 2013.

[190] Marcela V. Maus, Stephan A. Grupp, David L. Porter, and Carl H. June. Antibody-modified T cells: CARs take the front seat for hematologic malignancies. *Blood*, 123(17):2625–2635, apr 2014.

[191] Gianpietro Dotti, Stephen Gottschalk, Barbara Savoldo, and Malcolm K Brenner. Design and Development of Therapies using Chimeric Antigen Receptor-Expressing T cells. *Immunol. Rev.*, 257(1), jan 2014.

[192] Michael Hebeisen, Lukas Baitsch, Danilo Presotto, Petra Baumgaertner, Pedro Romero, Olivier Michielin, Daniel E. Speiser, and Nathalie Rufer. SHP-1 phosphatase activity counteracts increased T cell receptor affinity. *J. Clin. Invest.*, 123(3):1044–1056, mar 2013.

[193] Paul F. Robbins, Yong F. Li, Mona El-Gamil, Yangbing Zhao, Jennifer A. Wargo, Zhili Zheng, Hui Xu, Richard A. Morgan, Steven A. Feldman, Laura A. Johnson, Alan D. Bennett, Steven M. Dunn, Tara M. Mahon, Bent K. Jakobsen, and Steven A. Rosenberg. Single and Dual Amino Acid Substitutions in TCR CDRs Can Enhance Antigen-Specific T Cell Functions. *J. Immunol.*, 180(9):6116–6131, may 2008.

[194] Manfred Lehner, Gabriel Götz, Julia Proff, Niels Schaft, Jan Dörrie, Florian Full, Armin Ensser, Yves A. Muller, Adelheid Cerwenka, Hinrich Abken,

Ornella Parolini, Peter F. Ambros, Heinrich Kovar, and Wolfgang Holter. Redirecting T Cells to Ewing's Sarcoma Family of Tumors by a Chimeric NKG2D Receptor Expressed by Lentiviral Transduction or mRNA Transfection. *PLoS One*, 7(2):e31210, feb 2012.

[195] Ariel Talavera, Rosmarie Friemann, Silvia Gómez-Puerta, Carlos Martinez-Fleites, Greta Garrido, Ailem Rabasa, Alejandro López-Requena, Amaury Pupo, Rune F. Johansen, Oliberto Sánchez, Ute Krengel, and Ernesto Moreno. Nimotuzumab, an Antitumor Antibody that Targets the Epidermal Growth Factor Receptor, Blocks Ligand Binding while Permitting the Active Receptor Conformation. *Cancer Res.*, 69(14):5851–5859, jul 2009.

[196] Magdalena Nauerth, Bianca Weißbrich, Robert Knall, Tobias Franz, Georg Dössinger, Jeannette Bet, Paulina J. Paszkiewicz, Lukas Pfeifer, Mario Bunse, Wolfgang Uckert, Rafaela Holtappels, Dorothea Gillert-Marien, Michael Neuenhahn, Angela Krackhardt, Matthias J. Reddehase, Stanley R. Riddell, and Dirk H. Busch. TCR-Ligand koff Rate Correlates with the Protective Capacity of Antigen-Specific CD8+ T Cells for Adoptive Transfer. *Sci. Transl. Med.*, 5(192):192ra87–192ra87, jul 2013.

[197] Emily Corse, Rachel A. Gottschalk, and James P. Allison. Strength of TCRPeptide/MHC Interactions and In Vivo T Cell Responses. *J. Immunol.*, 186(9):5039–5045, may 2011.

[198] Haiyan Liu, Michele Rhodes, David L Wiest, and Dario A. A Vignali. On the Dynamics of TCR:CD3 Complex Cell Surface Expression and Downmodulation. *Immunity*, 13(5):665–675, nov 2000.

[199] Barry Flutter, Noha Edwards, Farnaz Fallah-Arani, Stephen Henderson, Jian-Guo Chai, Shivajanani Sivakumaran, Sara Ghorashian, Clare L. Bennett, Gordon J. Freeman, Megan Sykes, and Ronjon Chakraverty. Nonhematopoietic antigen blocks memory programming of alloreactive CD8+ T cells and

drives their eventual exhaustion in mouse models of bone marrow transplantation. *J. Clin. Invest.*, 120(11):3855–3868, nov 2010.

[200] E. John Wherry, Joseph N. Blattman, Kaja Murali-Krishna, Robbert van der Most, and Rafi Ahmed. Viral Persistence Alters CD8 T-Cell Immunodominance and Tissue Distribution and Results in Distinct Stages of Functional Impairment. *J. Virol.*, 77(8):4911–4927, apr 2003.

[201] Daniel T. Utzschneider, Francesca Alfei, Patrick Roelli, David Barras, Vijaykumar Chennupati, Stephanie Darbre, Mauro Delorenzi, Daniel D. Pinschewer, and Dietmar Zehn. High antigen levels induce an exhausted phenotype in a chronic infection without impairing T cell expansion and survival. *J. Exp. Med.*, 213(9):1819–1834, aug 2016.

[202] Kristen N. Pollizzi, Chirag H. Patel, Im-Hong Sun, Min-Hee Oh, Adam T. Waickman, Jiayu Wen, Greg M. Delgoffe, and Jonathan D. Powell. mTORC1 and mTORC2 selectively regulate CD8+ T cell differentiation. *J. Clin. Invest.*, 125(5):2090–2108, may 2015.

[203] Pedro Veliça, Mathias Zech, Sian Henson, Angelika Holler, Teresa Manzo, Rebecca Pike, Pedro Santos e Sousa, Lei Zhang, Bernhard Schiedlmeier, Martin Pule, Hans Stauss, and Ronjon Chakraverty. Genetic Regulation of Fate Decisions in Therapeutic T Cells to Enhance Tumor Protection and Memory Formation. *Cancer Res.*, 75(13):2641–2652, jul 2015.

[204] Koichi Araki, Alexandra P. Turner, Virginia Oliva Shaffer, Shivaprakash Gangappa, Susanne A. Keller, Martin F. Bachmann, Christian P. Larsen, and Rafi Ahmed. mTOR regulates memory CD8 T-cell differentiation. *Nature*, 460(7251):108–112, jul 2009.

[205] Laura A. Johnson and Carl H. June. Driving gene-engineered T cell immunotherapy of cancer. *Cell Res.*, dec 2016.

[206] Haina Shin and E John Wherry. CD8 T cell dysfunction during chronic viral infection. *Curr. Opin. Immunol.*, 19(4):408–415, aug 2007.

[207] Hélène D. Moreau, Fabrice Lemaître, Kym R. Garrod, Zacarias Garcia, Ana-Maria Lennon-Duménil, and Philippe Bousso. Signal strength regulates antigen-mediated T-cell deceleration by distinct mechanisms to promote local exploration or arrest. *Proc. Natl. Acad. Sci. U. S. A.*, 112(39):12151–12156, sep 2015.